Measurements of WH and ZH production with Higgs boson decays into bottom quarks and direct constraints on the charm Yukawa coupling in 13 TeV pp collisions with the ATLAS detector

The ATLAS Collaboration

A study of the Higgs boson decaying into bottom quarks ($H \rightarrow b\bar{b}$) and charm quarks ($H \rightarrow c\bar{c}$) is performed, in the associated production channel of the Higgs boson with a W or Z boson, using $140\,\text{fb}^{-1}$ of proton–proton collision data at $\sqrt{s} = 13$ TeV collected by the ATLAS detector. The individual production of WH and ZH with $H \rightarrow b\bar{b}$ is established with observed (expected) significances of 5.3 (5.5) and 4.9 (5.6). Differential cross-section measurements of the gauge boson transverse momentum within the simplified template cross-section framework are performed in a total of 13 kinematical fiducial regions.

The search for the $H \rightarrow c\bar{c}$ decay yields an observed (expected) upper limit at 95% confidence level of 11.5 (10.6) times the Standard Model prediction. The results are also used to set constraints on the charm coupling modifier, resulting in $|\kappa_c| < 4.2$ at 95% confidence level. Combining the $H \rightarrow b\bar{b}$ and $H \rightarrow c\bar{c}$ measurements constrains the absolute value of the ratio of Higgs-charm and Higgs-bottom coupling modifiers ($|\kappa_c/\kappa_b|$) to be less than 3.6 at 95% confidence level.

Contents

1 Introduction

The discovery of a heavy scalar particle with a mass of about 125 GeV by the ATLAS and CMS collaborations [1, 2] at the Large Hadron Collider (LHC), provided experimental confirmation of the Brout-Englert-Higgs (BEH) mechanism [3–8], which spontaneously breaks electroweak (EW) gauge symmetry and generates mass terms for the W and Z gauge bosons. The observation of Higgs boson decays into τ-leptons [9, 10], bottom-quarks [11, 12] and associated production with top-quarks [13, 14] provided strong evidence to support the BEH mechanism in the Standard Model (SM) where the fermion masses are generated via Yukawa interactions. All measured couplings are so far consistent with the SM [15, 16].

Since the decay of the Higgs boson into b-quarks has the largest branching fraction ($\mathcal{B}$) with a SM expectation of 58.2% for a mass of 125 GeV [17], the b-quark Yukawa coupling is of particular interest. It

is the most sensitive decay channel to study some of the rarer Higgs boson processes, such as associated production with a W or Z boson (VH) [18, 19], WH production via vector boson fusion [20], Higgs boson production at high transverse momentum [21–24] and Higgs boson pair production, in which the most sensitive channels have one or both Higgs bosons decaying into b-quarks [25–30]. In the SM the b-quark Yukawa coupling has the largest impact on the Higgs boson's width and thus measuring it is crucial to set constraints on phenomena beyond the SM [15, 16]. Furthermore, this decay mode has allowed differential measurements of the VH cross-section in kinematic fiducial volumes defined in the simplified template cross-section (STXS) framework [17].

The decay of the Higgs boson into c-quarks is much more challenging than its decay into b-quarks due to the smaller expected $\mathcal{B}$ (2.9% for a Higgs boson mass of 125 GeV [17]), the increased difficulty in identifying c-hadrons, due to their smaller lifetimes and masses, and the larger background from vector boson plus c-quark production. Phenomena beyond the Standard Model could significantly enhance the coupling of the Higgs boson to the charm-quark, and in turn the $H \rightarrow c\bar{c}$ branching fraction [31–37]. Searches in the VH channel [38, 39] offer the best direct constraints on the Higgs-charm coupling.

This paper reports on a combined study of $H \rightarrow b\bar{b}$ and $H \rightarrow c\bar{c}$ in the VH production mode, using 140 fb^{-1} of proton–proton collision data recorded with the ATLAS detector in the years 2015-2018 at a centre-of-mass energy of 13 TeV. The associated VH production mode is used as it provides a clean signature with the vector boson decaying into charged leptons or neutrinos and allows the separation of the $H \rightarrow b\bar{b}$ and $H \rightarrow c\bar{c}$ signals from the large multijet background. In the analysis presented in this paper, the W boson is searched for in its decays into an electron, muon or τ-lepton (ℓ) in addition to a neutrino and the Z boson in its decays into electron, muon or neutrino pairs. The channels are labelled as 0-,1- or 2-lepton corresponding to the number of reconstructed charged leptons in the final state. The vector boson must have a minimum transverse momentum (p_{T}^V) of 75 GeV in the 1- and 2-lepton channels and 150 GeV in the 0-lepton channel.

The Higgs boson is reconstructed either from two small-radius (small-R) jets or from a single large-radius (large-R) jet, whose definitions are given in Section 4. The $H \rightarrow b\bar{b}$ and $H \rightarrow c\bar{c}$ sensitive regions are defined according to flavour tagging information of the jets. The $H \rightarrow c\bar{c}$ search exclusively uses small-R jets. To reconstruct the Higgs boson decay products, the $H \rightarrow b\bar{b}$ analysis uses small-R jets for $p_{\mathrm{T}}^V < 400$ GeV (resolved regime) and large-radius jets for $p_{\mathrm{T}}^V > 400$ GeV (boosted regime). This approach offers good sensitivity across the p_{T}^V range. Events are further classified according to the transverse momentum of the vector boson and the number of jets. Multivariate discriminants, built from variables that describe the kinematics, jet flavour and missing transverse momentum content of the selected events, are used to maximise the analysis sensitivity in all signal regions. The output distributions are used as inputs to binned maximum-likelihood fits, which allows the yields and kinematics of both the signal and the background processes to be estimated. The measurements are validated using a diboson analysis, where the multivariate discriminant is modified to extract the VZ, $Z \rightarrow b\bar{b}$ and $Z \rightarrow c\bar{c}$ diboson processes. In addition to overall signal yields, differential STXS measurements of the VH cross-section in the $H \rightarrow b\bar{b}$ channel are presented. The results are also interpreted in the κ-framework [17, 40] to constrain the coupling modifiers of the Higgs boson to b- and c-quarks, κ_b and κ_c. In the following, the sensitive region targeting the $H \rightarrow b\bar{b}$ decay is referred to as the Hbb category and the sensitive region targeting the $H \rightarrow c\bar{c}$ decay is referred to as the Hcc category.

This paper updates previous results presented in Refs. [18, 22, 38], which used the same data sample as the present analysis, with several improvements: better reconstruction and calibration of leptons and jets, an improved flavour tagging algorithm that combines b- and c-jet identification and has a more precise calibration, extended acceptance for the WH process to events with $p_{\mathrm{T}}^V < 150$ GeV, re-optimisation of

multivariate discriminants and first application to the $H \rightarrow b\bar{b}$ boosted regime and $H \rightarrow c\bar{c}$ search, updated theoretical predictions, updated definition of signal and control regions and increased granularity of STXS measurements both at high transverse momentum and as a function of jet multiplicity.

2 ATLAS detector

The ATLAS detector [41] at the LHC covers nearly the entire solid angle around the collision point.[1] It consists of an inner tracking detector surrounded by a thin superconducting solenoid, electromagnetic and hadron calorimeters, and a muon spectrometer incorporating three large superconducting air-core toroidal magnets.

The inner-detector system (ID) is immersed in a 2 T axial magnetic field and provides charged-particle tracking in the range of $|\eta| < 2.5$. The high-granularity silicon pixel detector covers the vertex region and typically provides four measurements per track, the first hit normally being in the insertable B-layer (IBL) installed before Run 2 [42, 43]. It is followed by the SemiConductor Tracker (SCT), which usually provides eight measurements per track. These silicon detectors are complemented by the transition radiation tracker (TRT), which enables radially extended track reconstruction up to $|\eta| = 2.0$. The TRT also provides electron identification information based on the fraction of hits (typically 30 in total) above a higher energy-deposit threshold corresponding to transition radiation.

The calorimeter system covers the pseudorapidity range $|\eta| < 4.9$. Within the region $|\eta| < 3.2$, electromagnetic calorimetry is provided by barrel and endcap high-granularity lead/liquid-argon (LAr) calorimeters, with an additional thin LAr presampler covering $|\eta| < 1.8$ to correct for energy loss in material upstream of the calorimeters. Hadron calorimetry is provided by the steel/scintillator-tile calorimeter, segmented into three barrel structures within $|\eta| < 1.7$, and two copper/LAr hadron endcap calorimeters. The solid angle coverage is completed with forward copper/LAr and tungsten/LAr calorimeter modules optimised for electromagnetic and hadronic energy measurements respectively.

The muon spectrometer (MS) comprises separate trigger and high-precision tracking chambers measuring the deflection of muons in a magnetic field generated by the superconducting air-core toroidal magnets. The field integral of the toroids ranges between 2.0 and 6.0 T m across most of the detector. Three layers of precision chambers, each consisting of layers of monitored drift tubes, cover the region $|\eta| < 2.7$, complemented by cathode-strip chambers in the forward region, where the background is highest. The muon trigger system covers the range $|\eta| < 2.4$ with resistive-plate chambers in the barrel, and thin-gap chambers in the endcap regions.

The luminosity is measured mainly by the LUCID–2 [44] detector that records Cherenkov light produced by the quartz windows of photomultipliers located close to the beam pipe.

Events are selected by the first-level trigger system implemented in custom hardware, followed by selections made by algorithms implemented in software in the high-level trigger [45]. The first-level trigger accepts

---

[1] ATLAS uses a right-handed coordinate system with its origin at the nominal interaction point (IP) in the centre of the detector and the z-axis along the beam pipe. The x-axis points from the IP to the centre of the LHC ring, and the y-axis points upwards. Polar coordinates (r, ϕ) are used in the transverse plane, ϕ being the azimuthal angle around the z-axis. The pseudorapidity is defined in terms of the polar angle θ as $\eta = -\ln\tan(\theta/2)$ and is equal to the rapidity $y = \frac{1}{2}\ln\left(\frac{E+p_z}{E-p_z}\right)$ in the relativistic limit. Angular distance is measured in units of $\Delta R \equiv \sqrt{(\Delta y)^2 + (\Delta \phi)^2}$.

events from the 40 MHz bunch crossings at a rate below 100 kHz, which the high-level trigger further reduces to record events to disk at about 1 kHz.

A software suite [46] is used in data simulation, in the reconstruction and analysis of real and simulated data, in detector operations, and in the trigger and data acquisition systems of the experiment.

3 Data and simulated event samples

The data were collected using triggers that require an electron, a muon or large missing transverse transverse momentum in the event. Events are selected for analysis only if they are of good quality and if all the relevant detector components are known to be in good operating condition [47]. The recorded events contain an average of 34 inelastic pp collisions per bunch-crossing.

Monte Carlo (MC) simulated events are used to model most of the backgrounds from SM processes and the VH, $H \to b\bar{b}, c\bar{c}$ signal processes. A summary of all the generators used for the simulation of the signal and background processes is given in Table 1. In an update over the previous results [18, 22, 38], the V+jets and $qq \to VV$ diboson processes are now modelled using the SHERPA 2.2.11 generator, using the configuration described in Ref. [48]. These are multijet merged samples with next-to-leading-order (NLO) accuracy in the matrix element calculation. Virtual EW loop-terms are included at NLO accuracy for the V+jets and diboson processes. Furthermore, the default treatment of interference between the $t\bar{t}$ and Wt processes is now the diagram subtraction scheme [49] instead of the previously used diagram removal scheme [50], as it was found to give a better description of the data. Samples produced with alternative generators are used to estimate systematic uncertainties in the event modelling, as described in Section 7. All simulated processes are normalised using higher-order theoretical cross-section predictions and are generated to NLO accuracy at least, except for the $gg \to ZH$ and $gg \to VV$ processes, which are generated at leading-order (LO). For samples containing top-quarks or Higgs bosons, the EVTGEN 1.6.0 program [51] is used to model the decays of b- and c-hadrons.

All samples of simulated events are processed with the ATLAS detector simulation [89] based on GEANT4 [90]. The effects of multiple interactions in the same and nearby bunch crossings (pile-up) are modelled by overlaying minimum-bias events, simulated using the soft QCD processes of PYTHIA 8.186 with the A3 [91] set of tuned parameters (tune) and NNPDF2.3LO [92] parton distribution functions (PDFs).

4 Event reconstruction

Tracks measured in the inner detector are used to reconstruct interaction vertices [93], of which the one with the highest sum of squared transverse momenta of associated tracks is selected as the primary vertex of the hard interaction.

Electron candidates are reconstructed by matching ID tracks to clusters of energy deposited in the electromagnetic calorimeter. Electrons must have $p_T > 7$ GeV and $|\eta| < 2.47$. The associated track must have $|d_0|/\sigma_{d_0} < 5$ and $|z_0| \sin \theta < 0.5$ mm, where d_0 (z_0) is the transverse (longitudinal) impact parameter relative to the primary vertex and σ_{d_0} is the uncertainty in d_0. Candidates are identified with a likelihood method and must satisfy the 'loose' identification criteria and 'loose' isolation requirements as described

Table 1: Generators used for the simulation of the signal and background processes. If not specified, the order of the cross-section calculation refers to the expansion in the strong coupling constant (α_s). The acronyms ME, PS and UE stand for matrix element, parton shower and underlying event, respectively. ($\star$) The events are generated using the first PDF in the NNPDF3.0NLO set and subsequently reweighted to the PDF4LHC15NLO set [52] using the internal algorithm in Powheg Box v2. ($\dagger$) The NNLO(QCD)+NLO(EW) cross-section calculation for the $pp \rightarrow ZH$ process already includes the $gg \rightarrow ZH$ contribution. The $qq \rightarrow ZH$ process is normalised using the cross-section for the $pp \rightarrow ZH$ process, after subtracting the $gg \rightarrow ZH$ contribution. An additional scale factor is applied to the $qq \rightarrow VH$ processes as a function of the transverse momentum of the vector boson, up to $p_T^V = 1$ TeV, to account for electroweak (EW) corrections at NLO. This makes use of the VH differential cross-section computed with Hawk [53, 54]. Contributions from photon-quark processes are also included for $pp \rightarrow WH$ [55]. ($\ddagger$) For the diboson samples the cross-sections are calculated by the Monte Carlo generator at NLO accuracy in QCD.

Process	ME generator	ME PDF	PS and Hadronisation	UE tune	Cross-section order
Signal, mass set to 125 GeV and $b\bar{b}$ branching fraction to 58%					
$qq \rightarrow VH$	Powheg Box v2 [56] + GoSam [57]+ MiNLO [68, 69]	NNPDF3.0NLO $^{(\star)}$ [58]	Pythia 8.245 [59]	AZNLO [60]	NNLO(QCD)$^{(\dagger)}$+ NLO(EW) [61–67]
$gg \rightarrow ZH$	Powheg Box v2	NNPDF3.0NLO $^{(\star)}$	Pythia 8.245	AZNLO	NLO+ NLL [70–74]
Top quark, mass set to 172.5 GeV					
$t\bar{t}$	Powheg Box v2 [75]	NNPDF3.0NLO	Pythia 8.230	A14 [76]	NNLO+NNLL [77]
s-chan. single top	Powheg Box v2 [78]	NNPDF3.0NLO	Pythia 8.230	A14	NLO [79]
t-chan. single top	Powheg Box v2 [78]	NNPDF3.0NLO	Pythia 8.230	A14	NNLO [80]
Wt	Powheg Box v2 [81]	NNPDF3.0NLO	Pythia 8.230	A14	Approx. NNLO+NNLL [82]
Vector boson + jets					
V+jets	Sherpa 2.2.11 [83–85]	NNPDF3.0NNLO	Sherpa 2.2.11 [86, 87]	Default [88]	NNLO
Diboson					
$qq \rightarrow VV$	Sherpa 2.2.11	NNPDF3.0NNLO	Sherpa 2.2.11	Default	NLO$^{(\ddagger)}$
$gg \rightarrow VV$	Sherpa 2.2.2	NNPDF3.0NNLO	Sherpa 2.2.2	Default	NLO$^{(\ddagger)}$

in Ref. [94]. The electron energy is calibrated as described in Ref. [94]. The electron reconstruction, identification and trigger efficiencies in the simulation are corrected using comparisons with data [94].

Muon candidates are required to be reconstructed within the acceptance of the MS $|\eta| < 2.7$ and to have $p_T > 7$ GeV. They are further required to have $|d_0|/\sigma_{d_0} < 3$, and $|z_0| \sin\theta < 0.5$ mm. Muons are selected using a 'loose' quality criterion as described in Ref. [95] and a loose track isolation requirement. The muon momentum is calibrated as described in Ref. [96]. The muon reconstruction, identification and trigger efficiencies in the simulation are corrected using comparisons with data [95].

Hadronically decaying τ-lepton candidates (τ_{had}) are reconstructed [97] in the range of $|\eta| < 2.5$ and $p_T > 20$ GeV and identified using a tagger based on a recurrent neural network that uses tracking and calorimeter information. The 'loose' working point as described in Ref. [98] is used. No attempt is made to distinguish between leptonically decaying τ-leptons and electrons or muons.

The lepton selections as described above are used to remove overlaps between physics objects (see below) and classify the events into 0-, 1- and 2-lepton channels, but more stringent requirements are made in the
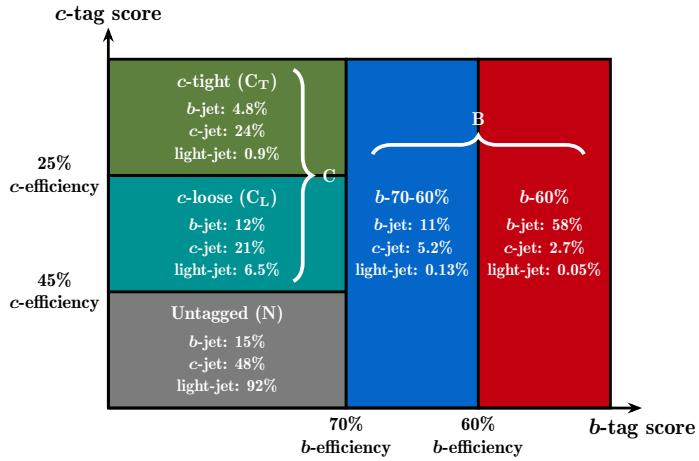
Figure 1: A schematic of the flavour tagging regions as used in the resolved regime. The efficiencies for the various jet flavours in the various regions are extracted from a simulated $t\bar{t}$ sample following the procedure detailed in Ref. [105].

1-lepton channel to suppress background from multijet processes: the quality is tightened to 'tight' for electrons and 'medium' for muons and 'HighPtCaloOnly' isolation is used for both lepton flavours [94, 95].

Small-R jets[2] are formed using objects from a particle-flow (PFlow) algorithm [99], which combines energy deposits in the calorimeter with inner detector tracks. The PFlow objects are combined into jets using the anti-k_t algorithm [100, 101] with a radius parameter $R = 0.4$. These jets are then initially calibrated to the particle level by applying a jet energy scale derived from simulation with in situ corrections based on the methodology derived in Ref. [102]. Central jets, i.e. those with $|\eta| < 2.5$, are required to have $p_T > 20$ GeV while forward jets ($2.5 < |\eta| < 4.5$) must satisfy the $p_T > 30$ GeV requirement. A jet-vertex-tagging technique using a multivariate likelihood [103, 104] is applied to central (forward) jets with $p_T < 60$ (120) GeV to suppress jets that are not associated with the event's primary vertex.

Simulated jets are labelled as b, c or τ_{had} by matching a b- or c-hadron or τ-lepton having $p_T \geq 5$ GeV within a cone of $\Delta R = 0.3$ [105] around the jet axis; the matching procedure prioritise b-hadrons over c-hadrons and τ-leptons, and c-hadrons over τ-leptons. Jets without a valid match are labelled as light (l) jets. The DL1r flavour tagger [105] computes for each jet the probability of containing a b-hadron, a c-hadron or being an l-jet (p_b, p_c, p_l); these probabilities are combined to define dedicated one-dimensional discriminant optimised to select b-jets (D_{DL1r}[3]) and c-jets (D^c_{DL1r}[4]). Central jets are then classified as either b-tagged, c-tagged or non-tagged in a scheme that is specifically designed for this analysis and is illustrated in Figure 1.

Any jet that satisfies the 70% b-tagging operating point of the D_{DL1r} discriminant (b-70%) [105] is classified as b-tagged. Jets that do not fall into this category are classified as c-tagged if they satisfy the a D^c_{DL1r} discriminant working point designed to have a 45% efficiency for c-jets. All other jets are classified as non-tagged. Jets that are c-tagged are further subdivided into loose and tight categories. In the $t\bar{t}$ simulation the fraction of b, c, l, and τ_{had} jets that satisfy the b-tagging selection is 69%, 8%, 0.2%,

---

[2] Unless explicitly stated the term 'jet' refers to small-R jets.
[3] $D_{DL1r} = \ln\left(p_b/(f_c \cdot p_c + (1 - f_c) \cdot p_l)\right)$ with $f_c = 0.018$.
[4] $D^c_{DL1r} = \ln\left(p_c/(f_b \cdot p_b + (1 - f_b) \cdot p_l)\right)$ with $f_b = 0.3$.

and 2.2% respectively. The corresponding fractions that satisfy the exclusive loose c-tagging selection are 11%, 21%, 7%, and 19% respectively, while those that satisfy the tight are 5%, 24%, 1%, and 20% respectively. A tighter 60% b-tagging working point is also used in the multi-variate analysis (MVA) as described in Section 6. The tagging efficiencies are measured with a data-driven method following the approaches described in Refs. [106–108] and the results are used to correct the simulation.

Large-R jets are formed from topological clusters of energy depositions [109] clustered with the anti-k_t algorithm with $R = 1.0$. They are trimmed [110, 111] to mitigate the effects of pile-up and soft radiation. The jet mass m_J is computed using tracking and calorimeter information and calibrated following the technique described in Ref. [112]. Such jets are required to have $p_T > 250$ GeV, $|\eta| < 2.0$ and a mass larger than 50 GeV. Track-jets with $p_T > 10$ GeV are used to identify the $H \to b\bar{b}$ decay within the large-R jet [22]. Track-jets are built with the anti-k_T algorithm with a variable radius (VR) p_T-dependent parameter, from tracks reconstructed in the ID [113–115]. Track-jets are ghost associated [116] to large-R jets. In a similar manner to small-R jets, the DL1r algorithm is used to b-tag track-jets. For the 85% working point chosen for the definition of the Higgs boson candidate, the fraction of b-, c- and l-track-jets that satisfy the b-tag selection in the $t\bar{t}$ simulation is 85%, 34% and 2% respectively. Tighter working points at 77%, 70% and 65% are used in the MVA. The tagging efficiencies are measured in a similar way to small-R jets.

To maximise the statistical power of the available MC samples, the tagging requirement is not applied to the V+ jets and s- and t-channel single-top-quark samples, or to the $t\bar{t}$ and Wt samples in just the boosted regime. Instead, events are weighted by the probabilities for each jet to fall into a given tagging category. The probabilities are extracted with a neutral network approach [117], which considers the flavour label and the kinematics of every jet in the event. In the Hcc category all jets are considered in the calculation of the event weight, while only light and c-jets are used in the Hbb category. This approach improves the simple jet-based parameterisation used in Ref. [38] since it is capable of directly capturing the dependency of the tagging efficiency on nearby jet activity.

Further corrections are applied to the four-momentum of the large-R jet or pair of small-R jets used to build the Higgs boson candidate to account for semileptonic decays of b- and c-hadrons and the different energy response of b-jets and c-jets compared with l-jets. Muons, before imposing the isolation requirement, that are within a p_T dependent ΔR cone[5] of the (track-) jet axis, are added to the jet four-momentum for both jet types [22, 118, 119] if the jets are b- or c-tagged. An additional MC-based correction is applied for small-R b-tagged jets to correct to the truth level using a similar method to Ref. [118]; a separate correction is applied to jets with and without an associated muon. In the 2-lepton channel, additional techniques are employed to improve the resolution on the reconstructed Higgs boson candidate mass (m_H). A per-event kinematic likelihood fit [118], primarily exploiting the excellent energy and momentum resolution of electrons and muons, is adopted for the boosted regime and events in the resolved regime with less than four jets. Finally in the resolved regime, if an additional central jet is sufficiently close to both of the two jets forming the Higgs boson candidate, the four-momentum of such a jet is added to the Higgs boson four-momentum H, to compute its invariant mass and other related quantities. The proximity criteria for the sum of the ΔR values between the jet and each of the two Higgs boson candidate jets, is optimised as a function of the reconstructed vector-boson p_T and varies between 2.85 at $p_T^V = 75$ GeV and 0.91 at $p_T^V = 400$ GeV. This procedure is referred to as final state radiation (FSR) recovery and aims at minimising the effect of hard QCD radiation of heavy quarks in the Higgs boson candiate reconstruction. The additional jet employed in this approach is not included in the jet multiplicity calculation. The combined effect of all these dedicated techniques improve the Higgs boson mass resolution by up to 12% in the 0-lepton and 1-lepton channels and by up to 40% in the 2-lepton channel.

---

[5] The cone size is optimised as a function of the reconstructed muon p_T as $\Delta R = \min\left(0.4, 0.04 + 10/(p_T \text{ [GeV]})\right)$

An overlap removal procedure is applied to avoid any double-counting between electrons, muons, τ_{had} candidates and jets. In the boosted regime, any small-R jet within a cone of $\Delta R = 1.0$ of the large-R jet axis is removed.

The missing transverse momentum, $\mathbf{E}_{\text{T}}^{\text{miss}}$, is reconstructed in each event as the negative vector sum of the transverse momenta of electrons, muons, τ_{had}s, jets, and a 'soft-term'. The soft-term is calculated as the vectorial sum of the p_{T} of tracks matched to the primary vertex but not associated with a reconstructed lepton or jet [120]. The magnitude of $\mathbf{E}_{\text{T}}^{\text{miss}}$ is referred to as $E_{\text{T}}^{\text{miss}}$.

The four-momentum of the vector-boson (V) is equivalent to $\mathbf{E}_{\text{T}}^{\text{miss}}$ in the 0-lepton channel. In the 1-lepton channel it is reconstructed as vector sum of the lepton and the neutrino where the transverse component of the neutrino momentum is identified with $\mathbf{E}_{\text{T}}^{\text{miss}}$ and the longitudinal component is obtained by applying a W mass constraint to the lepton-neutrino system. In the 2-lepton channel V is reconstructed from the two-lepton system. The transverse momentum of V is denoted by p_{T}^V.

5 Event selection and categorisation

5.1 Event selection

The events are classified into three channels depending on the number of charged leptons. 0-lepton events contain no electrons, muons or τ_{had} candidates. Events in the 1-lepton channel contain exactly one electron, muon or τ_{had} candidate. The electron or muon must fulfil the stricter lepton selection described in Section 4. Events in the 2-lepton channel have exactly two electrons or two muons. Since the signal-to-background ratio increases with p_{T}^V, the analysis focuses on the high p_{T}^V phase space: $\geq 150\,\text{GeV}$ in the 0-lepton channel and $\geq 75\,\text{GeV}$ in the 1- and 2-lepton channels. Jet cleaning criteria are used to identify jets arising from non-collision backgrounds or noise in the calorimeters, and events containing such jets are removed, using the 'tight cleaning' defined in Ref. [121].

Events are triggered either by the single electron, single muon or $E_{\text{T}}^{\text{miss}}$ triggers depending on the channel and p_{T}^V. Events with one or two electrons are collected with the single electron triggers [122]; for these events at least one electron must have an offline p_{T} greater than 27 GeV to ensure a high trigger efficiency. The single muon triggers [123] together with an offline muon requirement of $p_{\text{T}} > 25\,\text{GeV}$ are used for the 1-lepton muon sub-channel for $p_{\text{T}}^V < 150\,\text{GeV}$ and the 2-lepton muon sub-channel for $p_{\text{T}}^V < 250\,\text{GeV}$. The $E_{\text{T}}^{\text{miss}}$ triggers [124] are used for the 0-lepton channel, the 1-lepton τ sub-channel and at higher values of p_{T}^V in the 1- and 2-lepton muon sub-channels, where it becomes efficient because muons do not deposit much energy in the calorimeters. A requirement on the scalar sum of the transverse momenta of the jets, $H_{\text{T}} > 120\,(150)\,\text{GeV}$ for 2 (≥ 3) jet events, removes a region where the $E_{\text{T}}^{\text{miss}}$ trigger efficiency depends mildly on the number of jets in the event, corresponding to less than 1% of the phase space.

This section describes the main selection criteria for the signal regions (SRs). Most of the selections are also valid for the control regions (CRs), with any differences discussed in Section 5.2.

In the resolved Hbb category reconstruction, events must contain exactly two b-tagged jets (BB regions). These two jets are labelled j_1 and j_2 and define the Higgs boson candidate along with a possible FSR jet (see Section 4). Other jets in the event with $p_T > 30\,\text{GeV}$ are ordered in p_T and labelled j_i with $i > 2$. They are referred to in the following as 'additional jets'. Events in the Hcc category must contain at least one c-tagged jet and no b-tagged jets. The events are further separated into tight-tight ($C_{\text{T}}C_{\text{T}}$), tight-loose ($C_{\text{T}}C_{\text{L}}$) and tight-non-tagged ($C_{\text{T}}N$) categories. Loose-non-tagged ($C_{\text{L}}N$) events are used to
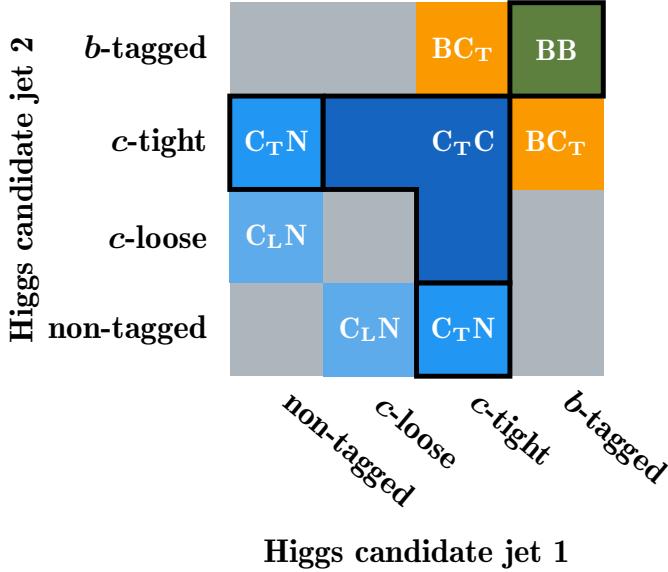
Figure 2: A representation of the analysis regions as defined by the tagging requirements for the Higgs boson jet candidates. The bold outline signifies the categories used in the SRs. The green regions are used in the Hbb category, the blue regions are used in the Hcc category, and the orange regions are used in the Top CRs, as defined in the text.

define dedicated CRs (see Section 5.2). The Higgs boson candidate jets j_1 and j_2 are the two c-tagged jets with the highest p_T or, for the $C_T N$ and $C_L N$ categories, the c-tagged jet and the leading non-tagged central jet. In the SRs, the $C_T C_T$ and $C_T C_L$ categories are combined into a $C_T C$ category and the flavour tagging scores of the jets are used in the boosted-decision-tree (BDT) training to further improve the signal-to-background separation as explained in Section 6. A further category, in which the event contains a b-tagged jet and a tight c-tagged jet (BC_T), is used to define a CR as described below. A representation of the various analysis regions as a function of the tagging requirements for the Higgs boson jet candidates is shown in Figure 2.

The resolved regimes require $m_H > 50$ GeV and the angular separation of the two Higgs boson candidate jets $\Delta R(j_1, j_2) < \pi$; the leading jet of the pair is further required to have $p_T > 45$ GeV.

In the boosted Hbb regime the Higgs boson is reconstructed from the large-R jet with the highest p_T. This jet must have $m_J > 50$ GeV and at least two matched track-jets. Exactly two of the three leading matched track-jets ordered in p_T must be b-tagged and are labelled j_1 and j_2 with the remaining track-jet labelled j_3 if present.

A dedicated event selection is then applied in each lepton channel with the aim to profit from the particular event topology to reduce key background contributions; the selection is optimised independently for the resolved and boosted regimes.

0-lepton channel: High E_T^{miss} in multijet events typically arises from mismeasured jets in the calorimeters; such events are efficiently removed by requirements on: the minimum azimuthal difference between $\mathbf{E}_T^{\mathrm{miss}}$ and any jet min $[\Delta\phi(\mathbf{E}_T^{\mathrm{miss}}, j_i)] > 20°$ (30°) for 2 jet (≥ 3 jet and boosted) events; the azimuthal difference between $\mathbf{E}_T^{\mathrm{miss}}$ and H, $\Delta\phi(\mathbf{E}_T^{\mathrm{miss}}, H) > 120°$; and the azimuthal difference between the two jets forming the Higgs boson candidate in the resolved category $\Delta\phi(j_1, j_2) < 140°$. Events with greater than two (one) additional jets are rejected in the Hbb (Hcc) resolved regime to reduce the top-quark background.

1-lepton channel: In the electron sub-channel an additional selection of $E_T^{miss} > 30$ (50) GeV is applied in the resolved (boosted) regime to reduce the background from multijet production; for similar reasons, the W boson transverse mass,[6] m_T^W, is requested to be larger than 20 GeV in events with $p_T^V < 150$ GeV. Multijet background in the τ sub-channel is suppressed using the same azimuthal requirements as in the 0-lepton channel, in addition to $m_T^W > 10$ GeV. Events with greater than one additional jet in the resolved regime are rejected to reduce top-quark background.

2-lepton channel: The invariant mass of the lepton pair ($m_{\ell\ell}$) must be close to the Z boson mass (81 GeV $< m_{\ell\ell} < 101$ GeV for the resolved regime and 66 GeV $< m_{\ell\ell} < 116$ GeV for the boosted regime). In di-muon events, the two muons are required to have opposite-sign charge. This requirement is not used in the electron sub-channel, where the charge misidentification rate is not negligible.

5.2 Event categorisation

Events are categorised according to the number of b- and c-tagged jets, the value of p_T^V and, in the resolved regime, the number of additional jets. Regions at larger p_T^V and those with no additional jets have higher signal purity. The Hcc category is split into regions of p_T^V with boundaries 75, 150 and 250 GeV. The Hbb category has additional p_T^V boundaries at 400 and 600 GeV where the boosted reconstruction is used. In the 2-lepton resolved regime, which can have larger jet multiplicities (defined as two more than the number of additional jets) than the other channels, regions with at least four (three) jets are combined in the Hbb (Hcc) category.

Events are divided into the SRs, which contain most of the signal events and several CRs, which are defined by changing exactly one selection criterion of the SR, such that they are orthogonal and extrapolations to the SR are small. The CRs are designed to control the contribution of specific backgrounds and allow theoretical uncertainties in the background predictions to be reduced.

A graphical summary of the analysis regions is given in Figure 3 and their composition is discussed in detail in Section 7.

Signal region events are defined with different criteria for the resolved and boosted regimes. The resolved SRs are defined using a continuous selection on $\Delta R(j_1, j_2)$, as a function of p_T^V following a procedure similar to that described in Ref. [38], but reoptimised for the present analysis. An upper requirement on $\Delta R(j_1, j_2)$ that depends also on jet multiplicity is designed to retain 95% (85%) of the signal in the SRs with exactly two (at least three) jet SRs. In the 1-lepton channel of the Hbb category, a lower limit on $\Delta R(j_1, j_2)$ is also applied to retain 90% of the diboson background in the SRs. This requirement ensures little signal loss, while retaining a large fraction of the diboson events that are used to validate the analysis (see Section 9). In the 0-and 1-lepton channels in the Hbb category the top-quark background is further reduced by rejecting the event if any additional jet is tight c-tagged. In the boosted regime, the events are required to have no b-tagged track-jet outside the large-R jet in order to reduce the top-quark contribution.

The $H \to c\bar{c}$ contamination in the Hbb category is negligible, while the expected $H \to b\bar{b}$ yield in the C_TC (C_TN) SRs of the $H \to c\bar{c}$ category is approximately 1.5 (1.9) times that of the expected $H \to c\bar{c}$ process. Due to the different tagging requirement, the Hbb and Hcc categories are not orthogonal for events with

---

[6] $m_T^W = \sqrt{2p_T^\ell p_T^\nu(1 - \cos(\phi^\ell - \phi^\nu))}$, where p_T^ℓ and ϕ^ℓ are the transverse momentum and azimuthal angle of the charged lepton and the corresponding quantities for the neutrino, p_T^ν and ϕ^ν, are reconstructed from $\mathbf{E}_T^{miss}$.
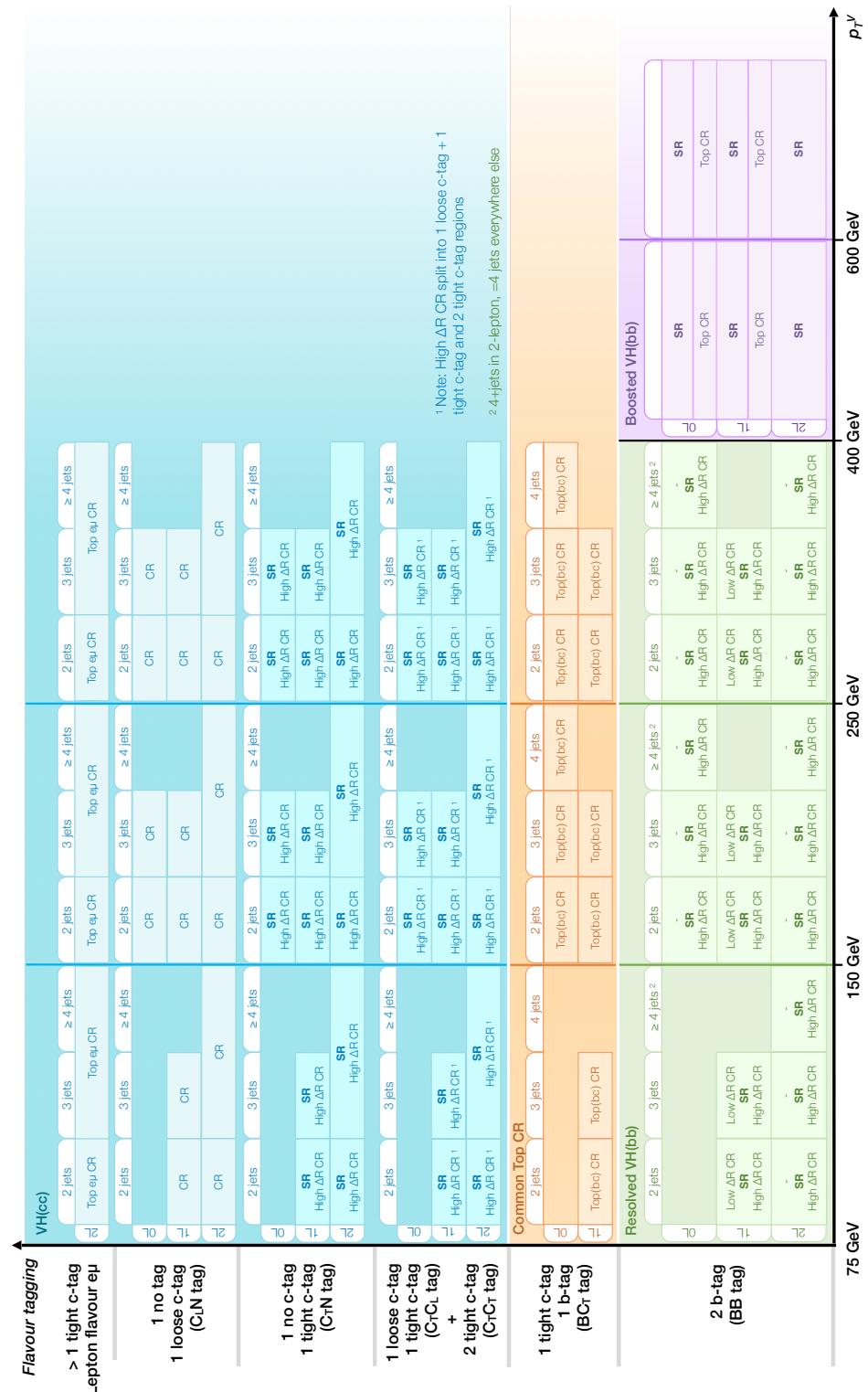
Figure 3: A schematic view of all the signal and control regions used in the analysis. The green regions are used in the Hbb category, the blue regions are used in the Hcc category, and the orange regions are used in the Top CRs, as defined in the text.

$p_T^V > 400\,$GeV. The VH, $H \to c\bar{c}$ signal (data) events selected by the boosted Hbb regime represents at most 1.9% (0.4%) of the total amount of VH, $H \to c\bar{c}$ signal (data) events selected in the Hcc category. This overlap has a negligible impact on the results.

High-ΔR control regions are defined by considering events with $\Delta R(j_1, j_2)$ above the upper boundary (see above). Such CRs are designed to have a similar composition of $V+$jets backgrounds to the SR and also serve to constrain the top-quark background. In the Hcc category $C_T C_T$ events are considered in separate regions from $C_T C_L$ events in order to better constrain different $V+$jets flavour components as discussed in Section 7.

BB Low-ΔR control regions are formed from 1-lepton Hbb resolved events that are below the lower boundary in $\Delta R(j_1, j_2)$. The CRs are dominated by $t\bar{t}$ and $W+$jets backgrounds with an enhanced contribution of $W+$jets with respect to the SRs and High-ΔR CRs.

C_LN $V+$light control regions mimic the Hcc SRs but consist of events in which one of the Higgs boson candidate jets is a loose c-tagged and the other is non-tagged. These CRs are use to constrain the backgrounds where a W or Z boson is associated with light jets. This background is primarily relevant in the Hcc category. These regions replace the previously 0 c-tag region used in Ref. [38].

BC_T Top control regions in the 0- and 1-lepton channels are defined with at least one tight c-tagged jet and at least one b-tagged jet and are used to constrain the top-quark background in the resolved regime. This CR targets the top-quark process where a b-jet and a c-jet from the same hadronically decaying top-quark are considered as a Higgs boson candidate.

Boosted Top control regions in the 0- and 1-lepton are defined by using the same SRs selection on the large-R jet, but requiring the presence of a b-tagged track-jet in the rest of the event. This CR enhances the fraction of $t\bar{t}$ events by effectively targeting events with two b-tagged jets with large angular separation.

Top eμ control regions are defined for the resolved regime by using the same selection as the SR but replacing the same-flavour lepton selection with a selection containing an electron and a muon in order to significantly increase the fraction of top-quark events. In the Hbb category, the $e\mu$ CRs directly provides the background prediction for the top-quark background in a data-driven way. as it is detailed in Section 7. In the Hcc category this data-driven method is not used due to low statistics. Instead, the $e\mu$ CRs are used to provide a constraint on the normalisation of the MC-based predictions. The CRs are not split according to jet tagging so events must have at least one tight c-tagged jet.

5.3 Categorisation for the simplified template cross-section measurement

In the Hbb category, cross-section measurements are conducted in an extended version of the VH, $V \to$ leptons stage-1.2 STXS region scheme [125, 126]. In this scheme, $qq \to ZH$ and $gg \to ZH$ are treated as a single ZH process, since there is currently not enough sensitivity to distinguish between them. The expected signal distributions and acceptance times efficiencies for each STXS region are estimated from the simulated signal samples by selecting events using information from the generator's 'truth' record, in particular the truth p_T^V, denoted by $p_T^{V,t}$, and the number of truth-level jets with $p_T > 30\,$GeV and $|\eta| < 4.5$ (additional truth jets, N_{jet}^t) reconstructed from stable truth particles after excluding the Higgs boson decay products. The truth templates are categorised as a function of $p_T^{V,t}$ following the same p_T^V boundaries used in the definition of the SRs. Only for the ZH process with $p_T^{V,t} < 400\,$GeV, a further separation is performed to distinguish between events with zero or at least one additional truth jet. The
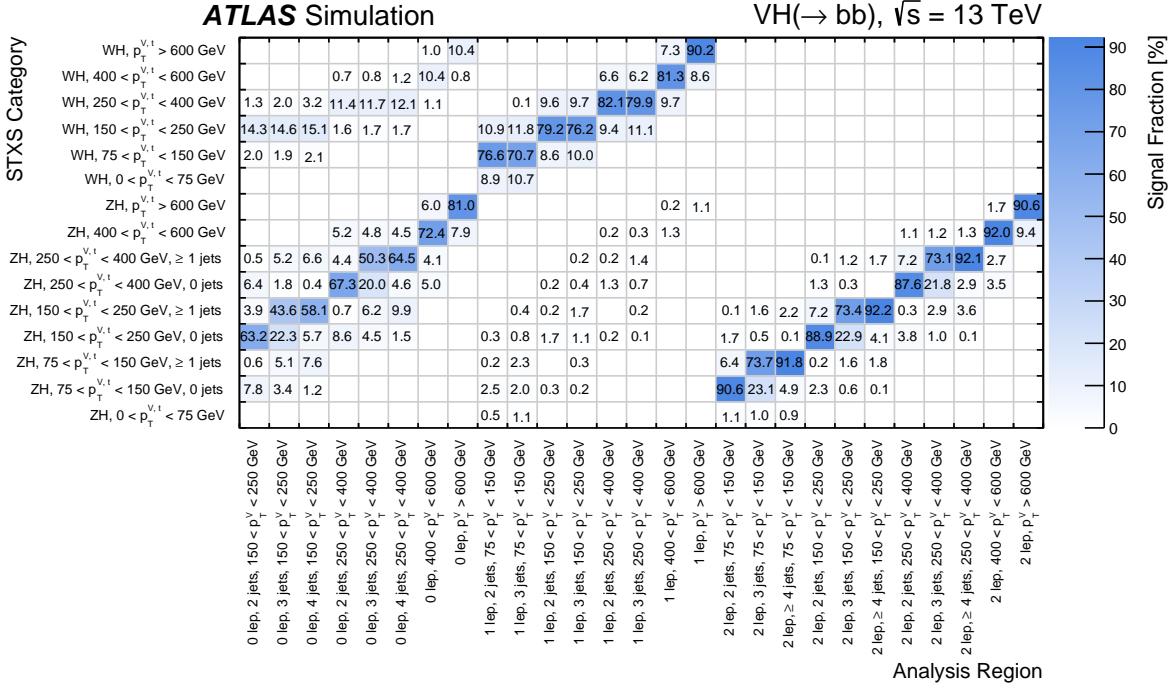
Figure 4: The predicted fraction of VH, $H \to b\bar{b}$ signal events passing all selection criteria (in percent) in every reconstructed-event category (x-axis) from each STXS category (y-axis). Entries with signal fractions below 0.1% are not shown.

choice is driven by the larger top-quark background in the 1-lepton channel in events with one additional jet. A set of measurements is also made without this split in jet multiplicity.

The fraction of events from each STXS category satisfying the requirements of the SRs of the Hbb category is shown in Figure 4. The correlation between 'truth' and reconstructed categories is improved with respect to the previous iteration of the analysis thanks to the dedicated treatment of the τ sub-channel, which reduces the WH contribution in the 0-lepton channel, and the increase in the p_T requirement from 20 to 30 GeV for the additional reconstructed central jets to align the definition with the targeted STXS observable.

6 Multivariate discriminants

A multivariate approach is used to maximise the sensitivity of the analysis. Several BDTs are used in the various signal regions of the analysis. A nominal set, referred to as BDT_{VH}, is designed to discriminate the VH signal from the background processes. A second set, BDT_{VZ}, which aims to separate the VZ diboson process from the VH signal and other background processes, is used to measure the WZ and ZZ processes, which serve as a validation of the analysis. Finally, in the 1-lepton channel Low-ΔR CR for the resolved Hbb category, additional BDTs are trained to separate the V+jets events from the other background, which is dominated by top-quark production, called $\mathrm{BDT}_{\text{Low-}\Delta R\,\text{CR}}$.

BDTs are generally trained separately for each SR but to reduce complexity, resolved SRs with ≥ 3 jets, or with $p_\mathrm{T}^V < 150\,\mathrm{GeV}$ or with $p_\mathrm{T}^V > 150\,\mathrm{GeV}$ are trained together. The same training procedures as those detailed in Ref. [18] are used.

The BDT input variables are listed in Table 2 and briefly discussed below. Different sets of variables are used for the 0-, 1- and 2-lepton channels in resolved and boosted regimes, but the Hcc category and Hbb category resolved channels use the same variables. The $\mathrm{BDT}_{\text{Low-}\Delta R\,\mathrm{CR}}$ uses the same variables as the 1-lepton resolved Hbb category. Variables are only included in the training if they improve the overall sensitivity. The distributions of all input variables of the BDTs are compared between data and simulation, and good agreement is found within the uncertainties.

The reconstructed Higgs boson mass m_H is the most discriminating variable, since no backgrounds peak at the same mass value. In the resolved channel the three jet system $m_{j_1 j_2 j_3}$ is used to reconstruct signal with FSR that does not satisfy the FSR criteria described in Section 5. The transverse momenta of the tagged jets or track-jets $p_\mathrm{T}^{j_1}$ and $p_\mathrm{T}^{j_2}$ are used together with the scalar sum of additional jets with $p_T > 20\,\mathrm{GeV}$ in the resolved channel, $\sum p_\mathrm{T}^{j_i}$ with $i > 2$, or the third track-jet $p_\mathrm{T}^{j_3}$ in the boosted regime. Flavour tagging information for j_1 and j_2 is taken into account by using the binned output of the D_{DL1r} tagging algorithm $\mathrm{bin}_{D_{\mathrm{DL1r}}}(j_1)$ and $\mathrm{bin}_{D_{\mathrm{DL1r}}}(j_2)$, with bin boundaries as listed in Section 4. All channels use p_T^V, which is equivalent to $E_\mathrm{T}^{\mathrm{miss}}$ in the 0-lepton channel. The 1-lepton channel uses $E_\mathrm{T}^{\mathrm{miss}}$ as an additional variable. In the 2-lepton resolved channel, where the signal does not have significant $E_\mathrm{T}^{\mathrm{miss}}$, the variable $E_\mathrm{T}^{\mathrm{miss}}/\sqrt{S_\mathrm{T}}$ is used, where S_T is the scalar sum of H_T and the p_T of the two leptons.

Angular variables include $\Delta R(j_1, j_2)$ and the minimum separation between either of the Higgs boson candidate jets and any other jet, $\min[\Delta R(j_i, j_1 \text{ or } j_2)]$ with $i > 2$, and the azimuthal and rapidity difference between the reconstructed Higgs boson and vector boson vectors, $|\Delta\phi(V, H)|$ and $|\Delta y(V, H)|$ respectively.

Variables that are used in all lepton channels of the boosted regime are the total number of track-jets in the Higgs boson candidate jet, the number of additional small-R jets in the event and 'colour ring', which is a variable designed to exploit the difference in colour-flow between gluon splitting and a decay from QCD singlet states [127]. Two variables are only used in the 0-lepton resolved channel: the pseudorapidity difference between the Higgs boson candidate jets $|\Delta\eta(j_1, j_2)|$ and the sum of H_T and $E_\mathrm{T}^{\mathrm{miss}}$. Variables that are only used in the 1-lepton resolved channel are m_T^W, and the reconstructed top-quark mass assuming the event contains a top-quark, m_{top} [18]. The transverse momentum of the lepton p_T^ℓ and $(p_\mathrm{T}^\ell - E_\mathrm{T}^{\mathrm{miss}})/p_\mathrm{T}^V$, which is a proxy for the W boson's lepton p_T asymmetry, are only used in the 1-lepton boosted channel. The dilepton mass $m_{\ell\ell}$ is used in the 2-lepton resolved channel and $\cos\theta^*(\ell^-, V)$, which is calculated using the lepton direction in the Z boson rest frame and the flight direction of the Z boson in the laboratory frame, is used both in the 2-lepton resolved and boosted regimes.

Table 2: Variables used for the multivariate discriminant in each of the channels. The ✓ symbol indicates the inclusion of a variable. The $\mathrm{BDT}_{\text{Low-}\Delta R\,\text{CR}}$ uses the same variables as the 1-lepton resolved Hbb category as described in the text.

Variable	Resolved VH, $H \to b\bar{b}, c\bar{c}$			Boosted VH, $H \to b\bar{b}$		
	0-lepton	1-lepton	2-lepton	0-lepton	1-lepton	2-lepton
m_H	✓	✓	✓	✓	✓	✓
$m_{j_1 j_2 j_3}$	✓	✓	✓			
$p_{\mathrm{T}}^{j_1}$	✓	✓	✓	✓	✓	✓
$p_{\mathrm{T}}^{j_2}$	✓	✓	✓	✓	✓	✓
$p_{\mathrm{T}}^{j_3}$				✓	✓	✓
$\sum p_{\mathrm{T}}^{j_i}, i > 2$	✓	✓	✓			
$\mathrm{bin}_{D_{\mathrm{DL1r}}}(j_1)$	✓	✓	✓	✓	✓	✓
$\mathrm{bin}_{D_{\mathrm{DL1r}}}(j_2)$	✓	✓	✓	✓	✓	✓
p_{T}^{V}	$\equiv E_{\mathrm{T}}^{\mathrm{miss}}$	✓	✓	$\equiv E_{\mathrm{T}}^{\mathrm{miss}}$	✓	✓
$E_{\mathrm{T}}^{\mathrm{miss}}$	✓	✓		✓	✓	
$E_{\mathrm{T}}^{\mathrm{miss}}/\sqrt{S_{\mathrm{T}}}$			✓			
$|\Delta\phi(\boldsymbol{V},\boldsymbol{H})|$	✓	✓	✓	✓	✓	✓
$|\Delta y(\boldsymbol{V},\boldsymbol{H})|$		✓	✓		✓	✓
$\Delta R(\boldsymbol{j_1},\boldsymbol{j_2})$	✓	✓	✓	✓	✓	✓
$\min[\Delta R(\boldsymbol{j_i},\boldsymbol{j_1} \text{ or } \boldsymbol{j_2})], i > 2$	✓	✓				
$N(\text{track-jets in } J)$				✓	✓	✓
$N(\text{add. small-}R \text{ jets})$				✓	✓	✓
colour ring				✓	✓	✓
$|\Delta\eta(\boldsymbol{j_1},\boldsymbol{j_2})|$	✓					
$H_{\mathrm{T}} + E_{\mathrm{T}}^{\mathrm{miss}}$	✓					
m_{T}^{W}		✓				
m_{top}		✓				
$\min[\Delta\phi(\boldsymbol{\ell},\boldsymbol{j_1} \text{ or } \boldsymbol{j_2})]$		✓				
p_{T}^{ℓ}					✓	
$(p_{\mathrm{T}}^{\ell} - E_{\mathrm{T}}^{\mathrm{miss}})/p_{\mathrm{T}}^{V}$					✓	
$m_{\ell\ell}$			✓			
$\cos\theta^*(\boldsymbol{\ell^-},\boldsymbol{V})$			✓			✓

Figure 5: The relative background composition in the signal and control regions with (a) $150\,\text{GeV} < p_{\text{T}}^V < 250\,\text{GeV}$ in the 0-lepton channel and (b) $250\,\text{GeV} < p_{\text{T}}^V < 400\,\text{GeV}$ in the 1-lepton channel. The ratio of the data to the total signal-plus-background (S+B) prediction is also shown. The background predictions are adjusted with the results of the VH fit to data described in Section 9 and the uncertainty band corresponds to the overall uncertainty in the background predictions.

7 Background predictions

The leading backgrounds affecting the analysis are $t\bar{t}$ and $V+$ jets production. Subleading contributions arise from single top-quark production, multijet production and diboson production (VV); for the latter case, the production of a vector boson and a Z boson (VZ) decaying into $b\bar{b}$ or $c\bar{c}$ represent a process with similar topology to the VH signal and is used to validate the analysis methodology.

Simulated event samples, which are summarised in Section 3, are used to model all background processes except for the $t\bar{t}$ background in the Hbb 2-lepton resolved channel and the multijet background in the 1-lepton channel, which are both estimated by using data-driven techniques. In the following, a brief overview of the composition of the leading backgrounds and the techniques used to estimate them is given.

The detailed composition of background processes varies greatly across signal and control regions. Examples of the background composition in a representative p_{T}^V intervals for each of the three lepton channels are shown in Figures 5 and 6.

$V+$ jets: $V+$ jets is a major background in all the SRs and its relative importance increases with p_{T}^V. The 2-lepton channel contribution is almost exclusively composed of $Z+$ jets events, while that of the 1-lepton channel is mostly $W+$ jet events. Both contributions are present in the 0-lepton channel with a predominance of $Z+$ jet events. Simulated MC events are categorised according to the flavours of j_1 and j_2: $V+lf$ when they are both light-flavour; $V+hf$ for cc and bb; mixed flavour ($V+mf$) for the remaining cases (cl, bl and bc). Events from the $V+bb$ process compose 85% to 95% of the $V+$ jets background in the resolved Hbb regions; the fraction drops to 50% in the boosted reconstruction regions due to the relaxed flavour

17
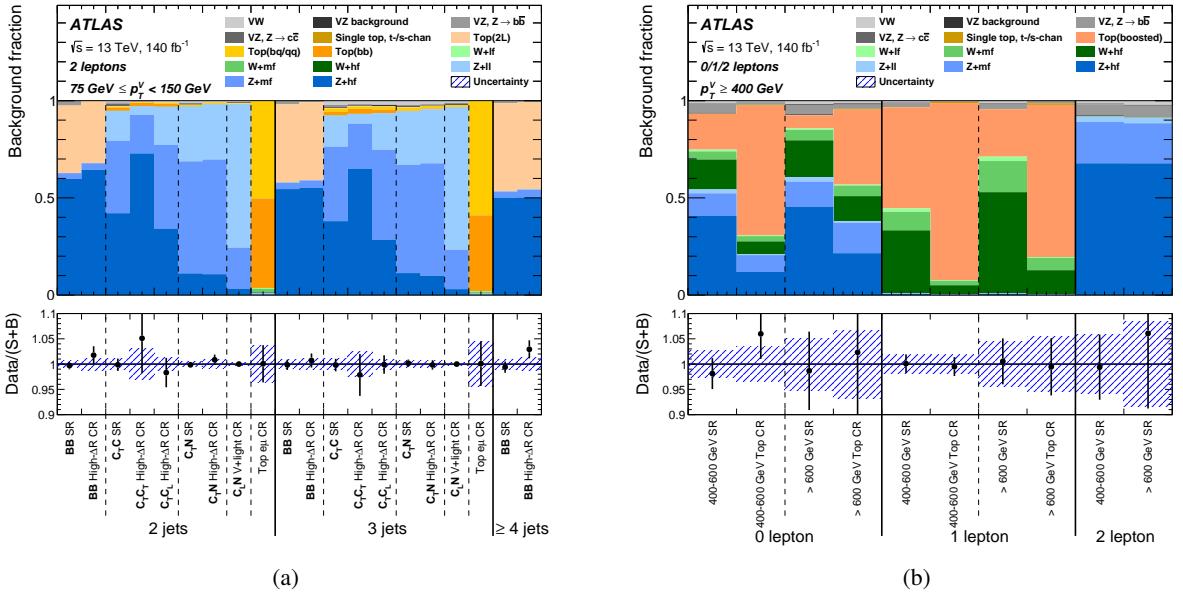
Figure 6: The relative background composition in the signal and control regions with (a) 75 GeV < p_T^V < 150 GeV in the 2-lepton channel and (b) all regions with p_T^V > 400 GeV. The ratio of the data to the total signal-plus-background (S+B) prediction is also shown. The background predictions are adjusted with the results of the VH fit to data described in Section 9 and the uncertainty band corresponds to the overall uncertainty in the background predictions.

tagging requirement.[7] In the Hcc category the flavour composition of V+ jets events is more diverse and strongly depends on the tagging requirements. In addition, the composition differs between W+ jets and Z+ jets processes due to W+c production, which significantly enhances the fraction of W+mf events. The C_TC SRs have a V+cc fraction of 30%–40% (15%–20%) for Z+ jets (W+ jets); the values roughly double in the C_TC_T High-ΔR CRs. Therefore, splitting the High-ΔR CR in C_TC_L and C_TC_T events provides better control of the V+ jets flavour composition. More than 60% of V+ jets events in the C_TN regions are populated by V+mf events; the composition is very consistent between SRs and High-ΔR CRs. Finally, C_LN CRs are dominated by V+lf events.

The normalisations of the V+hf, V+mf, and V+lf components in the resolved regime are free to float in the fits to data independently in different jet multiplicity (2-, or ≥ 3-jets) and p_T^V intervals. For Z+hf there are additional normalisation parameters for the regions with exactly three jets, to decouple the background normalisation between the 3-jet and ≥ 4-jet regions. In the boosted regime, V+hf and V+mf components are jointly free-floated in the two p_T^V ranges. The V+hf and V+mf components are constrained by the SRs, Low-ΔR and High-ΔR CRs, while the V+lf are constrained by the C_LN regions. In the 1-lepton channel of the resolved Hbb category, the W+hf normalisation constraints are significantly improved with the introduction of an MVA for the Low-ΔR CRs (BDT$_{\text{Low-}\Delta R\,\text{CR}}$) as described in Section 6. In comparison to a fit with only a single bin in the Low-ΔR CR, the uncertainty in the W+hf normalisation factor is reduced, in the 75 GeV < p_T^W < 150 GeV (150 GeV < p_T^W < 250 GeV) region by a factor of two (by 30%). In total, 42 free-floating normalisation factors are used in the fits to achieve an adequate V+ jets background model.

Top-quark background in 0- and 1-lepton channels: Top-quark processes represent the leading

---

[7] Approximately 15% of V+ jets events is V+cc in these regions.

background in several analysis regions of the 0-lepton and the 1-lepton channels; its contribution is more relevant in the Hbb category than in the Hcc ones, which have a veto on b-tagged jets. The relative contribution strongly increases with jet multiplicity and decreases as p_T^V increases.

The top-quark background primarily consists of $t\bar{t}$ production and Wt production, which are treated jointly given the very similar final state topology and to minimise the impact of interference effects. The relative fraction of Wt varies from 5% to 15% with increasing p_T^V in the Hbb category and from 15% to 20% in the Hcc category, depending on the tagging requirements. Single-top t-channel background is most relevant in the Hbb category of the 1-lepton channel, reaching almost 10% of the top-quark background in the low p_T^V SRs. The s-channel single-top process is negligible in all the analysis regions. The contributions of $t\bar{t}$ and Wt arise primarily from events where one of the W bosons decays leptonically and the other one hadronically; events enter the 0-lepton channel from cases where the lepton is not reconstructed, fails to meet the identification criteria or is outside the detector acceptance.

In a similar way as the V+jets background, top-quark backgrounds are categorised according to the truth flavour of j_1 and j_2. The top(bb) process primarily captures configurations where the Higgs boson candidate is built from the two b-jets from the top-quark decays.[8] The events are characterised by large values of m_H and $\Delta R(j_1, j_2)$ and represent the leading contribution in High-ΔR CRs of the Hbb category, while in the Hcc category the relative contribution reaches at most 15%. The top(bq) contribution describes configurations where the Higgs boson candidate is built from a b-jet and either a c- or light jet from the W boson decay; m_H is therefore bound by the top-quark mass and the event is more signal-like. The contribution increases with p_T^V and it represents up to 70% of the relative fraction of the total top-quark background in the SRs of both Hbb and Hcc categories a well as the BC$_T$ Top CRs; in the latter, the usage of m_{bc} as discriminating variable in the fits further contributes to isolating the contribution of this critical background. Finally, the top(qq) background captures events where the Higgs boson candidate is primarily built from jets from the hadronically decaying W boson; its contribution is negligible in the Hbb category, while it reaches up to 40% of the top-quark background for the loose tagging requirement regions in the Hcc category. In the boosted regime, the large-R jet naturally captures the full hadronic decay of the top-quark. In top(bq) events, particularly where one of the subjets is a c-jet, represent up to 85% of the total top-quark background contribution. The value is consistent between SRs and the Boosted Top CRs.

In the 0- and 1-lepton channels, separate free-floating normalisations are used for the top(bb) component and the combined top(bq) and top(qq) components, collectively referred to as the top($bq+qq$) component. The normalisation factors are further split depending on the jet multiplicity (2-, 3-, or 4-jet) and p_T^V intervals. In total, there are 18 free-floating normalisation factors for the top-quark background in the 0- and 1-lepton channels.

Top-quark background in 2-lepton channels: In the 2-lepton channels the top-quark background comes mainly from di-leptonic $t\bar{t}$ and Wt events. In the Hbb resolved category samples are defined in the data following a similar selection to the Top eμ CR described in Section 5. These samples have the same selection as the SRs but require an electron and a muon rather than two same-flavour leptons and are directly used as the background estimate. They provide very pure top-quark samples since most backgrounds and the signal are expected to contain same-flavour lepton pairs from a Z boson decay.

In the Hcc category, where the MC-based predictions are used, all components are correlated and there are five corresponding free-floating normalisation factors in the fits for the Hcc category, depending on p_T^V and jet multiplicity. Similarly for the boosted regime, since the top-quark background decreases rapidly with p_T^V and is small in this region, it is taken from MC simulation.

---

[8] The contribution of $t\bar{t}+hf$ is suppressed by the upper requirement on the jet multiplicity.

Diboson: Diboson production is comprised of the WW, WZ and ZZ processes and contributes primarily to the SRs. In the Hbb resolved category, the VZ, $Z \rightarrow b\bar{b}$ process contributes approximately to 90% of the overall diboson events; the fraction decreases to 60% for $p_T^V > 400\,\text{GeV}$ due the relaxed tagging requirement in the boosted reconstruction. In the Hcc category, the contribution from VZ, $Z \rightarrow c\bar{c}$ varies between 10% and 40% depending on the tagging requirements. The leading process is VW, $W \rightarrow cs$. The $Z \rightarrow b\bar{b}$ contamination in the Hcc category is always lower than 5% thanks to the excellent performance of the tagging algorithm, while the contribution from other hadronic Z-boson decays is only relevant in the $C_T N$ SRs.

Multijet: The production of events with multiple jets, multijet (MJ), has a large cross-section and thus, despite not being a source of genuine missing transverse momentum or prompt leptons, can contribute a non-negligible amount of background in the analysis regions. In the 1-lepton channel, the MJ background is estimated in each analysis region by performing a template fit to the m_T^W distribution, which offers discrimination between MJ and simulated backgrounds. The shape of the multijet template is evaluated from data using a dedicated CR, defined as the nominal event selection, except the strict lepton isolation requirement is inverted. Contributions from other backgrounds in this CR are estimated with simulation and subtracted. The MJ background was demonstrated to be negligible in both the 0- and 2-lepton channels and all boosted regions following the procedure decribed in Refs. [11, 22, 38].

8 Systematic uncertainties

The sources of systematic uncertainty can be broadly divided into three groups: those of an experimental nature, those related to the theoretical modelling of the backgrounds and those associated with the Higgs boson signal simulation. The estimation of the uncertainties builds upon the methodology outlined in Refs. [18, 22, 38] and is briefly summarised below. The breakdown of the systematic uncertainties and their impact on the signal strength extraction is shown in Section 10.

8.1 Experimental uncertainties

The dominant experimental uncertainties originate from the flavour-tagging performance, jet energy scale calibration and the modelling of the jet energy resolution.

The uncertainty in the flavour tagging correction factors (see Section 4) is decomposed into several orthogonal contributions. Additional simulation-based uncertainties are derived to cover the extrapolation to high-p_T regimes not covered by the data. Flavour-tagging uncertainties are treated as uncorrelated between small-R and VR track-jets.

For small-R jets, the uncertainties in the calibration of the energy scale and resolution, derived in Ref. [102], are correlated between different analysis regions. An additional uncertainty in the energy calibration of b- and c-jets is also included. An uncertainty is also assigned to the efficiency of the jet-vertex-tagging requirement on jets [103]. For large-R jets, the uncertainties in the energy and mass scales are based on a comparison of the ratio of calorimeter-based to track-based measurements in dijet data and simulation, as described in Ref. [112].

Uncertainties in the reconstruction, identification, isolation and trigger efficiencies of muons [95] and electrons [94] are considered, along with the uncertainty in their energy scale and resolution. The

uncertainties in the energy scale and resolution of the jets and leptons are propagated to the calculation of E_T^{miss}, which also has additional uncertainties from the modelling of the underlying event and momentum scale, momentum resolution and reconstruction efficiency of the tracks used to compute the soft-term [120]. A dedicated uncertainty in the E_T^{miss} trigger selection efficiency, derived from the comparison of data and simulation as explained in Refs. [18] and [38], is also included.

An uncertainty of 0.83% in the total integrated luminosity [128], obtained using the LUCID-2 detector [44] for the primary luminosity measurements and complemented by measurements using the inner detector and calorimeters, is assigned to physics processes whose normalisations are taken from simulation. An uncertainty arising from the correction of the pile-up distribution in simulation compared with that in data based on the measurement of the visible cross-section in minimum-bias events [129], is also considered.

8.2 Background uncertainties

Background modelling uncertainties for the simulated samples broadly cover three areas: absolute normalisation uncertainties; relative acceptance uncertainties that account for the relative normalisations between regions with a common floating normalisation factor; and shape uncertainties that account for uncertainties in the shapes of the different discriminants fit in the various regions, as listed in Table 3.

The BDT_S reweighting technique introduced in Ref. [18], is replaced by the neural-based Calibrated Likelihood Ratio Estimator (CARL) algorithm [130]. Utilising dense neural networks, the nominal and alternative (systematic variation) MC samples for a given physics process are used in a classification problem to train an optimal classifier, using the same kinematic variables as the ones used in the multivariate analysis described in Section 6. A transformation of the neural network output score is used to estimate the density ratio of the probability density functions for the alternative and nominal processes, as described in Ref. [131]. The CARL methodology then reweights the MC simulation to match the probability distribution of the alternative process. Due to the larger statistical sample size of the nominal dataset compared with the alternative, the reweighting process yields a pseudo estimate of the alternative MC prediction with higher statistical precision, thereby providing shape uncertainties that are less susceptible to statistical fluctuations.

V+jets production: The $V+$jets normalisation uncertainties and relative acceptance uncertainties are estimated by varying the renormalisation (μ_r) and factorisation (μ_f) scales by factors of 0.5 and 2.0, by varying the PDF, by varying the nominal scheme of the inclusion of the virtual NLO EW corrections compared with the NLO QCD corrections (*additive*) to alternative schemes (*multiplicative* and *exponentiated*), and by comparing the nominal SHERPA 2.2.11 sample to the alternative $V+$jets sample produced with MADGRAPH5_aMC@NLO+PYTHIA 8 [132] using FxFx merging [133]. The MADGRAPH5_aMC@NLO+PYTHIA 8 sample is produced with up to three additional partons at NLO accuracy and is described in more detail in Ref. [48]. All $V+$jets modelling uncertainties are treated as uncorrelated between $W+$jets and $Z+$jets processes.

Uncertainties are estimated for the relative normalisation of the heavy-flavour components that constitute the $V+hf$ and $V+mf$ backgrounds. These uncertainties account for the relative difference in the normalisation of the bb to cc, bl to bc, bl to cl, and bc to cl components, as a function of p_T^V and jet multiplicity. In the boosted regime, where $V+hf$ and $V+mf$ are floated coherently, additional uncertainties are also considered in the relative ratio of these components.

Relative acceptance uncertainties for the W+jets backgrounds are estimated for the ratio of the event yield in the 0-lepton channel to that in the 1-lepton channel. For the Z+jets backgrounds, there is a relative acceptance uncertainty in the ratio of the event yield in the 0-lepton channel to that in the 2-lepton channel. For both W+jets and Z+jets, relative acceptance uncertainties are estimated for the ratio of the event yield in the SR to that in the Low-ΔR and High-ΔR CRs. Furthermore, relative acceptance uncertainties are estimated for the ratio of the event yield between $400\,\text{GeV} < p_\text{T}^Z < 600\,\text{GeV}$ and $p_\text{T}^Z > 600\,\text{GeV}$ regions where there is a common Z+jets normalisation factor and for the 3-jet and 4-jet regions, which are covered by a common W+jets normalisation factor in the 0L Hbb category.

Shape uncertainties are estimated for the V+jets backgrounds using the CARL technique by reweighting the nominal SHERPA 2.2.11 sample to the alternative MADGRAPH5_AMC@NLO+PYTHIA 8 sample separately in two regions defined by the $\Delta R(j_1, j_2) = 1.0$ threshold.[9] The corrections obtained in the Low-ΔR CRs, which are sensitive to the modelling of the parton shower and the matching between matrix element and parton shower, are not necessarily applicable also to the High-ΔR CRs. Shape uncertainties are also derived for the QCD scale variations and variations in the scheme of the virtual NLO EW corrections. Furthermore, dedicated p_T^V shape uncertainties are derived in addition to the scale uncertainties by comparing the SHERPA 2.2.11 and SHERPA 2.2.1 MC samples separately for each V+jets component. These uncertainties are not covered by the QCD variations and provide the needed flexibility in the likelihood fit to correct the p_T^V spectra within a given p_T^V bin. The scale setting algorithms in SHERPA 2.2.11 were updated for better computational performance, as explained in Ref. [48], which lead to 10%-level differences in the p_T^V shape between the two samples. It is found that the central value of the p_T^V shape modelled by SHERPA 2.2.1 matches the data better in the $p_\text{T}^V < 400\,\text{GeV}$ region while the SHERPA 2.2.11 p_T^V shape matches the data better in the $p_\text{T}^V > 400\,\text{GeV}$ region. Most of these p_T^V shape uncertainties are constrained in the CRs by directly fitting the p_T^V distributions as summarised in Table 3.

$t\bar{t}$ **and** Wt **production:** Modelling systematic uncertainties are derived from comparisons between the nominal sample (POWHEG+PYTHIA 8) and alternative samples corresponding to matrix-element (MADGRAPH5_AMC@NLO+PYTHIA 8) and parton-shower (POWHEG+HERWIG 7 [134]) generator variations. The corresponding shape uncertainties are derived using CARL reweighting, similar to the V+jets background. In addition, the impact of additional radiation is assessed using (MADGRAPH5_AMC@NLO+PYTHIA 8) samples with modified parameter values for initial-state radiation (ISR) and FSR.

Uncertainties in the relative composition of the two commonly normalised components, top(bq) and top(qq), and the relative composition between the $t\bar{t}$ and Wt processes, are estimated from the difference in their relative rates between the nominal sample and the alternative matrix element and parton shower generator samples. Furthermore, relative acceptance uncertainties are estimated for the ratio of the top-quark event yields in the SRs to that in the Low-ΔR and High-ΔR CRs and for the 0-lepton to 1-lepton channel event yield ratios. Lastly, dedicated acceptance plus normalisation uncertainties are evaluated from comparisons between the nominal sample using the diagram subtraction scheme [49] and the diagram removal scheme [50] to account for the interference between Wt and $t\bar{t}$ production.

The uncertainty in the top-quark background in the 2-lepton Hbb resolved channel is dominated by the statistical uncertainty of the data control regions used to estimate it.

Single top t-/s-**channel:** The single top t-channel normalisation is constrained by the theory prediction with a normalisation uncertainty applied, derived from the internal MC scale variations. The acceptance uncertainties are estimated for the extrapolation between the SRs and Low-ΔR and High-ΔR CRs,

---

[9] The $\Delta R(j_1, j_2) = 1.0$ value approximately corresponds to the maximum kinematically allowed separation between two jets originating from gluon splitting with the ME+PS matching scale set at 20 GeV, following the $m^2 \approx p_\text{T}^{j_1} p_\text{T}^{j_2} \Delta R(j_1, j_2)^2$ relation.

between different p_T^V regions, between different jet multiplicities, and between the 0-lepton and 1-lepton channels. The shape uncertainties are derived using the CARL technique from comparisons between the nominal sample (POWHEG+PYTHIA 8) and alternative samples corresponding to matrix-element (MADGRAPH5_AMC@NLO+PYTHIA 8) and parton-shower (POWHEG+HERWIG 7) generator variations, and from the impact of additional radiation using MADGRAPH5_AMC@NLO+PYTHIA 8 samples with modified parameter values for ISR and FSR. For the single top s-channel, only a flat normalisation uncertainty is applied as its contribution to the total background is small.

Diboson production: The shape uncertainties, normalisation and relative acceptance uncertainties are estimated similarly to the $V+$jets processes: by comparing the nominal SHERPA 2.2.11 samples to the SHERPA 2.2.1 samples, by comparing the nominal samples to POWHEG+PYTHIA 8 diboson samples (also used in previous results [18, 22, 38]), by varying the renormalisation and factorisation scales, by varying the PDF, and by varying the scheme of the virtual NLO EW corrections. The shape uncertainties from two-sample comparisons are estimated by using the CARL technique. In addition to the different scale choice between SHERPA 2.2.11 and SHERPA 2.2.1 samples, SHERPA 2.2.11 samples have retuned heavy-flavour hadron production rates and b-hadron fragmentation functions [48], which lead to shape differences between the $Z \rightarrow b\bar{b}$ and $Z \rightarrow c\bar{c}$ dijet invariant mass distributions.

Multijet production: The shape and normalisation uncertainties in the multijet background in the 1-lepton channel are derived by following the procedure outlined in Ref. [11]. Two different uncertainty components are considered, those which alter the normalisation and those which alter the multijet template shape.

8.3 Signal uncertainties

The systematic uncertainties that affect the modelling of the signal are estimated with procedures that closely follow those outlined in Refs. [17, 135–137]. The systematic uncertainties in the calculations of the VH production cross-sections and the $H \rightarrow b\bar{b}$, $c\bar{c}$ branching fraction[10] are assigned following the recommendations of the LHC Higgs Cross Section Working Group [40, 74, 138, 139].

Uncertainties in acceptance and shape of the final multivariate discriminant are estimated, as described in Ref. [11], from scale variations, PDF and α_s (PDF+α_s) uncertainties, from varying the parton shower and underlying event (PS/UE) models using PYTHIA 8 internal variations and from comparisons with alternative parton-shower generator samples (POWHEG+HERWIG 7). The effects are treated as uncorrelated between qq-initiated and gg-initiated processes.

In addition, a systematic uncertainty from higher-order EW corrections is taken into account as a variation in the shape of the p_T^V distributions for VH production. Acceptance uncertainties, evaluated according to STXS regions, accounting for the migration and correlations between regions, are evaluated for the scale variations, PS/UE models and PDF+α_s. All the contributions, apart from the branching ratio uncertainties, are treated as fully correlated between the $H \rightarrow b\bar{b}$ and $H \rightarrow c\bar{c}$ processes.

For the STXS measurement, the signal uncertainties are separated into two groups. The first group contains uncertainties in the acceptance and shape of kinematic distributions, which alter the signal modelling (theoretical modelling uncertainties). The second set contains uncertainties in the prediction of the production cross-section for each kinematic region (theoretical cross-section uncertainties). Whilst theoretical modelling uncertainties enter the STXS measurements, theoretical cross-section uncertainties

---

[10] These systematic uncertainties are fully degenerate with the signal yield and do not affect the calculation of the significance relative to the background-only prediction and STXS cross-section measurement.

only affect the predictions with which they are compared, and are therefore not included in the likelihood function.

9 Statistical model

The statistical procedure is based on fits using a likelihood function $\mathcal{L}(\mu, \boldsymbol{\theta})$ constructed as the product of Poisson probability terms over the bins of the input distributions, with parameters of interest (POIs) μ extracted by maximising the likelihood. The effects of systematic uncertainties enter the likelihood as nuisance parameters (NP), $\boldsymbol{\theta}$. The normalisations of the largest backgrounds, top-quark and V+jets processes in several analysis regions, are determined by the fit, so they are left unconstrained in the likelihood. Experimental, background and signal systematic uncertainties, discussed in Section 7, are described by NPs that are constrained with Gaussian or log-normal probability density functions. The uncertainties due to the limited number of events in the simulated samples used for the background predictions are included using the "light" Beeston–Barlow technique [140]. As detailed in Ref. [141], systematic variations that are subject to large statistical fluctuations are smoothed, and systematic uncertainties that have a negligible impact on the final results are pruned away region-by-region (treating signal and control regions separately). Different fits are used to extract different sets of POIs.

The global likelihood fit comprises 59 signal regions (27 targeting $H \rightarrow b\bar{b}$ and 32 targeting $H \rightarrow c\bar{c}$), where BDT distributions are considered, and 97 control regions. The list of variables used in each CR of the resolved regime is shown in Table 3; in the boosted regime the mass of the large-R jet is considered in the Top CRs. The variables are selected by balancing fit complexity, data statistical uncertainty and the capability to control critical background modelling uncertainties.

The binning of the BDT distributions is determined following the algorithm defined in Ref. [118] to obtain a smoother distribution for the background processes and finer binning in the regions with the largest signal contribution, whilst ensuring that the statistical uncertainty of the simulated background is less than 20% in each bin. In addition, bins are require to have at least three expected events considering the sum of the total backgrounds and the SM expected signals. The final number of bins for each distribution varies from 15 to 3 depending on the expected number of background events. The analysis is run blinded so all selections, systematic uncertainties etc., are determined without looking at the data in any histogram bin with greater than 5% expected signal or looking at signal yields from the likelihood fit.

Multiple alternative sets of POIs are probed by the analysis. First in the VH fit, two signal strength parameters, μ_{VH}^{bb} and μ_{VH}^{cc}, are considered as multiplication factors that scale the expected VH, $H \rightarrow b\bar{b}$ and VH, $H \rightarrow c\bar{c}$ predictions respectively. An upper limit at 95% confidence level (CL) on the VH, $H \rightarrow c\bar{c}$ signal strength is computed using a modified frequentist CLs method [142], with the profile-likelihood ratio as the test statistic [143]. Second, a fit with four POI is performed to extract simultaneously the signal strength for the WH and ZH productions in $H \rightarrow b\bar{b}$ and $H \rightarrow c\bar{c}$ (μ_{WH}^{bb}, μ_{ZH}^{bb}, μ_{WH}^{cc}, μ_{ZH}^{cc}). Third, a 13-POI fit version measures the signal cross-section multiplied by the $H \rightarrow b\bar{b}$ and $V \rightarrow$leptons branching fractions in the STXS categories defined in Figure 4. For the categories with $p_{\mathrm{T}}^{V,t} < 75$ GeV no dedicated signal region exist and their contribution is fixed to the SM predictions including the full set of uncertainties described in Section 8.3. For this fit configuration, an inclusive signal strength is used for the VH, $H \rightarrow c\bar{c}$ component. Fourth, an additional 10-POI fit is performed where no split is considered in the number of jets (reduced STXS schema).

Table 3: A schematic of the fit variables used in the control regions. In the signal regions, the BDT output is used as the fit variable. The 'Norm. Only' label indicates that only the event yield is used in the fits and '—' indicates that the region is not used in the fits.

Channel	Region	BB	C_TN	C_TC_L	C_TC_T	BC_T	C_LN
0-lepton	High-ΔR CR	Norm. Only					—
	BC_T Top CR	—				$m_{j_1j_2}$	—
	$V+lf$ CR	—					Norm. Only
1-lepton	Low-ΔR CR	$\mathrm{BDT}_{\mathrm{Low}\text{-}\Delta R\,\mathrm{CR}}$	—				
	High-ΔR CR	p_T^V		$m_{j_1j_2}$			—
	BC_T Top CR	—				$m_{j_1j_2}$	—
	$V+lf$ CR	—					p_T^V
2-lepton	High-ΔR CR	p_T^V		$m_{j_1j_2}$			—
	Top eμ CR	—		Norm. Only		–	—
	$V+lf$ CR	—					p_T^V

Finally, an alternative fit is performed to extract signal strengths for the diboson processes μ_{VZ}^{bb} and μ_{VZ}^{cc} as a cross-check. A 4 POI VZ fit measures the signal strength of the WZ and ZZ, with $Z \to c\bar{c}$ or $Z \to b\bar{b}$. These fits use the BDT VZ output distributions instead of the VH BDT. The SM Higgs boson is included as a background process normalised to the predicted SM cross-section and including the full set of uncertainties described in Section 8.3.

10 Results

The post-fit normalisation factors of the unconstrained backgrounds in the VH fit are shown in Tables 4–6. The $V+$jets normalisation factors have a similar behaviour for $W+$jets and $Z+$jets; the normalisation factors increase with the number of additional jets and with p_T^V. The same trends are observed in a dedicated measurement of the $Z+hf$ processes in Ref. [144] for comparable multijet merged MC samples generated at NLO precision. The normalisation factors for the top-quark background processes show that the NLO Powheg+Pythia 8 generator set-up overshoots the data with increasing p_T^V, similarly to the trend observed in a dedicated measurement of the top-quark transverse momentum in $t\bar{t}$ events [145].

Figures 7–9 show the BDT$_{VH}$ output distribution for a selection of the most sensitive signal regions for both the $H \to b\bar{b}$ and $H \to c\bar{c}$ signals. The goodness-of-fit evaluated using a saturated model [146, 147] yields a probability of more than 75% for all fit configurations.

Table 4: The normalisation factors applied to the W+jets backgrounds processes in the analysis as obtained from the VH fit to data. The errors represent the combined statistical and systematic uncertainties.

p_{T}^{V} interval	Number of jets	$W+hf$	$W+mf$	$W+lf$
75–150 GeV	2	1.09 ± 0.06	1.20 ± 0.03	1.03 ± 0.04
	≥ 3	1.30 ± 0.07	1.16 ± 0.04	1.07 ± 0.05
150–250 GeV	2	1.00 ± 0.05	1.31 ± 0.03	1.08 ± 0.03
	≥ 3	1.28 ± 0.07	1.31 ± 0.04	1.07 ± 0.04
250–400 GeV	2	0.97 ± 0.08	1.35 ± 0.07	1.05 ± 0.03
	≥ 3	1.46 ± 0.12	1.32 ± 0.07	1.10 ± 0.04
400–600 GeV	-	1.49 ± 0.25		$-$
> 600 GeV	-	2.03 ± 0.25		$-$

Table 5: The normalisation factors applied to the Z+jets backgrounds processes in the analysis as obtained from the VH fit to data. The $3/\geq 3$ value is an additional correction factor applied to $Z+hf$ in categories with exactly three jets on top of the ≥ 3 normalisation factors. The errors represent the combined statistical and systematic uncertainties.

p_{T}^{V} intervsl	Number of jets	$Z+hf$	$Z+mf$	$Z+lf$
75–150 GeV	2	1.20 ± 0.04	1.04 ± 0.04	1.12 ± 0.03
	≥ 3	1.49 ± 0.06	1.11 ± 0.05	1.12 ± 0.05
	$3/\geq 3$	0.77 ± 0.03	$-$	$-$
150–250 GeV	2	1.30 ± 0.04	1.08 ± 0.04	1.17 ± 0.02
	≥ 3	1.59 ± 0.07	1.14 ± 0.05	1.17 ± 0.04
	$3/\geq 3$	0.80 ± 0.04	$-$	$-$
250–400 GeV	2	1.40 ± 0.07	1.31 ± 0.08	1.16 ± 0.03
	≥ 3	1.78 ± 0.09	1.32 ± 0.07	1.20 ± 0.04
	$3/\geq 3$	0.74 ± 0.04	$-$	$-$
>400 GeV	-	1.63 ± 0.13		$-$

Table 6: The normalisation factors applied to the top-quark background processes in the analysis as obtained from the VH fit to data. The errors represent the combined statistical and systematic uncertainties.

p_{T}^{V} interval	Number of jets	Top(bb)	Top(bq,qq)	Top 2L
75–150 GeV	2	1.02 ± 0.04	0.98 ± 0.05	1.05 ± 0.05
	3	0.97 ± 0.03	0.98 ± 0.03	0.98 ± 0.05
150–250 GeV	2	0.89 ± 0.05	0.83 ± 0.04	1.07 ± 0.16
	3	0.91 ± 0.03	0.86 ± 0.03	0.95 ± 0.14
	4	0.97 ± 0.02	0.95 ± 0.03	
250–400 GeV	2	0.78 ± 0.08	0.82 ± 0.05	
	3	0.83 ± 0.04	0.80 ± 0.03	1.10 ± 0.50
	4	0.93 ± 0.05	0.86 ± 0.04	
400–600 GeV	-	0.83 ± 0.05		$-$
>600 GeV	-	0.69 ± 0.07		$-$
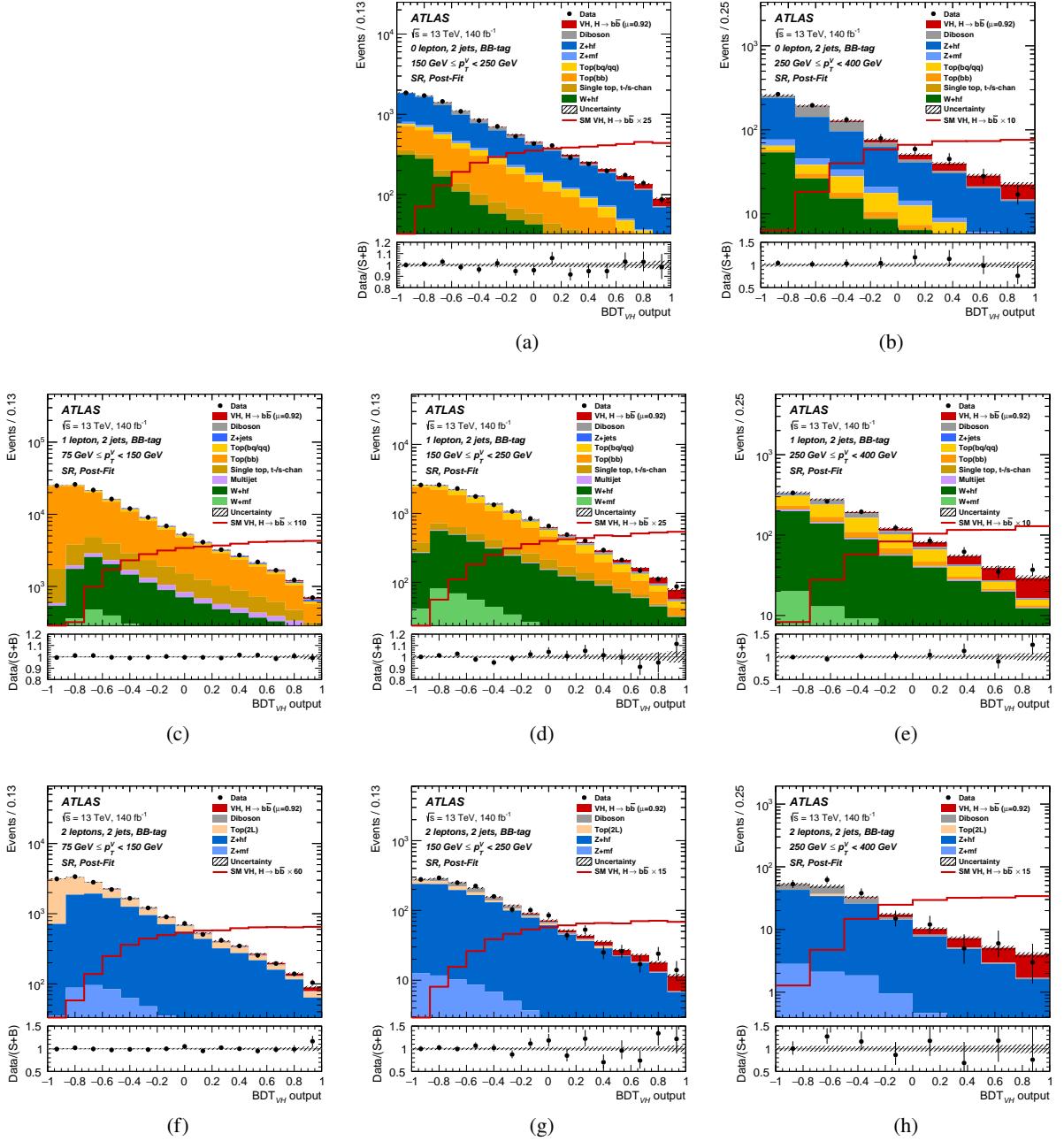
Figure 7: The BDT$_{VH}$ post-fit distributions in the (a) $150\,\text{GeV} < p_\text{T}^V < 250\,\text{GeV}$ and (b) $250\,\text{GeV} < p_\text{T}^V < 400\,\text{GeV}$ signal regions of the Hbb category in the 0-lepton, (c) $75\,\text{GeV} < p_\text{T}^V < 150\,\text{GeV}$, (d) $150\,\text{GeV} < p_\text{T}^V < 250\,\text{GeV}$ and (e) $250\,\text{GeV} < p_\text{T}^V < 400\,\text{GeV}$ in the 1-lepton and (f) $75\,\text{GeV} < p_\text{T}^V < 150\,\text{GeV}$, (g) $150\,\text{GeV} < p_\text{T}^V < 250\,\text{GeV}$ and (h) $250\,\text{GeV} < p_\text{T}^V < 400\,\text{GeV}$ in the 2-lepton channel for events with 2 jets. The background contributions after the VH fit are shown as filled histograms. The Higgs boson signal VH, $H \to b\bar{b}$ is shown as a filled histogram on top of the fitted backgrounds normalised to the signal yield extracted from data ($\mu = 0.92$), and unstacked as an unfilled histogram, scaled by a value reported in the legend for better visualisation. The size of the combined statistical and systematic uncertainties for the sum of the fitted signal and background (S+B) are indicated by the hatched band. The ratios of the data to the sum of the fitted signal and background are shown in the lower panel.

Figure 8: The BDT$_{VH}$ post-fit distributions in the (a) $150\,\text{GeV} < p_{\text{T}}^{V} < 250\,\text{GeV}$ and (b) $250\,\text{GeV} < p_{\text{T}}^{V} < 400\,\text{GeV}$ signal regions of the Hcc C$_{\text{T}}$C category in the 0-lepton, (c) $75\,\text{GeV} < p_{\text{T}}^{V} < 150\,\text{GeV}$, (d) $150\,\text{GeV} < p_{\text{T}}^{V} < 250\,\text{GeV}$ and (e) $250\,\text{GeV} < p_{\text{T}}^{V} < 400\,\text{GeV}$ in the 1-lepton and (f) $75\,\text{GeV} < p_{\text{T}}^{V} < 150\,\text{GeV}$, (g) $150\,\text{GeV} < p_{\text{T}}^{V} < 250\,\text{GeV}$ and (h) $250\,\text{GeV} < p_{\text{T}}^{V} < 400\,\text{GeV}$ in the 2-lepton channel for events with 2 jets. The background contributions after the VH fit are shown as filled histograms. The VH, $H \to c\bar{c}$ signal and the contribution from VH, $H \to b\bar{b}$ are shown unstacked as unfilled histograms, scaled by the factor indicated in the legend. The size of the combined statistical and systematic uncertainties for the sum of the fitted signal and background (S+B) are indicated by the hatched band. The ratios of the data to the sum of the fitted signal and background are shown in the lower panel.

28
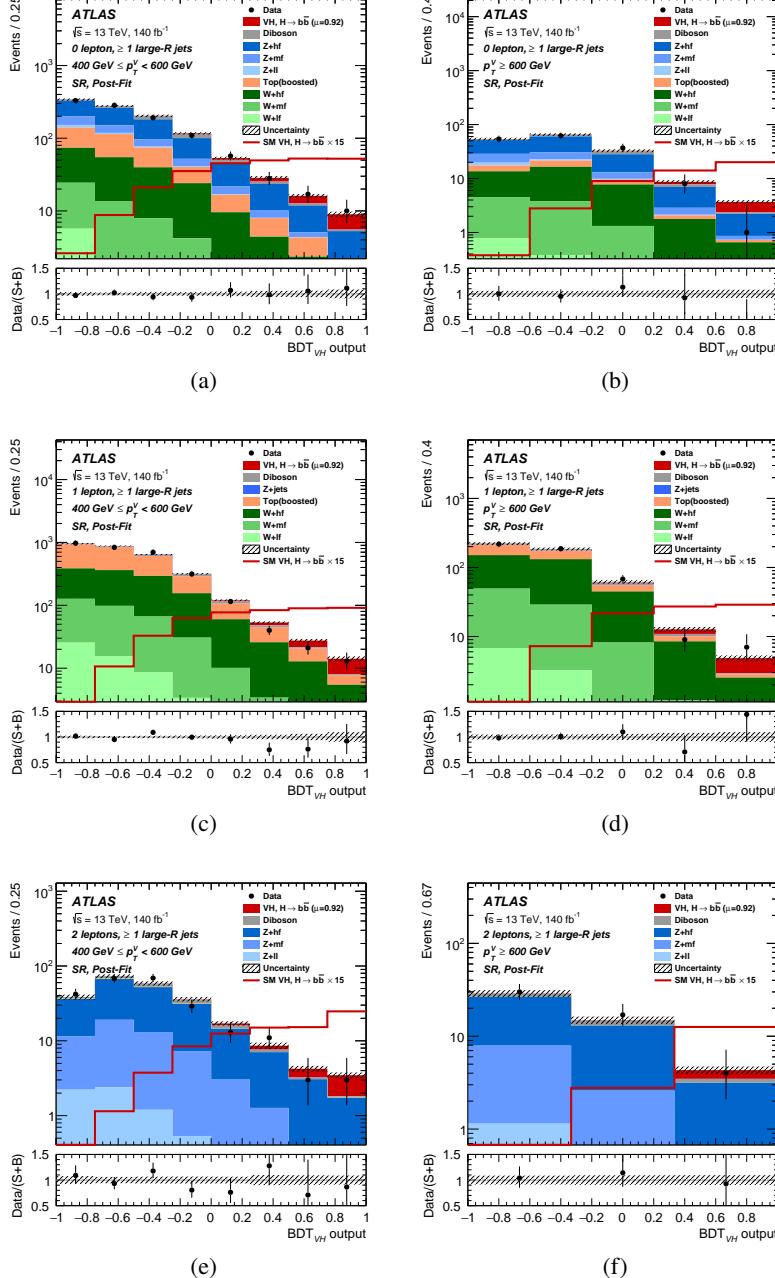
Figure 9: The BDT$_{VH}$ post-fit distributions in the (a) 400 GeV $< p_\text{T}^V <$ 600 GeV and (b) $p_\text{T}^V >$ 600 GeV signal regions of the boosted regime in the 0-lepton, (c) 400 GeV $< p_\text{T}^V <$ 600 GeV and (d) $p_\text{T}^V >$ 600 GeV in the 1-lepton and (e) 400 GeV $< p_\text{T}^V <$ 600 GeV and (f) $p_\text{T}^V >$ 600 GeV in the 2-lepton channels. The background contributions after the VH fit are shown as filled histograms. The Higgs boson signal VH, $H \rightarrow b\bar{b}$ is shown as a filled histogram on top of the fitted backgrounds normalised to the signal yield extracted from data ($\mu = 0.92$), and unstacked as an unfilled histogram, scaled by a value reported in the legend for better visualisation. The size of the combined statistical and systematic uncertainties for the sum of the fitted signal and background (S+B) are indicated by the hatched band. The ratios of the data to the sum of the fitted signal and background are shown in the lower panel.
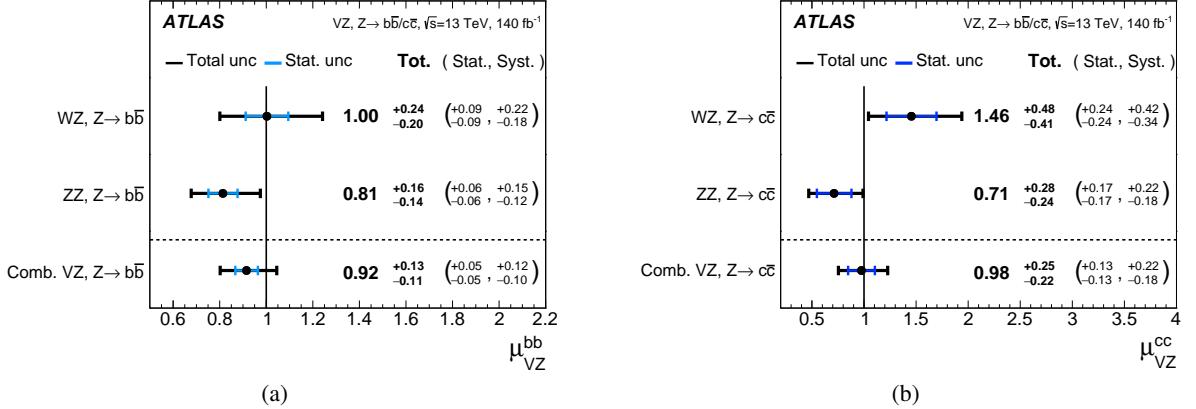
Figure 10: The fitted values of the VZ signal strengths for the (a) $Z \rightarrow b\bar{b}$ and (b) $Z \rightarrow c\bar{c}$ processes. The values for the WZ and ZZ signal strengths are obtained from a simultaneous fit with the signal strengths for each of the WZ and ZZ processes floating independently for the two decay modes.

10.1 Diboson signal strength measurements

Measurements of VZ production, which are used to validate the Higgs boson analysis, yield signal strengths of

$$\mu_{VZ}^{bb} = 0.92^{+0.13}_{-0.11} = 0.92 \pm 0.05 \text{ (stat.)}^{+0.12}_{-0.10} \text{ (syst.)},$$
$$\mu_{VZ}^{cc} = 0.98^{+0.25}_{-0.22} = 0.98 \pm 0.13 \text{ (stat.)}^{+0.22}_{-0.18} \text{ (syst.)},$$

in good agreement with the SM predictions. The correlation between the two measurements is +46% primarily driven by signal modelling uncertainties, which also represent the leading contribution to the overall uncertainty. For the VZ, $Z \rightarrow c\bar{c}$ process, the observed (expected) significance over the background-only prediction is 5.2 (5.3) standard deviations. The VZ, $Z \rightarrow b\bar{b}$ process is observed with a significance greater than 10 standard deviations. A fit is also performed with separate signal strengths for the WZ and ZZ processes in the two decay modes of the Z boson; the results are shown in Figure 10. The WZ, $Z \rightarrow b\bar{b}$ process is observed (expected) at 6.4 (6.5) standard deviations, while the significance is greater than 10 standard deviations for ZZ, $Z \rightarrow b\bar{b}$. Evidence for both WZ and ZZ with $Z \rightarrow c\bar{c}$ is found with an observed (expected) significance of 3.9 (2.7) and 3.1 (4.3) standard deviations respectively.

10.2 VH signal strength measurements

The measured signal strength for the $H \rightarrow b\bar{b}$ and $H \rightarrow c\bar{c}$ signals are:

$$\mu_{VH}^{bb} = 0.92^{+0.16}_{-0.15} = 0.92 \pm 0.10 \text{ (stat.)}^{+0.13}_{-0.11} \text{ (syst.)},$$
$$\mu_{VH}^{cc} = 1.0^{+5.4}_{-5.2} = 1.0^{+4.0}_{-3.9} \text{ (stat.)}^{+3.7}_{-3.5} \text{ (syst.)}.$$

The results are shown in Figure 11 together with the expected and observed 68% and 95% CL contours. Both measurements show good agreement with the SM and their correlation is +5%.
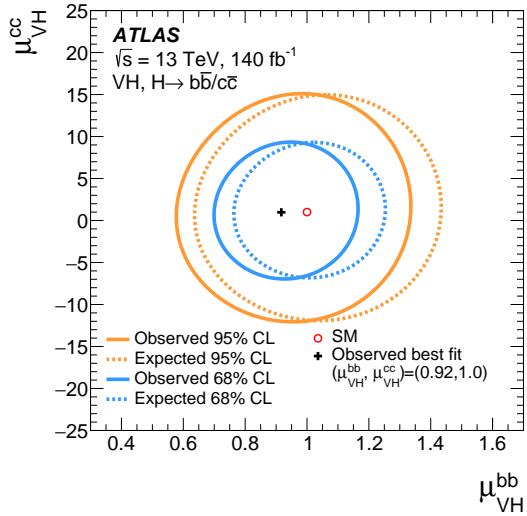
Figure 11: The observed (solid lines) and expected (dashed lines) 68% and 95% CL contours of the VH, $H \to b\bar{b}$ and VH, $H \to c\bar{c}$ signal strengths, along with their best-fit values.
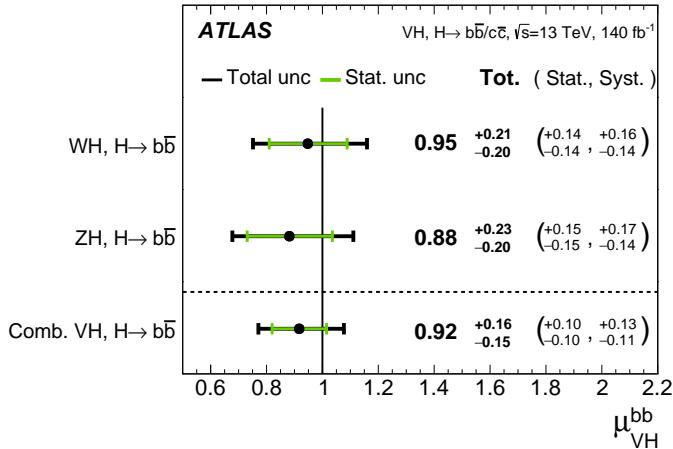
Figure 12: The fitted values of the WH, $H \to b\bar{b}$ and ZH, $H \to b\bar{b}$ signal strengths, along with their combination.

The measurement of μ_{VH}^{bb} has an observed (expected) significance of 7.4 (8.0) standard deviations. The measured $H \to b\bar{b}$ signal strengths of the WH and ZH processes separately are shown in Figure 12, in agreement with the SM predictions. The ZH, $H \to b\bar{b}$ measurement has an observed (expected) significance of 4.9 (5.6) standard deviations, while the observed (expected) significance for WH, $H \to b\bar{b}$ is 5.3 (5.5) standard deviations. This is the first observation of the WH, $H \to b\bar{b}$ process.

The effects of systematic uncertainties in the measurement of the VH, $H \to b\bar{b}$, WH, $H \to b\bar{b}$, ZH, $H \to b\bar{b}$ and VH, $H \to c\bar{c}$ signal strengths are shown in Table 7. The impact of a set of systematic uncertainties is defined as the difference in quadrature between the uncertainty in μ computed when all NPs are fitted and that when the NPs in the set are fixed to their best-fit values. The total statistical uncertainty is defined as the uncertainty on μ when all the NPs are fixed to their best-fit values. The total systematic uncertainty is defined as the difference in quadrature between the total uncertainty in μ and the total statistical uncertainty.

Table 7: The breakdown of contributions to the uncertainty in the fitted value of the signal strengths (σ_μ) for $VH, H \to b\bar{b}$, $WH, H \to b\bar{b}$, $ZH, H \to b\bar{b}$ and $VH, H \to c\bar{c}$. The sum in quadrature of uncertainties from different sources may differ from the total due to correlations. In cases where the upward and downward systematic variations have different values, the mean of the absolute values is shown.

Source of uncertainty		σ_μ			
		$VH, H \to b\bar{b}$	$WH, H \to b\bar{b}$	$ZH, H \to b\bar{b}$	$VH, H \to c\bar{c}$
Total		0.153	0.204	0.216	5.31
Statistical		0.097	0.139	0.153	3.94
Systematic		0.118	0.149	0.153	3.57
Statistical uncertainties					
Data statistical		0.090	0.129	0.139	3.67
$t\bar{t}$ $e\mu$ control region		0.009	0.014	0.027	0.08
Background floating normalisations		0.034	0.049	0.042	1.24
Other VH floating normalisation		0.007	0.018	0.014	0.33
Simulation samples size		0.023	0.033	0.030	1.62
Experimental uncertainties					
Jets		0.027	0.035	0.030	1.02
$E_{\mathrm{T}}^{\mathrm{miss}}$		0.010	0.005	0.021	0.23
Leptons		0.003	0.002	0.010	0.25
	b-jets	0.020	0.018	0.026	0.29
b-tagging	c-jets	0.013	0.017	0.012	0.73
	light-flavour jets	0.005	0.008	0.008	0.66
Pile-up		0.008	0.017	0.002	0.23
Luminosity		0.006	0.007	0.006	0.08
Theoretical and modelling uncertainties					
Signal		0.076	0.074	0.101	0.72
Z + jets		0.042	0.018	0.081	1.77
W + jets		0.054	0.087	0.026	1.42
$t\bar{t}$ and Wt		0.018	0.033	0.018	1.02
Single top-quark (s-, t-ch.)		0.010	0.018	0.002	0.16
Diboson		0.033	0.039	0.049	0.52
Multijet		0.005	0.010	0.005	0.55

For the WH and ZH signal strength measurements the total statistical and systematic uncertainties are similar in size. The background modelling, in particular W+jets and Z+jets production, and signal modelling represent the largest contribution to the total systematic uncertainty while detector-related systematic uncertainties, primarily jet and flavour tagging, have a subdominant effect.

An improvement of 23% (10%) is observed in the total uncertainty of the WH (ZH) measurement compared with the previous $VH, H \to b\bar{b}$ result in Ref. [18]; the WH channel, in particular, profits from the 25% increased c-jet rejection of the D_{DL1r} algorithm for a similar b-jet efficiency, improved treatment of τ_{had} candidates, addition of the $75\,\mathrm{GeV} < p_{\mathrm{T}}^W < 150\,\mathrm{GeV}$ region, use of $\mathrm{BDT_{Low\text{-}\Delta R\,CR}}$, and the dedicated CRs
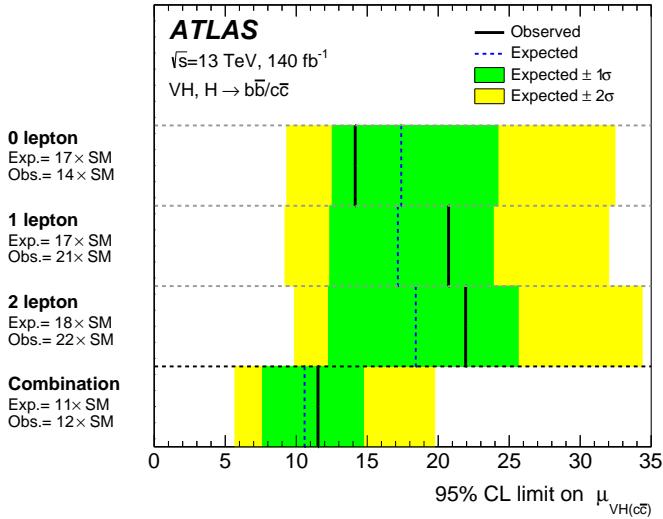
Figure 13: The observed and expected 95% CL upper limits on the VH, $H \to c\bar{c}$ signal strength in each lepton channel and for the combined fit. The single-channel limits are obtained in a fit in which each channel has a separate VH, $H \to c\bar{c}$ signal strength. A single parameter of interest is used in both fits for the VH, $H \to b\bar{b}$ signal strength.

to constrain the top(bq) background. Additional reasons for the improved performance are more precise flavour tagging and jet calibrations, larger signal-background separation of re-optimised MVAs, improved boosted $H \to b\bar{b}$ reconstruction and identification, and up to a 50% increase in the effective size of the MC simulated samples primarily in the V+jets background.

The μ_{VH}^{cc} results corresponds to an observed upper limit of 11.5 times the SM predictions at 95% CL, while a limit of 10.6 is expected in the case of no $H \to c\bar{c}$ process. The upper limits at 95% CL on VH, $H \to c\bar{c}$ for each individual channel and the combinations are shown in Figure 13. The impacts of statistical and systematic uncertainties in the observed signal strength for VH, $H \to c\bar{c}$ are at a similar level. The modelling of the V+jets background, jet and flavour tagging related calibration and the impact of the finite Monte Carlo statistics have comparable effects. The expected sensitivity has improved by roughly a factor of three compared with the previous iteration of the analysis [38]. Several interconnected factors contribute to this. The improved flavour tagging algorithms reduced the contamination of non c-jet background by roughly 40% while maintaining the same signal efficiency; at the same time the usage of an additional looser working point allows the signal acceptance to be increased, while maintaining the background contamination under control. The combined effect of the new working points and event classification is estimated as a 25% improvement on the previous result. A more efficient generator set-up for V+jets events, bringing up to a factor of five times more effective statistics, and the more advanced technique to parameterise the tagging probabilities has significantly reduced the uncertainty due to the finite size of the MC simulated samples. Furthermore, an additional 40% improvement in the expected sensitivity is obtained by deploying a multivariate discriminant over using dijet invariant mass as fit variable.[11] Finally, fitting the normalisation of the $V + hf$ components in Hbb and Hcc categories simultaneously reduces the related modelling uncertainties by up to a factor of two, improving the expected sensitivity by 6%.

Figure 14 shows the data, background (B) and signal (S) yields, where the bins of the MVA discriminants in

---

[11] In the current configuration, the BDT is further using flavour tagging information and has the capability to separate $C_T C_T$ and $C_T C_L$ events.
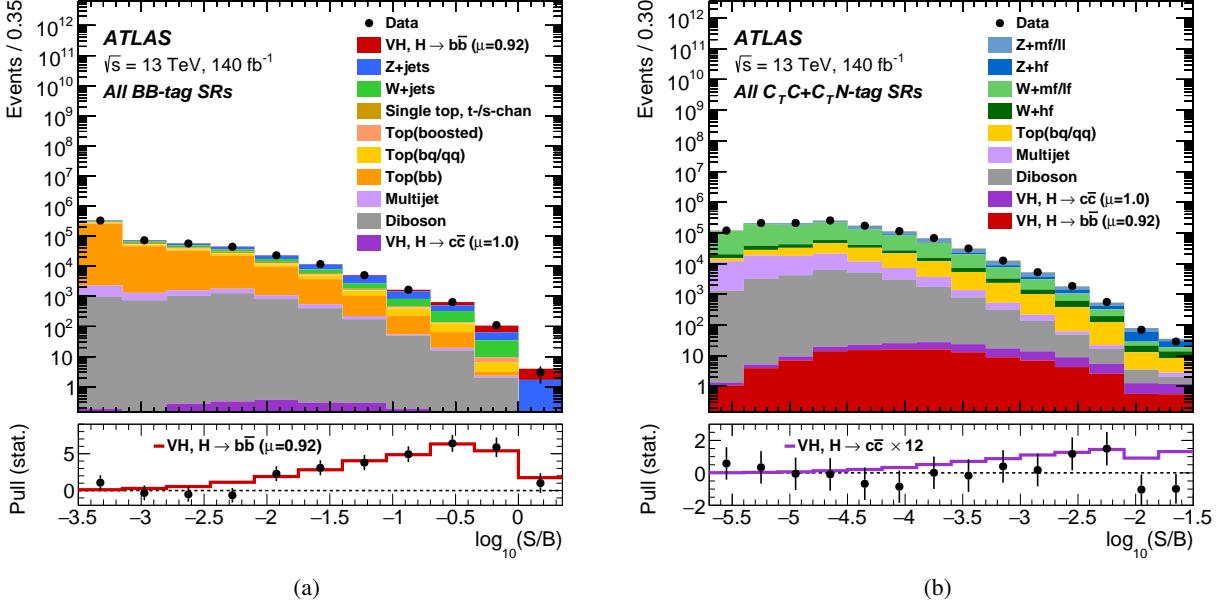
Figure 14: The event yields as a function of $\log_{10}(S/B)$ for data, background and a Higgs boson signal for the nominal VH fit. Final-discriminant bins in the (a) Hbb and (b) Hcc regions are combined into bins of $\log_{10}(S/B)$ with S being the fitted VH, $H \to b\bar{b}$ and $H \to c\bar{c}$ contribution respectively and B the fitted background yields. The Higgs boson contributions in the top pad are shown after rescaling the SM cross-section according to the value of the signal strength extracted from data: 0.92 for $H \to b\bar{b}$ and 1.0 for $H \to c\bar{c}$. In the lower panel, the pull of the data relative to the background (the statistical significance of the difference between data and fitted background) is shown with statistical uncertainties only. The full line indicates the pull expected from the sum of fitted signal and background relative to the fitted background; in the $H \to c\bar{c}$ case, the fitted signal is scaled to the value of the observed upper limit.

SRs are combined into bins of $\log_{10}(S/B)$. Distributions are shown separately for Hbb and Hcc categories where the definition to S is adapted to specifically consider only one specific Higgs boson decay mode at a time.

10.3 STXS result

The measured values of the product of the VH cross-sections and the $H \to b\bar{b}$ and $V \to$ leptons branching fractions, together with the SM predictions in the selected STXS regions, are summarised in Table 8. The cross-sections are consistent with the SM expectations within one standard deviation except in the $400\,\mathrm{GeV} < p_\mathrm{T}^{W,t} < 600\,\mathrm{GeV}$ and $p_\mathrm{T}^{Z,t} > 600\,\mathrm{GeV}$ categories, where the observed cross-sections are lower than the SM predictions by more than one standard deviation, but less than two standard deviations. Overall, the compatibility with the SM predictions is 90%.

Figure 15 shows the result for a configuration with no categorisation as a function of additional truth jets. In the WH channel, the relative uncertainty in the cross-sections is the smallest for the $250\,\mathrm{GeV} < p_\mathrm{T}^{W,t} < 400\,\mathrm{GeV}$ category at 25%. In the ZH channel the smallest relative error of 33% is in the $150\,\mathrm{GeV} < p_\mathrm{T}^{W,t} < 250\,\mathrm{GeV}$ category. The available statistics and the smaller systematic uncertainties in the ZH channel allows a further split of the measurements into the $N_\mathrm{jet}^\mathrm{t} = 0$ and $N_\mathrm{jet}^\mathrm{t} \geq 1$ categories for
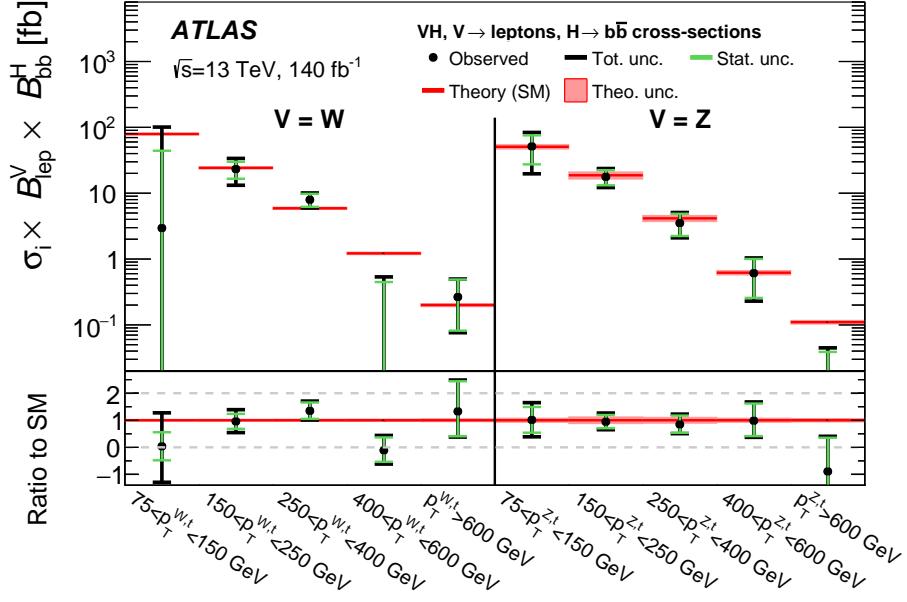
Figure 15: The measured VH cross-sections times the $V \to$ leptons and $H \to b\bar{b}$ branching fractions in the reduced STXS scheme with no split in the number of jets.
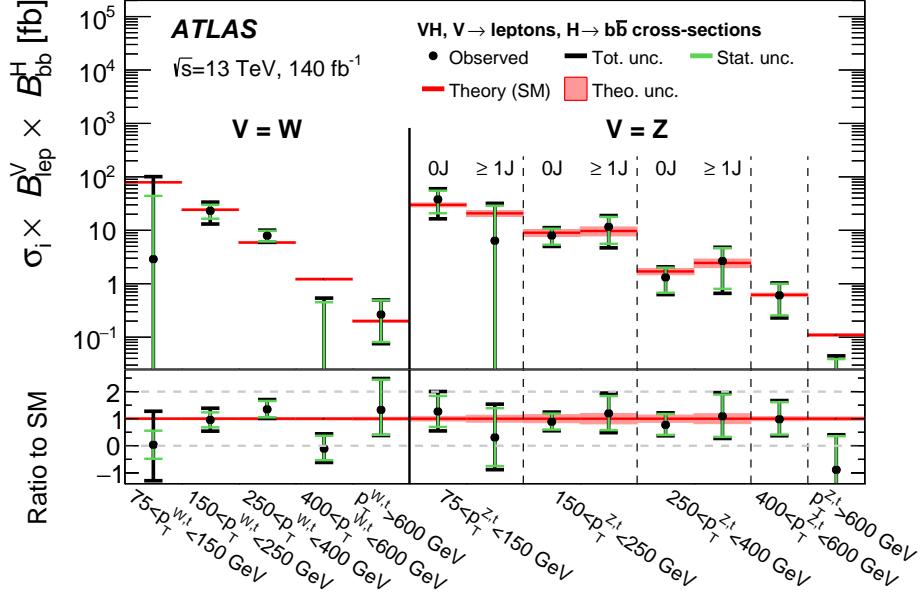
Figure 16: The measured VH cross-sections times the $V \to$ leptons and $H \to b\bar{b}$ branching fractions in the extended STXS scheme.

$75\,\text{GeV} < p_{\text{T}}^{Z,t} < 400\,\text{GeV}$ as shown in Figure 16. The $N_{\text{jet}}^{\text{t}} = 0$ categories have a relative uncertainty roughly a factor two smaller than the corresponding $N_{\text{jet}}^{\text{t}} \geq 1$ categories in the same $p_{\text{T}}^{V,t}$ interval. The categories with $p_{\text{T}}^{Z,t} > 400\,\text{GeV}$ remain inclusive.

In all cases, the uncertainties are dominated by the data statistical uncertainty, which also includes the

Table 8: The best-fit values and uncertainties for the measured VH cross-sections times the $V \to$ leptons and the $H \to b\bar{b}$ branching fraction, in the extended 1.2 STXS scheme. For the ZH process, inclusive results in truth jet multiplicity are also reported. Such results are obtained from an alternative fit configuration described in Section 9; the cross-section results for other categories are unchanged in this alternative configuration within the precision considered. The SM predictions for each region, computed using the inclusive cross-section calculations and the simulated event samples are also shown. The symmetrised contributions to the total measurement uncertainty from statistical (Stat. unc.) or systematic uncertainties (Syst. unc.) related to the signal prediction (Th. sig.), background prediction (Th. bkg.), and the experimental performance (Exp.) are given separately. The total systematic uncertainty, equal to the difference in quadrature between the total uncertainty and the statistical uncertainty, differs from the sum in quadrature of the Th. sig., Th. bkg., and Exp. systematic uncertainties due to correlations. All leptonic decays of the V bosons (including those to τ-leptons, $\ell = e, \mu, \tau$) are considered.

STXS region			SM prediction [fb]			Measurement [fb]			Stat. unc. [fb]	Syst. unc. [fb]		
Process	$p_{\mathrm{T}}^{V,\mathrm{t}}$ interval	$N_{\mathrm{jet}}^{\mathrm{t}}$								Th. sig.	Th. bkg.	Exp.
$W(\ell\nu)H$	75–150 GeV	≥ 0	79.2	$\pm$	2.8	3	$\pm$	102	41	13	89	36
	150–250 GeV	≥ 0	24.3	$\pm$	1.0	23	$\pm$	10	7	2	7	3
	250–400 GeV	≥ 0	5.90	$\pm$	0.25	7.9	$\pm$	2.1	1.8	0.5	0.8	0.3
	400–600 GeV	≥ 0	1.03	$\pm$	0.05	-0.11	$\pm$	0.54	0.46	0.05	0.25	0.09
	> 600 GeV	≥ 0	0.20	$\pm$	0.01	0.26	$\pm$	0.21	0.20	0.02	0.04	0.03
$Z(\ell\ell/\nu\nu)H$	75–150 GeV	≥ 0	50.7	$\pm$	3.9	51	$\pm$	32	24	5	18	11
		$= 0$	29.9	$\pm$	2.5	38	$\pm$	22	17	3	12	6
		≥ 1	20.7	$\pm$	2.6	6	$\pm$	25	22	4	9	8
	150–250 GeV	≥ 0	18.7	$\pm$	3.5	17.7	$\pm$	5.8	4.6	1.7	3.0	1.0
		$= 0$	9.0.	$\pm$	1.3	8.0	$\pm$	3.1	2.7	0.6	1.4	0.5
		≥ 1	9.7	$\pm$	1.9	11.6	$\pm$	7.1	6.1	1.0	3.2	1.4
	250–400 GeV	≥ 0	4.15	$\pm$	0.45	3.5	$\pm$	1.5	1.3	0.4	0.5	0.2
		$= 0$	1.70	$\pm$	0.22	1.31	$\pm$	0.72	0.66	0.14	0.25	0.10
		≥ 1	2.45	$\pm$	0.45	2.7	$\pm$	2.1	1.9	0.3	0.7	0.3
	400–600 GeV	≥ 0	0.62	$\pm$	0.05	0.61	$\pm$	0.40	0.37	0.05	0.12	0.08
	> 600 GeV	≥ 0	0.11	$\pm$	0.01	-0.10	$\pm$	0.12	0.12	0.01	0.03	0.01

contribution from the floating normalisation factors on the leading background contributions and other signal categories, except in the $75\,\mathrm{GeV} < p_{\mathrm{T}}^{W,t} < 150\,\mathrm{GeV}$ and $150\,\mathrm{GeV} < p_{\mathrm{T}}^{W,t} < 250\,\mathrm{GeV}$ categories, where the systematic uncertainties are the largest contributions to the total uncertainty. Compared to the previous $VH, H \to b\bar{b}$ STXS result in Ref. [148], the finer binning with a split at $p_{\mathrm{T}}^{V,t} = 400\,\mathrm{GeV}$ was made as a result of the 50% improvement in the expected sensitivity of the boosted Hbb category, due to the use of a multivariate discriminant over the dijet invariant mass as the fit variable and the improved performance of the flavour tagging algorithms.

The largest sources of systematic uncertainties are the modelling of $Z + hf$ production, primarily for the ZH categories and the modelling of the $W + hf$ production and top-quark background for the WH categories. Uncertainties related to the jet calibration, both small- and large-R jets, and b-tagging are the leading detector-related effects, but their contribution is small compared with the modelling uncertainties. The relative impact of the limited size of the MC sample is the third largest component, and is similar across all the regions. For the ZH measurements, the signal uncertainties also have a significant contribution due to the limited precision of the theoretical calculations of the gluon-initiated process, for which the lowest order is a box or triangle diagram.
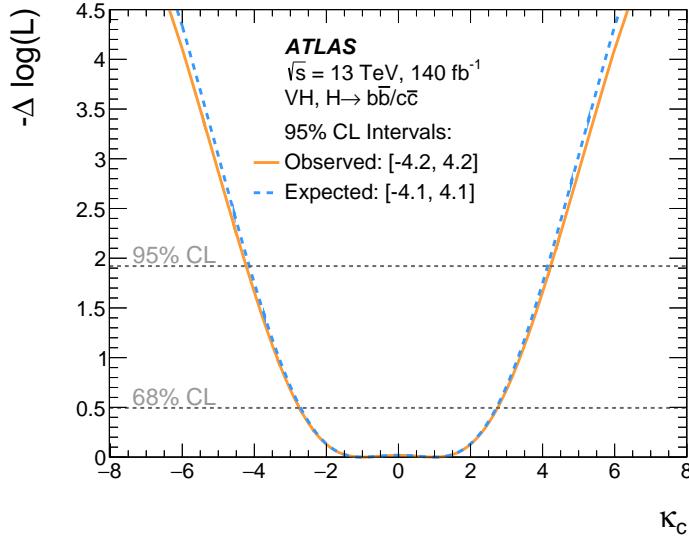
Figure 17: The observed (solid) and expected (dashed) values of the negative profile log-likelihood ratio as a function of κ_c, is obtained in a fit with κ_b fixed to unity. The signal strength μ_{VH}^{bb} is not parameterised but taken as a single parameter of interest in the fit.

11 Interpretation in the κ-framework

The best-fit values of the VH signal strength are interpreted in the context of the κ-framework [17, 40] by reparameterising the μ_{VH}^{bb} and μ_{VH}^{cc} in the likelihood function in terms of the Higgs-bottom and Higgs-charm multiplicative coupling modifiers, κ_b and κ_c, assuming that they affect only the Higgs boson decays.[12] Including effects in both the partial and full width, considering only SM decays and setting all other couplings to their SM predictions, the parameterisation is:

$$\mu_{VH}^{bb} = \frac{\kappa_b^2}{1 + B_{Hbb}^{\mathrm{SM}}(\kappa_b^2 - 1) + B_{Hcc}^{\mathrm{SM}}(\kappa_c^2 - 1)}, \tag{1}$$

$$\mu_{VH}^{cc} = \frac{\kappa_c^2}{1 + B_{Hbb}^{\mathrm{SM}}(\kappa_b^2 - 1) + B_{Hcc}^{\mathrm{SM}}(\kappa_c^2 - 1)}, \tag{2}$$

where B_{Hbb}^{SM} and B_{Hcc}^{SM} are the $H \to b\bar{b}$ and $H \to c\bar{c}$ branching fraction predictions in the SM.

First, the direct κ_c constraint from the VH, $H \to c\bar{c}$ process is extracted by setting $\kappa_b = 1$ in Eq. 2 and not parameterising μ_{VH}^{bb}. Constraints on κ_c are set using the profile-likelihood ratio test statistic and are shown in Figure 17. The result from the full fit achieves an observed (expected) constraint of $|\kappa_c| < 4.2$ ($|\kappa_c| < 4.1$) at 95% CL. An equivalent approach for κ_b yields an observed (expected) 95% CL interval of $0.65 < |\kappa_b| < 1.37$ ($0.72 < |\kappa_b| < 1.62$).

Second, a simultaneous determination of κ_b and κ_c is performed using Eqs. 1 and 2. The contours at 68% CL and 95% CL extracted from a likelihood scan are reported in Figure 18(a). For most values of κ_b, a value of κ_c is allowed at 95% CL that compensates for the effect of κ_b via the width of the Higgs boson

---

[12] The effect of anomalous κ values on the $ggZH$ production process is found to be negligible within the the range of parameters probed by this analysis.
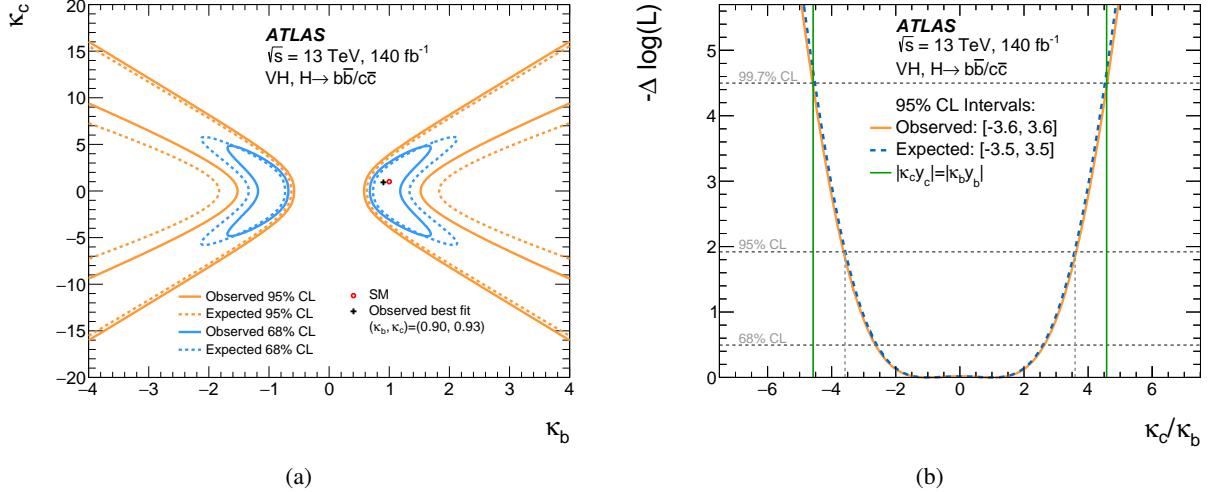
Figure 18: (a) The observed (solid) and expected (dashed) constraints on κ_b and κ_c at 68% CL and 95% CL confidence levels. (b) The observed and expected values of the combined negative profile log-likelihood ratio as a function of κ_c/κ_b where μ_{VH}^{bb} is a free parameter. The solid vertical lines correspond to the values of $|\kappa_c/\kappa_b|$ for which the Higgs-charm and Higgs-bottom couplings are equal.

and vice versa. The best-fit value is $(\kappa_b, \kappa_c) = (0.90, 0.93)$, but no 95% CL contours can be set on each parameter independent of the other in this model. These constraints complement those from measurements of the Higgs boson p_T spectrum [149].

An alternative parameterisation is performed targeting the ratio $|\kappa_c/\kappa_b|$, which can be performed without assumptions on the Higgs boson's width. The signal strength μ_{VH}^{bb} is a profiled free parameter in the fit absorbing both the effect of potentially anomalous κ_b and width values; this assumes that the width is still negligible relative to the experimental resolution, which is more than 1000 times worse than the SM intrinsic width of the Higgs boson. The $VH, H \rightarrow c\bar{c}$ signal strength is parameterised as $\mu_{VH}^{cc} = (\kappa_c/\kappa_b)^2 \mu_{VH}^{bb}$. The results are shown in Figure 18(b) reporting the profile likelihood scan as a function of $|\kappa_c/\kappa_b|$. The observed (expected) upper limit on $|\kappa_c/\kappa_b|$ is 3.6 (3.5) at 95% CL. Both upper limits are smaller than the ratio of the b- and c-quark masses, 4.578 [150], evaluated at a renormalisation scale equal to 125 GeV, confirming that the coupling of the Higgs boson to charm-quarks is weaker than the coupling of the Higgs boson to bottom-quarks.

12 Conclusion

The study of the Higgs boson decay into a $b\bar{b}$ or $c\bar{c}$ pair, when produced in association with a W or Z boson, is presented using data collected by the ATLAS experiment in proton–proton collisions from Run 2 of the LHC. The data correspond to an integrated luminosity of 140 fb^{-1} collected at a centre-of-mass energy of $\sqrt{s}$ =13 TeV.

The measurements of the diboson processes WZ and ZZ with $Z \rightarrow b\bar{b}$ and $Z \rightarrow c\bar{c}$ decays are used as a validation of the analysis methodology. All four processes are observed with significances larger than 3 standard deviations. The $WZ, Z \rightarrow b\bar{b}$ process is measured with a significance of 6.4 standard deviations,

while the ZZ, $Z \to b\bar{b}$ process has a significance more than 10 standard deviations. For the first time in ATLAS, the VZ, $Z \to c\bar{c}$ process is observed with a significance greater than five standard deviations. No significant deviations are observed from the SM predictions.

For a Higgs boson with a mass of 125 GeV produced in association with either a W or Z boson, the signal strengths relative to the SM prediction in the $H \to b\bar{b}$ and $H \to c\bar{c}$ decay channels are measured to be $\mu_{VH}^{bb} = 0.92_{-0.14}^{+0.16}$ and $\mu_{VH}^{cc} = 1.0_{-5.2}^{+5.4}$ respectively. The measurement of μ_{VH}^{bb} has an observed (expected) significance of 7.4 (8.0) standard deviations, while the μ_{VH}^{cc} results correspond to an observed upper limit at 95% confidence level of 11.5 times the SM prediction, with an expected limit of 10.6 times the SM prediction in the case of no $H \to c\bar{c}$ process. The uncertainties in the signal strengths have improved by 15% in the $H \to b\bar{b}$ channel and roughly a factor of three in the $H \to c\bar{c}$ channel compared with the previous ATLAS results. Measurements made separately for the WH or ZH processes, are in agreement with the SM predictions.

Differential cross-sections of WH and ZH production with $H \to b\bar{b}$ decays are made as a function of the vector boson transverse momentum in kinematic fiducial volumes within the simplified template cross-section framework. For the first time at ATLAS, the ZH measurements are further split into events with 0 and 1 or more jets in addition to those associated with the Higgs boson decay and the granularity of the VH cross section measurement has been extended including dedicated signal extraction for $p_{\mathrm{T}}^{V,t} > 600$ GeV. All measurements are in agreement with the SM predictions.

The results are also used to set constraints on a charm Yukawa coupling modifier; $|\kappa_c| < 4.2$ at 95% confidence level. The $H \to b\bar{b}$ and $H \to c\bar{c}$ data constrain the absolute value of the ratio of the coupling modifiers of the Higgs boson to c- and b-quarks ($|\kappa_c/\kappa_b|$) to less than 3.6 at 95% confidence level, confirming that the coupling of the Higgs boson to charm-quarks is weaker than the coupling of the Higgs boson to bottom quarks.

Acknowledgements

References

[1] ATLAS Collaboration, *Observation of a new particle in the search for the Standard Model Higgs boson with the ATLAS detector at the LHC*, Phys. Lett. B **716** (2012) 1, arXiv: 1207.7214 [hep-ex].

[2] CMS Collaboration, *Observation of a new boson at a mass of 125 GeV with the CMS experiment at the LHC*, Phys. Lett. B **716** (2012) 30, arXiv: 1207.7235 [hep-ex].

[3] F. Englert and R. Brout, *Broken Symmetry and the Mass of Gauge Vector Mesons*, Phys. Rev. Lett. **13** (1964) 321.

[4] P. W. Higgs, *Broken symmetries, massless particles and gauge fields*, Phys. Lett. **12** (1964) 132.

[5] P. W. Higgs, *Broken Symmetries and the Masses of Gauge Bosons*, Phys. Rev. Lett. **13** (1964) 508.

[6] G. S. Guralnik, C. R. Hagen and T. W. B. Kibble, *Global Conservation Laws and Massless Particles*, Phys. Rev. Lett. **13** (1964) 585.

[7] P. W. Higgs, *Spontaneous Symmetry Breakdown without Massless Bosons*, Phys. Rev. **145** (1966) 1156.

[8] T. W. B. Kibble, *Symmetry Breaking in Non-Abelian Gauge Theories*, Phys. Rev. **155** (1967) 1554.

[9] CMS Collaboration, *Observation of the Higgs boson decay to a pair of τ leptons with the CMS detector*, Phys. Lett. B **779** (2018) 283, arXiv: 1708.00373 [hep-ex].

[10] ATLAS Collaboration, *Cross-section measurements of the Higgs boson decaying into a pair of τ-leptons in proton–proton collisions at $\sqrt{s} = 13$ TeV with the ATLAS detector*, Phys. Rev. D **99** (2019) 072001, arXiv: 1811.08856 [hep-ex].

[11] ATLAS Collaboration, *Observation of $H \to b\bar{b}$ decays and VH production with the ATLAS detector*, Phys. Lett. B **786** (2018) 59, arXiv: 1808.08238 [hep-ex].

[12] CMS Collaboration, *Observation of Higgs Boson Decay to Bottom Quarks*, Phys. Rev. Lett. **121** (2018) 121801, arXiv: 1808.08242 [hep-ex].

[13] CMS Collaboration, *Observation of $t\bar{t}H$ Production*, Phys. Rev. Lett. **120** (2018) 231801, arXiv: 1804.02610 [hep-ex].

[14] ATLAS Collaboration, *Observation of Higgs boson production in association with a top quark pair at the LHC with the ATLAS detector*, Phys. Lett. B **784** (2018) 173, arXiv: 1806.00425 [hep-ex].

[15] ATLAS Collaboration, *A detailed map of Higgs boson interactions by the ATLAS experiment ten years after the discovery*, Nature **607** (2022) 52, arXiv: 2207.00092 [hep-ex], Erratum: Nature **612** (2022) E24.

[16] CMS Collaboration, *A portrait of the Higgs boson by the CMS experiment ten years after the discovery*, Nature **607** (2022) 60, arXiv: 2207.00043 [hep-ex], Erratum: Nature **623** (2023) E4.

[17] D. de Florian et al., *Handbook of LHC Higgs Cross Sections: 4. Deciphering the Nature of the Higgs Sector*, (2017), arXiv: 1610.07922 [hep-ph].

[18] ATLAS Collaboration, *Measurements of WH and ZH production in the $H \to b\bar{b}$ decay channel in pp collisions at* 13 *TeV with the ATLAS detector*, Eur. Phys. J. C **81** (2021) 178, arXiv: 2007.02873 [hep-ex].

[19] CMS Collaboration, *Measurement of simplified template cross sections of the Higgs boson produced in association with W or Z bosons in the $H \to b\bar{b}$ decay channel in proton–proton collisions at $\sqrt{s} = 13$ TeV*, Phys. Rev. D **109** (2024) 092011, arXiv: 2312.07562 [hep-ex].

[20] ATLAS Collaboration, *Determination of the relative sign of the Higgs boson couplings to W and Z bosons using WH production via vector-boson fusion with the ATLAS detector*, Phys. Rev. Lett. **133** (2024) 141801, arXiv: 2402.00426 [hep-ex].

[21] CMS Collaboration, *Inclusive search for highly boosted Higgs bosons decaying to bottom quark-antiquark pairs in proton–proton collisions at $\sqrt{s} = 13$ TeV*, JHEP **12** (2020) 085, arXiv: 2006.13251 [hep-ex].

[22] ATLAS Collaboration, *Measurement of the associated production of a Higgs boson decaying into b-quarks with a vector boson at high transverse momentum in pp collisions at $\sqrt{s} = 13$ TeV with the ATLAS detector*, Phys. Lett. B **816** (2021) 136204, arXiv: 2008.02508 [hep-ex].

[23] ATLAS Collaboration, *Constraints on Higgs boson production with large transverse momentum using $H \to b\bar{b}$ decays in the ATLAS detector*, Phys. Rev. D **105** (2022) 092003, arXiv: 2111.08340 [hep-ex].

[24] ATLAS Collaboration, *Study of High-Transverse-Momentum Higgs Boson Production in Association with a Vector Boson in the qqbb Final State with the ATLAS Detector*, Phys. Rev. Lett. **132** (2024) 131802, arXiv: 2312.07605 [hep-ex].

[25] CMS Collaboration, *Search for nonresonant Higgs boson pair production in final states with two bottom quarks and two photons in proton–proton collisions at $\sqrt{s} = 13$ TeV*, JHEP **03** (2021) 257, arXiv: 2011.12373 [hep-ex].

[26] CMS Collaboration, *Search for Higgs Boson Pair Production in the Four b Quark Final State in Proton–Proton Collisions at $\sqrt{s} = 13$ TeV*, Phys. Rev. Lett. **129** (2022) 081802, arXiv: 2202.09617 [hep-ex].

[27] CMS Collaboration, *Search for nonresonant Higgs boson pair production in final state with two bottom quarks and two tau leptons in proton–proton collisions at $\sqrt{s} = 13$ TeV*, Phys. Lett. B **842** (2023) 137531, arXiv: 2206.09401 [hep-ex].

[28] ATLAS Collaboration, *Search for resonant and non-resonant Higgs boson pair production in the $b\bar{b}\tau^+\tau^-$ decay channel using* 13 *TeV pp collision data from the ATLAS detector*, JHEP **07** (2023) 040, arXiv: 2209.10910 [hep-ex].

[29] ATLAS Collaboration, *Search for nonresonant pair production of Higgs bosons in the $b\bar{b}b\bar{b}$ final state in pp collisions at $\sqrt{s} = 13$ TeV with the ATLAS detector*, Phys. Rev. D **108** (2023) 052003, arXiv: 2301.03212 [hep-ex].

[30] ATLAS Collaboration, *Studies of new Higgs boson interactions through nonresonant HH production in the $b\bar{b}\gamma\gamma$ final state in pp collisions at $\sqrt{s} = 13$ TeV with the ATLAS detector*, JHEP **01** (2024) 066, arXiv: 2310.12301 [hep-ex].

[31] C. Delaunay, T. Golling, G. Perez and Y. Soreq, *Enhanced Higgs boson coupling to charm pairs*, Phys. Rev. D **89** (2014) 033014, arXiv: 1310.7029 [hep-ph].

[32] G. Perez, Y. Soreq, E. Stamou and K. Tobioka,
Constraining the charm Yukawa and Higgs-quark coupling universality,
Phys. Rev. D **92** (2015) 033016, arXiv: 1503.00290 [hep-ph].

[33] F. Botella, G. Branco, M. Rebelo and J. Silva-Marcos, *What if the masses of the first two quark families are not generated by the standard model Higgs boson?*, Phys. Rev. D **94** (2016) 115031,
arXiv: 1602.08011 [hep-ph].

[34] S. Bar-Shalom and A. Soni, *Universally enhanced light-quarks Yukawa couplings paradigm*,
Phys. Rev. D **98** (2018) 055001, arXiv: 1804.02400 [hep-ph].

[35] D. Ghosh, R. S. Gupta and G. Perez, *Is the Higgs mechanism of fermion mass generation a fact? A Yukawa-less first-two-generation model*, Phys. Lett. B **755** (2016) 504,
arXiv: 1508.01501 [hep-ph].

[36] D. Egana-Ugrinovic, S. Homiller and P. Meade, *Aligned and Spontaneous Flavor Violation*,
Phys. Rev. Lett. **123** (2019) 031802, arXiv: 1811.00017 [hep-ph].

[37] D. Egana-Ugrinovic, S. Homiller and P. Meade, *Higgs bosons with large couplings to light quarks*,
Phys. Rev. D **100** (2019) 115041, arXiv: 1908.11376 [hep-ph].

[38] ATLAS Collaboration, *Direct constraint on the Higgs-charm coupling from a search for Higgs boson decays into charm quarks with the ATLAS detector*, Eur. Phys. J. C **82** (2022) 717,
arXiv: 2201.11428 [hep-ex].

[39] CMS Collaboration, *Search for Higgs Boson Decay to a Charm Quark-Antiquark Pair in Proton–Proton Collisions at $\sqrt{s} = 13\,TeV$*, Phys. Rev. Lett. **131** (2023) 061801,
arXiv: 2205.05550 [hep-ex].

[40] S. Heinemeyer et al., *Handbook of LHC Higgs Cross Sections: 3. Higgs Properties*,
CERN-2013-004 (2013), arXiv: 1307.1347 [hep-ph].

[41] ATLAS Collaboration, *The ATLAS Experiment at the CERN Large Hadron Collider*,
JINST **3** (2008) S08003.

[42] ATLAS Collaboration, *ATLAS Insertable B-Layer: Technical Design Report*,
ATLAS-TDR-19; CERN-LHCC-2010-013, 2010,
URL: https://cds.cern.ch/record/1291633, Addendum: ATLAS-TDR-19-ADD-1;
CERN-LHCC-2012-009, 2012, URL: https://cds.cern.ch/record/1451888.

[43] B. Abbott et al., *Production and integration of the ATLAS Insertable B-Layer*,
JINST **13** (2018) T05008, arXiv: 1803.00844 [physics.ins-det].

[44] G. Avoni et al., *The new LUCID-2 detector for luminosity measurement and monitoring in ATLAS*,
JINST **13** (2018) P07017.

[45] ATLAS Collaboration, *Performance of the ATLAS trigger system in 2015*,
Eur. Phys. J. C **77** (2017) 317, arXiv: 1611.09661 [hep-ex].

[46] ATLAS Collaboration, *Software and computing for Run 3 of the ATLAS experiment at the LHC*,
(2024), arXiv: 2404.06335 [hep-ex].

[47] ATLAS Collaboration,
ATLAS data quality operations and performance for 2015–2018 data-taking,
JINST **15** (2020) P04003, arXiv: 1911.04632 [physics.ins-det].

[48] ATLAS Collaboration, *Modelling and computational improvements to the simulation of single vector-boson plus jet processes for the ATLAS experiment*, JHEP **08** (2022) 089, arXiv: `2112.09588 [hep-ex]`.

[49] S. Frixione, P. Nason and C. Oleari, *Matching NLO QCD computations with parton shower simulations: the POWHEG method*, JHEP **11** (2007) 070, arXiv: `0709.2092 [hep-ph]`.

[50] S. Frixione, E. Laenen, P. Motylinski, C. White and B. R. Webber, *Single-top hadroproduction in association with a W boson*, JHEP **07** (2008) 029, arXiv: `0805.3067 [hep-ph]`.

[51] D. J. Lange, *The EvtGen particle decay simulation package*, Nucl. Instrum. Meth. A **462** (2001) 152.

[52] J. Butterworth et al., *PDF4LHC recommendations for LHC Run II*, J. Phys. G **43** (2016) 023001, arXiv: `1510.03865 [hep-ph]`.

[53] A. Denner, S. Dittmaier, S. Kallweit and A. Mück, *Electroweak corrections to Higgs-strahlung off W/Z bosons at the Tevatron and the LHC with Hawk*, JHEP **03** (2012) 075, arXiv: `1112.5142 [hep-ph]`.

[54] A. Denner, S. Dittmaier, S. Kallweit and A. Mück, *HAWK 2.0: A Monte Carlo program for Higgs production in vector-boson fusion and Higgs strahlung at hadron colliders*, Comput. Phys. Commun. **195** (2015) 161, arXiv: `1412.5390 [hep-ph]`.

[55] J. de Favereau de Jeneret et al., *High energy photon interactions at the LHC*, (2009), arXiv: `0908.2020 [hep-ph]`.

[56] S. Alioli, P. Nason, C. Oleari and E. Re, *A general framework for implementing NLO calculations in shower Monte Carlo programs: the POWHEG BOX*, JHEP **06** (2010) 043, arXiv: `1002.2581 [hep-ph]`.

[57] G. Cullen et al., *Automated one-loop calculations with GoSam*, Eur. Phys. J. C **72** (2012) 1889, arXiv: `1111.2034 [hep-ph]`.

[58] NNPDF Collaboration, R. D. Ball et al., *Parton distributions for the LHC run II*, JHEP **04** (2015) 040, arXiv: `1410.8849 [hep-ph]`.

[59] T. Sjöstrand, S. Mrenna and P. Skands, *A brief introduction to PYTHIA 8.1*, Comput. Phys. Commun. **178** (2008) 852, arXiv: `0710.3820 [hep-ph]`.

[60] ATLAS Collaboration, *Measurement of the Z/γ^* boson transverse momentum distribution in pp collisions at $\sqrt{s} = 7$ TeV with the ATLAS detector*, JHEP **09** (2014) 145, arXiv: `1406.3660 [hep-ex]`.

[61] M. L. Ciccolini, S. Dittmaier and M. Krämer, *Electroweak radiative corrections to associated WH and ZH production at hadron colliders*, Phys. Rev. D **68** (2003) 073003, arXiv: `hep-ph/0306234 [hep-ph]`.

[62] O. Brein, A. Djouadi and R. Harlander, *NNLO QCD corrections to the Higgs-strahlung processes at hadron colliders*, Phys. Lett. B **579** (2004) 149, arXiv: `hep-ph/0307206`.

[63] G. Ferrera, M. Grazzini and F. Tramontano, *Associated Higgs-W-Boson Production at Hadron Colliders: A Fully Exclusive QCD Calculation at NNLO*, Phys. Rev. Lett. **107** (2011) 152003, arXiv: `1107.1164 [hep-ph]`.

[64] O. Brein, R. V. Harlander, M. Wiesemann and T. Zirke,
Top-quark mediated effects in hadronic Higgs-Strahlung, Eur. Phys. J. C **72** (2012) 1868,
arXiv: 1111.0761 [hep-ph].

[65] G. Ferrera, M. Grazzini and F. Tramontano,
Higher-order QCD effects for associated WH production and decay at the LHC,
JHEP **04** (2014) 039, arXiv: 1312.1669 [hep-ph].

[66] G. Ferrera, M. Grazzini and F. Tramontano,
Associated ZH production at hadron colliders: The fully differential NNLO QCD calculation,
Phys. Lett. B **740** (2015) 51, arXiv: 1407.4747 [hep-ph].

[67] J. M. Campbell, R. K. Ellis and C. Williams, *Associated production of a Higgs boson at NNLO*,
JHEP **06** (2016) 179, arXiv: 1601.00658 [hep-ph].

[68] K. Hamilton, P. Nason and G. Zanderighi, *MINLO: multi-scale improved NLO*,
JHEP **10** (2012) 155, arXiv: 1206.3572 [hep-ph].

[69] G. Luisoni, P. Nason, C. Oleari and F. Tramontano, *HW$^{\pm}$/HZ + 0 and 1 jet at NLO with the
POWHEG BOX interfaced to GoSam and their merging within MiNLO*, JHEP **10** (2013) 083,
arXiv: 1306.2542 [hep-ph].

[70] L. Altenkamp, S. Dittmaier, R. V. Harlander, H. Rzehak and T. J. E. Zirke,
Gluon-induced Higgs-strahlung at next-to-leading order QCD, JHEP **02** (2013) 078,
arXiv: 1211.5015 [hep-ph].

[71] B. Hespel, F. Maltoni and E. Vryonidou,
Higgs and Z boson associated production via gluon fusion in the SM and the 2HDM,
JHEP **06** (2015) 065, arXiv: 1503.01656 [hep-ph].

[72] R. V. Harlander, A. Kulesza, V. Theeuwes and T. Zirke,
Soft gluon resummation for gluon-induced Higgs Strahlung, JHEP **11** (2014) 082,
arXiv: 1410.0217 [hep-ph].

[73] R. V. Harlander, S. Liebler and T. Zirke,
Higgs Strahlung at the Large Hadron Collider in the 2-Higgs-doublet model, JHEP **02** (2014) 023,
arXiv: 1307.8122 [hep-ph].

[74] O. Brein, R. V. Harlander and T. J. E. Zirke, *vh@nnlo – Higgs Strahlung at hadron colliders*,
Comput. Phys. Commun. **184** (2013) 998, arXiv: 1210.5347 [hep-ph].

[75] S. Frixione, G. Ridolfi and P. Nason,
A positive-weight next-to-leading-order Monte Carlo for heavy flavour hadroproduction,
JHEP **09** (2007) 126, arXiv: 0707.3088 [hep-ph].

[76] ATLAS Collaboration, *ATLAS Pythia 8 tunes to 7 TeV data*, ATL-PHYS-PUB-2014-021, 2014,
URL: https://cds.cern.ch/record/1966419.

[77] M. Czakon and A. Mitov,
Top++: A program for the calculation of the top-pair cross-section at hadron colliders,
Comput. Phys. Commun. **185** (2014) 2930, arXiv: 1112.5675 [hep-ph].

[78] S. Alioli, P. Nason, C. Oleari and E. Re,
NLO single-top production matched with shower in POWHEG: s- and t-channel contributions,
JHEP **09** (2009) 111, arXiv: 0907.4076 [hep-ph], Erratum: JHEP **02** (2010) 011.

[79] N. Kidonakis,
Next-to-next-to-leading logarithm resummation for s-channel single top quark production,
Phys. Rev. D **81** (2010) 054028, arXiv: `1001.5034 [hep-ph]`.

[80] J. Campbell, T. Neumann and Z. Sullivan, *Single-top-quark production in the t-channel at NNLO*,
JHEP **02** (2021) 040, arXiv: `2012.01574 [hep-ph]`.

[81] E. Re,
Single-top Wt-channel production matched with parton showers using the POWHEG method,
Eur. Phys. J. C **71** (2011) 1547, arXiv: `1009.2450 [hep-ph]`.

[82] N. Kidonakis,
Two-loop soft anomalous dimensions for single top quark associated production with a W^- or H^-,
Phys. Rev. D **82** (2010) 054018, arXiv: `1005.4451 [hep-ph]`.

[83] E. Bothmann et al., *Event generation with Sherpa 2.2*, SciPost Phys. **7** (2019) 034,
arXiv: `1905.09127 [hep-ph]`.

[84] F. Cascioli, P. Maierhöfer and S. Pozzorini, *Scattering Amplitudes with Open Loops*,
Phys. Rev. Lett. **108** (2012) 111601, arXiv: `1111.5206 [hep-ph]`.

[85] T. Gleisberg and S. Höche, *Comix, a new matrix element generator*, JHEP **12** (2008) 039,
arXiv: `0808.3674 [hep-ph]`.

[86] S. Schumann and F. Krauss,
A parton shower algorithm based on Catani–Seymour dipole factorisation, JHEP **03** (2008) 038,
arXiv: `0709.1027 [hep-ph]`.

[87] S. Höche, F. Krauss, M. Schönherr and F. Siegert,
QCD matrix elements + parton showers. The NLO case, JHEP **04** (2013) 027,
arXiv: `1207.5030 [hep-ph]`.

[88] S. Catani, L. Cieri, G. Ferrera, D. de Florian and M. Grazzini, *Vector Boson Production at Hadron Colliders: A Fully Exclusive QCD Calculation at Next-to-Next-to-Leading Order*,
Phys. Rev. Lett. **103** (2009) 082001, arXiv: `0903.2120 [hep-ph]`.

[89] ATLAS Collaboration, *The ATLAS Simulation Infrastructure*, Eur. Phys. J. C **70** (2010) 823,
arXiv: `1005.4568 [physics.ins-det]`.

[90] S. Agostinelli et al., *Geant4 – a simulation toolkit*, Nucl. Instrum. Meth. A **506** (2003) 250.

[91] ATLAS Collaboration, *The Pythia 8 A3 tune description of ATLAS minimum bias and inelastic measurements incorporating the Donnachie–Landshoff diffractive model*,
ATL-PHYS-PUB-2016-017, 2016, URL: `https://cds.cern.ch/record/2206965`.

[92] NNPDF Collaboration, R. D. Ball et al., *Parton distributions with LHC data*,
Nucl. Phys. B **867** (2013) 244, arXiv: `1207.1303 [hep-ph]`.

[93] ATLAS Collaboration, *Vertex Reconstruction Performance of the ATLAS Detector at $\sqrt{s} = 13$ TeV*,
ATL-PHYS-PUB-2015-026, 2015, URL: `https://cds.cern.ch/record/2037717`.

[94] ATLAS Collaboration, *Electron and photon performance measurements with the ATLAS detector using the 2015–2017 LHC proton–proton collision data*, JINST **14** (2019) P12006,
arXiv: `1908.00005 [hep-ex]`.

[95] ATLAS Collaboration, *Muon reconstruction and identification efficiency in ATLAS using the full Run 2 pp collision data set at $\sqrt{s} = 13$ TeV*, Eur. Phys. J. C **81** (2021) 578,
arXiv: `2012.00578 [hep-ex]`.

[96] ATLAS Collaboration, *Studies of the muon momentum calibration and performance of the ATLAS detector with pp collisions at $\sqrt{s}$ = 13 TeV*, Eur. Phys. J. C **83** (2023) 686, arXiv: 2212.07338 [hep-ex].

[97] ATLAS Collaboration, *Reconstruction, Energy Calibration, and Identification of Hadronically Decaying Tau Leptons in the ATLAS Experiment for Run-2 of the LHC*, ATL-PHYS-PUB-2015-045, 2015, URL: https://cds.cern.ch/record/2064383.

[98] ATLAS Collaboration, *Identification of hadronic tau lepton decays using neural networks in the ATLAS experiment*, ATL-PHYS-PUB-2019-033, 2019, URL: https://cds.cern.ch/record/2688062.

[99] ATLAS Collaboration, *Jet reconstruction and performance using particle flow with the ATLAS Detector*, Eur. Phys. J. C **77** (2017) 466, arXiv: 1703.10485 [hep-ex].

[100] M. Cacciari, G. P. Salam and G. Soyez, *The anti-k_t jet clustering algorithm*, JHEP **04** (2008) 063, arXiv: 0802.1189 [hep-ph].

[101] M. Cacciari, G. P. Salam and G. Soyez, *FastJet user manual*, Eur. Phys. J. C **72** (2012) 1896, arXiv: 1111.6097 [hep-ph].

[102] ATLAS Collaboration, *Jet energy scale and resolution measured in proton–proton collisions at $\sqrt{s}$ = 13 TeV with the ATLAS detector*, Eur. Phys. J. C **81** (2021) 689, arXiv: 2007.02645 [hep-ex].

[103] ATLAS Collaboration, *Performance of pile-up mitigation techniques for jets in pp collisions at $\sqrt{s}$ = 8 TeV using the ATLAS detector*, Eur. Phys. J. C **76** (2016) 581, arXiv: 1510.03823 [hep-ex].

[104] ATLAS Collaboration, *Forward jet vertex tagging using the particle flow algorithm*, ATL-PHYS-PUB-2019-026, 2019, URL: https://cds.cern.ch/record/2683100.

[105] ATLAS Collaboration, *ATLAS flavour-tagging algorithms for the LHC Run 2 pp collision dataset*, Eur. Phys. J. C **83** (2023) 681, arXiv: 2211.16345 [physics.data-an].

[106] ATLAS Collaboration, *ATLAS b-jet identification performance and efficiency measurement with $t\bar{t}$ events in pp collisions at $\sqrt{s}$ = 13 TeV*, Eur. Phys. J. C **79** (2019) 970, arXiv: 1907.05120 [hep-ex].

[107] ATLAS Collaboration, *Measurement of the c-jet mistagging efficiency in $t\bar{t}$ events using pp collision data at $\sqrt{s}$ = 13 TeV collected with the ATLAS detector*, Eur. Phys. J. C **82** (2022) 95, arXiv: 2109.10627 [hep-ex].

[108] ATLAS Collaboration, *Calibration of the light-flavour jet mistagging efficiency of the b-tagging algorithms with Z+jets events using 139 fb^{-1} of ATLAS proton–proton collision data at $\sqrt{s}$ = 13 TeV*, Eur. Phys. J. C **83** (2023) 728, arXiv: 2301.06319 [hep-ex].

[109] ATLAS Collaboration, *Topological cell clustering in the ATLAS calorimeters and its performance in LHC Run 1*, Eur. Phys. J. C **77** (2017) 490, arXiv: 1603.02934 [hep-ex].

[110] D. Krohn, J. Thaler and L.-T. Wang, *Jet Trimming*, JHEP **02** (2010) 084, arXiv: 0912.1342 [hep-ph].

[111] ATLAS Collaboration, *Optimisation of large-radius jet reconstruction for the ATLAS detector in* 13 *TeV proton–proton collisions*, Eur. Phys. J. C **81** (2021) 334, arXiv: 2009.04986 [hep-ex].

[112] ATLAS Collaboration, *In situ calibration of large-radius jet energy and mass in* 13 *TeV proton–proton collisions with the ATLAS detector*, Eur. Phys. J. C **79** (2019) 135, arXiv: 1807.09477 [hep-ex].

[113] D. Krohn, J. Thaler and L.-T. Wang, *Jets with Variable R*, JHEP **06** (2009) 059, arXiv: 0903.0392 [hep-ph].

[114] ATLAS Collaboration, *Variable Radius, Exclusive-k_T, and Center-of-Mass Subjet Reconstruction for Higgs($\to b\bar{b}$) Tagging in ATLAS*, ATL-PHYS-PUB-2017-010, 2017, URL: https://cds.cern.ch/record/2268678.

[115] ATLAS Collaboration, *Identification of boosted, hadronically decaying W bosons and comparisons with ATLAS data taken at $\sqrt{s}$ = 8 TeV*, Eur. Phys. J. C **76** (2016) 154, arXiv: 1510.05821 [hep-ex].

[116] M. Cacciari, G. P. Salam and G. Soyez, *The Catchment Area of Jets*, JHEP **04** (2008) 005, arXiv: 0802.1188 [hep-ph].

[117] ATLAS Collaboration, *Flavor Tagging Efficiency Parametrisations with Graph Neural Networks*, ATL-PHYS-PUB-2022-041, 2022, URL: https://cds.cern.ch/record/2825433.

[118] ATLAS Collaboration, *Evidence for the $H \to b\bar{b}$ decay with the ATLAS detector*, JHEP **12** (2017) 024, arXiv: 1708.03299 [hep-ex].

[119] ATLAS Collaboration, *Identification of boosted Higgs bosons decaying into b-quark pairs with the ATLAS detector at* 13 *TeV*, Eur. Phys. J. C **79** (2019) 836, arXiv: 1906.11005 [hep-ex].

[120] ATLAS Collaboration, *The performance of missing transverse momentum reconstruction and its significance with the ATLAS detector using* $140 fb^{-1}$ *of $\sqrt{s}$ = 13 TeV pp collisions*, (2024), arXiv: 2402.05858 [hep-ex].

[121] ATLAS Collaboration, *Selection of jets produced in* 13 *TeV proton–proton collisions with the ATLAS detector*, ATLAS-CONF-2015-029, 2015, URL: https://cds.cern.ch/record/2037702.

[122] ATLAS Collaboration, *Performance of electron and photon triggers in ATLAS during LHC Run 2*, Eur. Phys. J. C **80** (2020) 47, arXiv: 1909.00761 [hep-ex].

[123] ATLAS Collaboration, *Performance of the ATLAS muon triggers in Run 2*, JINST **15** (2020) P09015, arXiv: 2004.13447 [physics.ins-det].

[124] ATLAS Collaboration, *Performance of the missing transverse momentum triggers for the ATLAS detector during Run-2 data taking*, JHEP **08** (2020) 080, arXiv: 2005.09554 [hep-ex].

[125] J. R. Andersen et al., *Les Houches 2015: Physics at TeV Colliders Standard Model Working Group Report*, (2016), arXiv: 1605.04692 [hep-ph].

[126] N. Berger et al., *Simplified Template Cross Sections - Stage 1.1*, (2019), arXiv: 1906.02754 [hep-ph].

[127] A. Buckley, G. Callea, A. J. Larkoski and S. Marzani, *An Optimal Observable for Color Singlet Identification*, SciPost Phys. **9** (2020) 026, arXiv: 2006.10480 [hep-ph].

[128] ATLAS Collaboration,
Luminosity determination in pp collisions at $\sqrt{s} = 13\,TeV$ using the ATLAS detector at the LHC,
Eur. Phys. J. C **83** (2023) 982, arXiv: 2212.09379 [hep-ex].

[129] ATLAS Collaboration, *Measurement of the Inelastic Proton–Proton Cross Section at $\sqrt{s} = 13\,TeV$ with the ATLAS Detector at the LHC*, Phys. Rev. Lett. **117** (2016) 182002,
arXiv: 1606.02625 [hep-ex].

[130] K. Cranmer, J. Pavez and G. Louppe,
Approximating Likelihood Ratios with Calibrated Discriminative Classifiers, (2016),
arXiv: 1506.02169 [stat.AP], URL: https://arxiv.org/abs/1506.02169.

[131] S. Rizvi, M. Pettee and B. Nachman, *Learning likelihood ratios with neural network classifiers*,
JHEP **02** (2024) 136, arXiv: 2305.10500 [hep-ph].

[132] J. Alwall et al., *The automated computation of tree-level and next-to-leading order differential cross sections, and their matching to parton shower simulations*, JHEP **07** (2014) 079,
arXiv: 1405.0301 [hep-ph].

[133] R. Frederix and S. Frixione, *Merging meets matching in MC@NLO*, JHEP **12** (2012) 061,
arXiv: 1209.6215 [hep-ph].

[134] J. Bellm et al., *Herwig 7.0/Herwig++ 3.0 release note*, Eur. Phys. J. C **76** (2016) 196,
arXiv: 1512.01178 [hep-ph].

[135] ATLAS Collaboration, *Measurement of VH, $H \rightarrow b\bar{b}$ production as a function of the vector-boson transverse momentum in 13 TeV pp collisions with the ATLAS detector*, JHEP **05** (2019) 141,
arXiv: 1903.04618 [hep-ex].

[136] ATLAS Collaboration, *Evaluation of theoretical uncertainties for simplified template cross section measurements of V-associated production of the Higgs boson*, ATL-PHYS-PUB-2018-035, 2018,
URL: https://cds.cern.ch/record/2649241.

[137] J. Bendavid et al.,
Les Houches 2017: Physics at TeV Colliders Standard Model Working Group Report, (2018),
arXiv: 1803.07977 [hep-ph].

[138] S. Dittmaier et al., *Handbook of LHC Higgs Cross Sections: 1. Inclusive Observables*,
CERN-2011-002 (2011), arXiv: 1101.0593 [hep-ph].

[139] S. Dittmaier et al., *Handbook of LHC Higgs Cross Sections: 2. Differential Distributions*,
CERN-2012-002 (2012), arXiv: 1201.3084 [hep-ph].

[140] R. Barlow and C. Beeston, *Fitting using finite Monte Carlo samples*,
Comput. Phys. Commun. **77** (1993) 219.

[141] ATLAS Collaboration, *Search for the $b\bar{b}$ decay of the Standard Model Higgs boson in associated $(W/Z)H$ production with the ATLAS detector*, JHEP **01** (2015) 069,
arXiv: 1409.6212 [hep-ex].

[142] A. L. Read, *Presentation of search results: the CL_S technique*, J. Phys. G **28** (2002) 2693.

[143] G. Cowan, K. Cranmer, E. Gross and O. Vitells,
Asymptotic formulae for likelihood-based tests of new physics, Eur. Phys. J. C **71** (2011) 1554,
arXiv: 1007.1727 [physics.data-an], Erratum: Eur. Phys. J. C **73** (2013) 2501.

[144] ATLAS Collaboration, *Measurements of the production cross-section for a Z boson in association with b- or c-jets in proton–proton collisions at $\sqrt{s}$ = 13 TeV with the ATLAS detector*, Eur. Phys. J. C **84** (2024) 984, arXiv: `2403.15093 [hep-ex]`.

[145] ATLAS Collaboration, *Measurements of differential cross-sections in top-quark pair events with a high transverse momentum top quark and limits on beyond the Standard Model contributions to top-quark pair production with the ATLAS detector at $\sqrt{s}$ = 13 TeV*, JHEP **06** (2022) 063, arXiv: `2202.12134 [hep-ex]`.

[146] S. Baker and R. D. Cousins, *Clarification of the use of CHI-square and likelihood functions in fits to histograms*, Nucl. Instrum. Meth. **221** (1984) 437.

[147] R. D. Cousins, *Generalization of Chisquare Goodness-of Fit Test for Binned Data Using Saturated Models, with Application to Histograms*, 2013, URL: `https://www.physics.ucla.edu/~cousins/stats/cousins_saturated.pdf`.

[148] ATLAS Collaboration, *Combination of measurements of Higgs boson production in association with a W or Z boson in the $b\bar{b}$ decay channel with the ATLAS experiment at $\sqrt{s}$ = 13 TeV*, ATLAS-CONF-2021-051, 2021, URL: `https://cds.cern.ch/record/2782535`.

[149] ATLAS Collaboration, *Measurement of the total and differential Higgs boson production cross-sections at $\sqrt{s}$ = 13 TeV with the ATLAS detector by combining the $H \to ZZ^* \to 4\ell$ and $H \to \gamma\gamma$ decay channels*, JHEP **05** (2023) 028, arXiv: `2207.08615 [hep-ex]`.

[150] A. Bazavov et al., *Up-, down-, strange-, charm-, and bottom-quark masses from four-flavor lattice QCD*, Phys. Rev. D **98** (0218) 054517, arXiv: `1802.04248 [hep-ph]`.

[151] ATLAS Collaboration, *ATLAS Computing Acknowledgements*, ATL-SOFT-PUB-2023-001, 2023, URL: `https://cds.cern.ch/record/2869272`.

The ATLAS Collaboration

G. Aad [104], E. Aakvaag [17], B. Abbott [123], S. Abdelhameed [119a], K. Abeling [56], N.J. Abicht [50],
S.H. Abidi [30], M. Aboelela [45], A. Aboulhorma [36e], H. Abramowicz [155], H. Abreu [154],
Y. Abulaiti [120], B.S. Acharya [70a,70b,k], A. Ackermann [64a], C. Adam Bourdarios [4],
L. Adamczyk [87a], S.V. Addepalli [27], M.J. Addison [103], J. Adelman [118], A. Adiguzel [22c],
T. Adye [137], A.A. Affolder [139], Y. Afik [40], M.N. Agaras [13], J. Agarwala [74a,74b],
A. Aggarwal [102], C. Agheorghiesei [28c], F. Ahmadov [39,y], W.S. Ahmed [106], S. Ahuja [97],
X. Ai [63e], G. Aielli [77a,77b], A. Aikot [166], M. Ait Tamlihat [36e], B. Aitbenchikh [36a],
M. Akbiyik [102], T.P.A. Åkesson [100], A.V. Akimov [38], D. Akiyama [171], N.N. Akolkar [25],
S. Aktas [22a], K. Al Khoury [42], G.L. Alberghi [24b], J. Albert [168], P. Albicocco [54], G.L. Albouy [61],
S. Alderweireldt [53], Z.L. Alegria [124], M. Aleksa [37], I.N. Aleksandrov [39], C. Alexa [28b],
T. Alexopoulos [10], F. Alfonsi [24b], M. Algren [57], M. Alhroob [170], B. Ali [135], H.M.J. Ali [93,s],
S. Ali [32], S.W. Alibocus [94], M. Aliev [34c], G. Alimonti [72a], W. Alkakhi [56], C. Allaire [67],
B.M.M. Allbrooke [150], J.S. Allen [103], J.F. Allen [53], C.A. Allendes Flores [140f], P.P. Allport [21],
A. Aloisio [73a,73b], F. Alonso [92], C. Alpigiani [142], Z.M.K. Alsolami [93], M. Alvarez Estevez [101],
A. Alvarez Fernandez [102], M. Alves Cardoso [57], M.G. Alviggi [73a,73b], M. Aly [103],
Y. Amaral Coutinho [84b], A. Ambler [106], C. Amelung[37], M. Amerl [103], C.G. Ames [111],
D. Amidei [108], B. Amini [55], K.J. Amirie [158], S.P. Amor Dos Santos [133a], K.R. Amos [166],
D. Amperiadou [156], S. An[85], V. Ananiev [128], C. Anastopoulos [143], T. Andeen [11], J.K. Anders [37],
A.C. Anderson [60], S.Y. Andrean [48a,48b], A. Andreazza [72a,72b], S. Angelidakis [9], A. Angerami [42],
A.V. Anisenkov [38], A. Annovi [75a], C. Antel [57], E. Antipov [149], M. Antonelli [54], F. Anulli [76a],
M. Aoki [85], T. Aoki [157], M.A. Aparo [150], L. Aperio Bella [49], C. Appelt [19], A. Apyan [27],
S.J. Arbiol Val [88], C. Arcangeletti [54], A.T.H. Arce [52], J-F. Arguin [110], S. Argyropoulos [156],
J.-H. Arling [49], O. Arnaez [4], H. Arnold [149], G. Artoni [76a,76b], H. Asada [113], K. Asai [121],
S. Asai [157], N.A. Asbah [37], R.A. Ashby Pickering [170], K. Assamagan [30], R. Astalos [29a],
K.S.V. Astrand [100], S. Atashi [162], R.J. Atkin [34a], M. Atkinson[165], H. Atmani[36f],
P.A. Atmasiddha [131], K. Augsten [135], S. Auricchio [73a,73b], A.D. Auriol [21], V.A. Austrup [103],
G. Avolio [37], K. Axiotis [57], G. Azuelos [110,ad], D. Babal [29b], H. Bachacou [138], K. Bachas [156,o],
A. Bachiu [35], E. Bachmann [51], F. Backman [48a,48b], A. Badea [40], T.M. Baer [108],
P. Bagnaia [76a,76b], M. Bahmani [19], D. Bahner [55], K. Bai [126], J.T. Baines [137], L. Baines [96],
O.K. Baker [175], E. Bakos [16], D. Bakshi Gupta [8], L.E. Balabram Filho [84b], V. Balakrishnan [123],
R. Balasubramanian [4], E.M. Baldin [38], P. Balek [87a], E. Ballabene [24b,24a], F. Balli [138],
L.M. Baltes [64a], W.K. Balunas [33], J. Balz [102], I. Bamwidhi [119b], E. Banas [88],
M. Bandieramonte [132], A. Bandyopadhyay [25], S. Bansal [25], L. Barak [155], M. Barakat [49],
E.L. Barberio [107], D. Barberis [58b,58a], M. Barbero [104], M.Z. Barel [117], T. Barillari [112],
M-S. Barisits [37], T. Barklow [147], P. Baron [125], D.A. Baron Moreno [103], A. Baroncelli [63a],
A.J. Barr [129], J.D. Barr [98], F. Barreiro [101], J. Barreiro Guimarães da Costa [14], U. Barron [155],
M.G. Barros Teixeira [133a], S. Barsov [38], F. Bartels [64a], R. Bartoldus [147], A.E. Barton [93],
P. Bartos [29a], A. Basan [102], M. Baselga [50], A. Bassalat [67,b], M.J. Basso [159a], S. Bataju [45],
R. Bate [167], R.L. Bates [60], S. Batlamous[101], B. Batool [145], M. Battaglia [139], D. Battulga [19],
M. Bauce [76a,76b], M. Bauer [80], P. Bauer [25], L.T. Bazzano Hurrell [31], J.B. Beacham [52],
T. Beau [130], J.Y. Beaucamp [92], P.H. Beauchemin [161], P. Bechtle [25], H.P. Beck [20,n],
K. Becker [170], A.J. Beddall [83], V.A. Bednyakov [39], C.P. Bee [149], L.J. Beemster [16],
T.A. Beermann [37], M. Begalli [84d], M. Begel [30], A. Behera [149], J.K. Behr [49], J.F. Beirer [37],
F. Beisiegel [25], M. Belfkir [119b], G. Bella [155], L. Bellagamba [24b], A. Bellerive [35], P. Bellos [21],

K. Beloborodov [38], D. Benchekroun [36a], F. Bendebba [36a], Y. Benhammou [155],
K.C. Benkendorfer [62], L. Beresford [49], M. Beretta [54], E. Bergeaas Kuutmann [164], N. Berger [4],
B. Bergmann [135], J. Beringer [18a], G. Bernardi [5], C. Bernius [147], F.U. Bernlochner [25],
F. Bernon [37], A. Berrocal Guardia [13], T. Berry [97], P. Berta [136], A. Berthold [51], S. Bethke [112],
A. Betti [76a,76b], A.J. Bevan [96], N.K. Bhalla [55], S. Bhatta [149], D.S. Bhattacharya [169],
P. Bhattarai [147], Z.M. Bhatti [120], K.D. Bhide [55], V.S. Bhopatkar [124], R.M. Bianchi [132],
G. Bianco [24b,24a], O. Biebel [111], R. Bielski [126], M. Biglietti [78a], C.S. Billingsley [45], Y. Bimgdi [36f],
M. Bindi [56], A. Bingul [22b], C. Bini [76a,76b], G.A. Bird [33], M. Birman [172], M. Biros [136],
S. Biryukov [150], T. Bisanz [50], E. Bisceglie [44b,44a], J.P. Biswal [137], D. Biswas [145], I. Bloch [49],
A. Blue [60], U. Blumenschein [96], J. Blumenthal [102], V.S. Bobrovnikov [38], M. Boehler [55],
B. Boehm [169], D. Bogavac [37], A.G. Bogdanchikov [38], L.S. Boggia [130], C. Bohm [48a],
V. Boisvert [97], P. Bokan [37], T. Bold [87a], M. Bomben [5], M. Bona [96], M. Boonekamp [138],
C.D. Booth [97], A.G. Borbély [60], I.S. Bordulev [38], G. Borissov [93], D. Bortoletto [129],
D. Boscherini [24b], M. Bosman [13], J.D. Bossio Sola [37], K. Bouaouda [36a], N. Bouchhar [166],
L. Boudet [4], J. Boudreau [132], E.V. Bouhova-Thacker [93], D. Boumediene [41], R. Bouquet [58b,58a],
A. Boveia [122], J. Boyd [37], D. Boye [30], I.R. Boyko [39], L. Bozianu [57], J. Bracinik [21],
N. Brahimi [4], G. Brandt [174], O. Brandt [33], F. Braren [49], B. Brau [105], J.E. Brau [126],
R. Brener [172], L. Brenner [117], R. Brenner [164], S. Bressler [172], G. Brianti [79a,79b], D. Britton [60],
D. Britzger [112], I. Brock [25], R. Brock [109], G. Brooijmans [42], E.M. Brooks [159b], E. Brost [30],
L.M. Brown [168], L.E. Bruce [62], T.L. Bruckler [129], P.A. Bruckman de Renstrom [88], B. Brüers [49],
A. Bruni [24b], G. Bruni [24b], M. Bruschi [24b], N. Bruscino [76a,76b], T. Buanes [17], Q. Buat [142],
D. Buchin [112], A.G. Buckley [60], O. Bulekov [38], B.A. Bullard [147], S. Burdin [94], C.D. Burgard [50],
A.M. Burger [37], B. Burghgrave [8], O. Burlayenko [55], J. Burleson [165], J.T.P. Burr [33],
J.C. Burzynski [146], E.L. Busch [42], V. Büscher [102], P.J. Bussey [60], J.M. Butler [26], C.M. Buttar [60],
J.M. Butterworth [98], W. Buttinger [137], C.J. Buxo Vazquez [109], A.R. Buzykaev [38],
S. Cabrera Urbán [166], L. Cadamuro [67], D. Caforio [59], H. Cai [132], Y. Cai [14,114c], Y. Cai [114a],
V.M.M. Cairo [37], O. Cakir [3a], N. Calace [37], P. Calafiura [18a], G. Calderini [130], P. Calfayan [69],
G. Callea [60], L.P. Caloba [84b], D. Calvet [41], S. Calvet [41], M. Calvetti [75a,75b], R. Camacho Toro [130],
S. Camarda [37], D. Camarero Munoz [27], P. Camarri [77a,77b], M.T. Camerlingo [73a,73b],
D. Cameron [37], C. Camincher [168], M. Campanelli [98], A. Camplani [43], V. Canale [73a,73b],
A.C. Canbay [3a], E. Canonero [97], J. Cantero [166], Y. Cao [165], F. Capocasa [27], M. Capua [44b,44a],
A. Carbone [72a,72b], R. Cardarelli [77a], J.C.J. Cardenas [8], G. Carducci [44b,44a], T. Carli [37],
G. Carlino [73a], J.I. Carlotto [13], B.T. Carlson [132,p], E.M. Carlson [168,159a], J. Carmignani [94],
L. Carminati [72a,72b], A. Carnelli [138], M. Carnesale [37], S. Caron [116], E. Carquin [140f],
I.B. Carr [107], S. Carrá [72a], G. Carratta [24b,24a], A.M. Carroll [126], M.P. Casado [13,h], M. Caspar [49],
F.L. Castillo [4], L. Castillo Garcia [13], V. Castillo Gimenez [166], N.F. Castro [133a,133e],
A. Catinaccio [37], J.R. Catmore [128], T. Cavaliere [4], V. Cavaliere [30], N. Cavalli [24b,24a],
L.J. Caviedes Betancourt [23b], Y.C. Cekmecelioglu [49], E. Celebi [83], S. Cella [37],
M.S. Centonze [71a,71b], V. Cepaitis [57], K. Cerny [125], A.S. Cerqueira [84a], A. Cerri [150],
L. Cerrito [77a,77b], F. Cerutti [18a], B. Cervato [145], A. Cervelli [24b], G. Cesarini [54], S.A. Cetin [83],
D. Chakraborty [118], J. Chan [18a], W.Y. Chan [157], J.D. Chapman [33], E. Chapon [138],
B. Chargeishvili [153b], D.G. Charlton [21], M. Chatterjee [20], C. Chauhan [136], Y. Che [114a],
S. Chekanov [6], S.V. Chekulaev [159a], G.A. Chelkov [39,a], A. Chen [108], B. Chen [155], B. Chen [168],
H. Chen [114a], H. Chen [30], J. Chen [63c], J. Chen [146], M. Chen [129], S. Chen [89], S.J. Chen [114a],
X. Chen [63c], X. Chen [15,ac], Y. Chen [63a], C.L. Cheng [173], H.C. Cheng [65a], S. Cheong [147],
A. Cheplakov [39], E. Cheremushkina [49], E. Cherepanova [117], R. Cherkaoui El Moursli [36e],
E. Cheu [7], K. Cheung [66], L. Chevalier [138], V. Chiarella [54], G. Chiarelli [75a], N. Chiedde [104],

G. Chiodini [71a], A.S. Chisholm [21], A. Chitan [28b], M. Chitishvili [166], M.V. Chizhov [39,q], K. Choi [11], Y. Chou [142], E.Y.S. Chow [116], K.L. Chu [172], M.C. Chu [65a], X. Chu [14,114c], Z. Chubinidze [54], J. Chudoba [134], J.J. Chwastowski [88], D. Cieri [112], K.M. Ciesla [87a], V. Cindro [95], A. Ciocio [18a], F. Cirotto [73a,73b], Z.H. Citron [172], M. Citterio [72a], D.A. Ciubotaru[28b], A. Clark [57], P.J. Clark [53], N. Clarke Hall [98], C. Clarry [158], J.M. Clavijo Columbie [49], S.E. Clawson [49], C. Clement [48a,48b], Y. Coadou [104], M. Cobal [70a,70c], A. Coccaro [58b], R.F. Coelho Barrue [133a], R. Coelho Lopes De Sa [105], S. Coelli [72a], L.S. Colangeli [158], B. Cole [42], J. Collot [61], P. Conde Muiño [133a,133g], M.P. Connell [34c], S.H. Connell [34c], E.I. Conroy [129], F. Conventi [73a,ae], H.G. Cooke [21], A.M. Cooper-Sarkar [129], F.A. Corchia [24b,24a], A. Cordeiro Oudot Choi [130], L.D. Corpe [41], M. Corradi [76a,76b], F. Corriveau [106,x], A. Cortes-Gonzalez [19], M.J. Costa [166], F. Costanza [4], D. Costanzo [143], B.M. Cote [122], J. Couthures [4], G. Cowan [97], K. Cranmer [173], L. Cremer [50], D. Cremonini [24b,24a], S. Crépé-Renaudin [61], F. Crescioli [130], M. Cristinziani [145], M. Cristoforetti [79a,79b], V. Croft [117], J.E. Crosby [124], G. Crosetti [44b,44a], A. Cueto [101], H. Cui [98], Z. Cui [7], W.R. Cunningham [60], F. Curcio [166], J.R. Curran [53], P. Czodrowski [37], M.J. Da Cunha Sargedas De Sousa [58b,58a], J.V. Da Fonseca Pinto [84b], C. Da Via [103], W. Dabrowski [87a], T. Dado [37], S. Dahbi [152], T. Dai [108], D. Dal Santo [20], C. Dallapiccola [105], M. Dam [43], G. D'amen [30], V. D'Amico [111], J. Damp [102], J.R. Dandoy [35], D. Dannheim [37], G. D'anniballe [75b], M. Danninger [146], V. Dao [149], G. Darbo [58b], S.J. Das [30], F. Dattola [49], S. D'Auria [72a,72b], A. D'Avanzo [73a,73b], C. David [34a], T. Davidek [136], I. Dawson [96], H.A. Day-hall [135], K. De [8], R. De Asmundis [73a], N. De Biase [49], S. De Castro [24b,24a], N. De Groot [116], P. de Jong [117], H. De la Torre [118], A. De Maria [114a], A. De Salvo [76a], U. De Sanctis [77a,77b], F. De Santis [71a,71b], A. De Santo [150], J.B. De Vivie De Regie [61], J. Debevc [95], D.V. Dedovich[39], J. Degens [94], A.M. Deiana [45], F. Del Corso [24b,24a], J. Del Peso [101], L. Delagrange [130], F. Deliot [138], C.M. Delitzsch [50], M. Della Pietra [73a,73b], D. Della Volpe [57], A. Dell'Acqua [37], L. Dell'Asta [72a,72b], M. Delmastro [4], C.C. Delogu [102], P.A. Delsart [61], S. Demers [175], M. Demichev [39], S.P. Denisov [38], L. D'Eramo [41], D. Derendarz [88], F. Derue [130], P. Dervan [94], K. Desch [25], C. Deutsch [25], F.A. Di Bello [58b,58a], A. Di Ciaccio [77a,77b], L. Di Ciaccio [4], A. Di Domenico [76a,76b], C. Di Donato [73a,73b], A. Di Girolamo [37], G. Di Gregorio [37], A. Di Luca [79a,79b], B. Di Micco [78a,78b], R. Di Nardo [78a,78b], K.F. Di Petrillo [40], M. Diamantopoulou [35], F.A. Dias [117], T. Dias Do Vale [146], M.A. Diaz [140a,140b], F.G. Diaz Capriles [25], A.R. Didenko [39], M. Didenko [166], E.B. Diehl [108], S. Díez Cornell [49], C. Diez Pardos [145], C. Dimitriadi [164], A. Dimitrievska [21], J. Dingfelder [25], T. Dingley [129], I-M. Dinu [28b], S.J. Dittmeier [64b], F. Dittus [37], M. Divisek [136], B. Dixit [94], F. Djama [104], T. Djobava [153b], C. Doglioni [103,100], A. Dohnalova [29a], J. Dolejsi [136], Z. Dolezal [136], K. Domijan [87a], K.M. Dona [40], M. Donadelli [84d], B. Dong [109], J. Donini [41], A. D'Onofrio [73a,73b], M. D'Onofrio [94], J. Dopke [137], A. Doria [73a], N. Dos Santos Fernandes [133a], P. Dougan [103], M.T. Dova [92], A.T. Doyle [60], M.A. Draguet [129], M.P. Drescher [56], E. Dreyer [172], I. Drivas-koulouris [10], M. Drnevich [120], M. Drozdova [57], D. Du [63a], T.A. du Pree [117], F. Dubinin [38], M. Dubovsky [29a], E. Duchovni [172], G. Duckeck [111], O.A. Ducu [28b], D. Duda [53], A. Dudarev [37], E.R. Duden [27], M. D'uffizi [103], L. Duflot [67], M. Dührssen [37], I. Duminica [28g], A.E. Dumitriu [28b], M. Dunford [64a], S. Dungs [50], K. Dunne [48a,48b], A. Duperrin [104], H. Duran Yildiz [3a], M. Düren [59], A. Durglishvili [153b], B.L. Dwyer [118], G.I. Dyckes [18a], M. Dyndal [87a], B.S. Dziedzic [37], Z.O. Earnshaw [150], G.H. Eberwein [129], B. Eckerova [29a], S. Eggebrecht [56], E. Egidio Purcino De Souza [84e], L.F. Ehrke [57], G. Eigen [17], K. Einsweiler [18a], T. Ekelof [164], P.A. Ekman [100], S. El Farkh [36b], Y. El Ghazali [63a], H. El Jarrari [37], A. El Moussaouy [36a], V. Ellajosyula [164], M. Ellert [164], F. Ellinghaus [174], N. Ellis [37], J. Elmsheuser [30], M. Elsawy [119a], M. Elsing [37], D. Emeliyanov [137], Y. Enari [85], I. Ene [18a],

S. Epari [13], P.A. Erland [88], D. Ernani Martins Neto [88], M. Errenst [174], M. Escalier [67],
C. Escobar [166], E. Etzion [155], G. Evans [133a], H. Evans [69], L.S. Evans [97], A. Ezhilov [38],
S. Ezzarqtouni [36a], F. Fabbri [24b,24a], L. Fabbri [24b,24a], G. Facini [98], V. Fadeyev [139],
R.M. Fakhrutdinov [38], D. Fakoudis [102], S. Falciano [76a], L.F. Falda Ulhoa Coelho [37],
F. Fallavollita [112], G. Falsetti [44b,44a], J. Faltova [136], C. Fan [165], K.Y. Fan [65b], Y. Fan [14],
Y. Fang [14,114c], M. Fanti [72a,72b], M. Faraj [70a,70b], Z. Farazpay [99], A. Farbin [8], A. Farilla [78a],
T. Farooque [109], S.M. Farrington [53], F. Fassi [36e], D. Fassouliotis [9], M. Faucci Giannelli [77a,77b],
W.J. Fawcett [33], L. Fayard [67], P. Federic [136], P. Federicova [134], O.L. Fedin [38,a], M. Feickert [173],
L. Feligioni [104], D.E. Fellers [126], C. Feng [63b], Z. Feng [117], M.J. Fenton [162], L. Ferencz [49],
R.A.M. Ferguson [93], S.I. Fernandez Luengo [140f], P. Fernandez Martinez [68], M.J.V. Fernoux [104],
J. Ferrando [93], A. Ferrari [164], P. Ferrari [117,116], R. Ferrari [74a], D. Ferrere [57], C. Ferretti [108],
D. Fiacco [76a,76b], F. Fiedler [102], P. Fiedler [135], S. Filimonov [38], A. Filipčič [95], E.K. Filmer [159a],
F. Filthaut [116], M.C.N. Fiolhais [133a,133c,c], L. Fiorini [166], W.C. Fisher [109], T. Fitschen [103],
P.M. Fitzhugh [138], I. Fleck [145], P. Fleischmann [108], T. Flick [174], M. Flores [34d,aa],
L.R. Flores Castillo [65a], L. Flores Sanz De Acedo [37], F.M. Follega [79a,79b], N. Fomin [33],
J.H. Foo [158], A. Formica [138], A.C. Forti [103], E. Fortin [37], A.W. Fortman [18a], M.G. Foti [18a],
L. Fountas [9,i], D. Fournier [67], H. Fox [93], P. Francavilla [75a,75b], S. Francescato [62],
S. Franchellucci [57], M. Franchini [24b,24a], S. Franchino [64a], D. Francis [37], L. Franco [116],
V. Franco Lima [37], L. Franconi [49], M. Franklin [62], G. Frattari [27], Y.Y. Frid [155], J. Friend [60],
N. Fritzsche [37], A. Froch [55], D. Froidevaux [37], J.A. Frost [129], Y. Fu [63a],
S. Fuenzalida Garrido [140f], M. Fujimoto [104], K.Y. Fung [65a], E. Furtado De Simas Filho [84e],
M. Furukawa [157], J. Fuster [166], A. Gaa [56], A. Gabrielli [24b,24a], A. Gabrielli [158], P. Gadow [37],
G. Gagliardi [58b,58a], L.G. Gagnon [18a], S. Gaid [163], S. Galantzan [155], J. Gallagher [1],
E.J. Gallas [129], B.J. Gallop [137], K.K. Gan [122], S. Ganguly [157], Y. Gao [53],
F.M. Garay Walls [140a,140b], B. Garcia [30], C. García [166], A. Garcia Alonso [117],
A.G. Garcia Caffaro [175], J.E. García Navarro [166], M. Garcia-Sciveres [18a], G.L. Gardner [131],
R.W. Gardner [40], N. Garelli [161], D. Garg [81], R.B. Garg [147], J.M. Gargan [53], C.A. Garner [158],
C.M. Garvey [34a], V.K. Gassmann [161], G. Gaudio [74a], V. Gautam [13], P. Gauzzi [76a,76b],
J. Gavranovic [95], I.L. Gavrilenko [38], A. Gavrilyuk [38], C. Gay [167], G. Gaycken [126],
E.N. Gazis [10], A.A. Geanta [28b], C.M. Gee [139], A. Gekow [122], C. Gemme [58b], M.H. Genest [61],
A.D. Gentry [115], S. George [97], W.F. George [21], T. Geralis [47], P. Gessinger-Befurt [37],
M.E. Geyik [174], M. Ghani [170], K. Ghorbanian [96], A. Ghosal [145], A. Ghosh [162], A. Ghosh [7],
B. Giacobbe [24b], S. Giagu [76a,76b], T. Giani [117], A. Giannini [63a], S.M. Gibson [97], M. Gignac [139],
D.T. Gil [87b], A.K. Gilbert [87a], B.J. Gilbert [42], D. Gillberg [35], G. Gilles [117], L. Ginabat [130],
D.M. Gingrich [2,ad], M.P. Giordani [70a,70c], P.F. Giraud [138], G. Giugliarelli [70a,70c], D. Giugni [72a],
F. Giuli [77a,77b], I. Gkialas [9,i], L.K. Gladilin [38], C. Glasman [101], G.R. Gledhill [126], G. Glemža [49],
M. Glisic [126], I. Gnesi [44b], Y. Go [30], M. Goblirsch-Kolb [37], B. Gocke [50], D. Godin [110],
B. Gokturk [22a], S. Goldfarb [107], T. Golling [57], M.G.D. Gololo [34g], D. Golubkov [38],
J.P. Gombas [109], A. Gomes [133a,133b], G. Gomes Da Silva [145], A.J. Gomez Delegido [166],
R. Gonçalo [133a], L. Gonella [21], A. Gongadze [153c], F. Gonnella [21], J.L. Gonski [147],
R.Y. González Andana [53], S. González de la Hoz [166], R. Gonzalez Lopez [94],
C. Gonzalez Renteria [18a], M.V. Gonzalez Rodrigues [49], R. Gonzalez Suarez [164],
S. Gonzalez-Sevilla [57], L. Goossens [37], B. Gorini [37], E. Gorini [71a,71b], A. Gorišek [95],
T.C. Gosart [131], A.T. Goshaw [52], M.I. Gostkin [39], S. Goswami [124], C.A. Gottardo [37],
S.A. Gotz [111], M. Gouighri [36b], V. Goumarre [49], A.G. Goussiou [142], N. Govender [34c],
R.P. Grabarczyk [129], I. Grabowska-Bold [87a], K. Graham [35], E. Gramstad [128],
S. Grancagnolo [71a,71b], C.M. Grant [1,138], P.M. Gravila [28f], F.G. Gravili [71a,71b], H.M. Gray [18a],

54

M. Greco [71a,71b], M.J. Green [1], C. Grefe [25], A.S. Grefsrud [17], I.M. Gregor [49], K.T. Greif [162],
P. Grenier [147], S.G. Grewe[112], A.A. Grillo [139], K. Grimm [32], S. Grinstein [13,t], J.-F. Grivaz [67],
E. Gross [172], J. Grosse-Knetter [56], L. Guan [108], J.G.R. Guerrero Rojas [166], G. Guerrieri [37],
R. Gugel [102], J.A.M. Guhit [108], A. Guida [19], E. Guilloton [170], S. Guindon [37], F. Guo [14,114c],
J. Guo [63c], L. Guo [49], L. Guo [14], Y. Guo [108], A. Gupta [50], R. Gupta [132], S. Gurbuz [25],
S.S. Gurdasani [55], G. Gustavino [76a,76b], P. Gutierrez [123], L.F. Gutierrez Zagazeta [131],
M. Gutsche [51], C. Gutschow [98], C. Gwenlan [129], C.B. Gwilliam [94], E.S. Haaland [128],
A. Haas [120], M. Habedank [60], C. Haber [18a], H.K. Hadavand [8], A. Hadef [51], S. Hadzic [112],
A.I. Hagan [93], J.J. Hahn [145], E.H. Haines [98], M. Haleem [169], J. Haley [124], G.D. Hallewell [104],
L. Halser [20], K. Hamano [168], M. Hamer [25], E.J. Hampshire [97], J. Han [63b], L. Han [114a],
L. Han [63a], S. Han [18a], Y.F. Han [158], K. Hanagaki [85], M. Hance [139], D.A. Hangal [42],
H. Hanif [146], M.D. Hank [131], J.B. Hansen [43], P.H. Hansen [43], D. Harada [57], T. Harenberg [174],
S. Harkusha [176], M.L. Harris [105], Y.T. Harris [25], J. Harrison [13], N.M. Harrison [122],
P.F. Harrison[170], N.M. Hartman [112], N.M. Hartmann [111], R.Z. Hasan [97,137], Y. Hasegawa [144],
F. Haslbeck [129], S. Hassan [17], R. Hauser [109], C.M. Hawkes [21], R.J. Hawkings [37],
Y. Hayashi [157], D. Hayden [109], C. Hayes [108], R.L. Hayes [117], C.P. Hays [129], J.M. Hays [96],
H.S. Hayward [94], F. He [63a], M. He [14,114c], Y. He [49], Y. He [98], N.B. Heatley [96], V. Hedberg [100],
A.L. Heggelund [128], N.D. Hehir [96,*], C. Heidegger [55], K.K. Heidegger [55], J. Heilman [35],
S. Heim [49], T. Heim [18a], J.G. Heinlein [131], J.J. Heinrich [126], L. Heinrich [112,ab], J. Hejbal [134],
A. Held [173], S. Hellesund [17], C.M. Helling [167], S. Hellman [48a,48b], R.C.W. Henderson[93],
L. Henkelmann [33], A.M. Henriques Correia[37], H. Herde [100], Y. Hernández Jiménez [149],
L.M. Herrmann [25], T. Herrmann [51], G. Herten [55], R. Hertenberger [111], L. Hervas [37],
M.E. Hesping [102], N.P. Hessey [159a], J. Hessler [112], M. Hidaoui [36b], N. Hidic [136], E. Hill [158],
S.J. Hillier [21], J.R. Hinds [109], F. Hinterkeuser [25], M. Hirose [127], S. Hirose [160],
D. Hirschbuehl [174], T.G. Hitchings [103], B. Hiti [95], J. Hobbs [149], R. Hobincu [28e], N. Hod [172],
M.C. Hodgkinson [143], B.H. Hodkinson [129], A. Hoecker [37], D.D. Hofer [108], J. Hofer [166],
T. Holm [25], M. Holzbock [37], L.B.A.H. Hommels [33], B.P. Honan [103], J.J. Hong [69], J. Hong [63c],
T.M. Hong [132], B.H. Hooberman [165], W.H. Hopkins [6], M.C. Hoppesch [165], Y. Horii [113],
M.E. Horstmann [112], S. Hou [152], A.S. Howard [95], J. Howarth [60], J. Hoya [6], M. Hrabovsky [125],
A. Hrynevich [49], T. Hryn'ova [4], P.J. Hsu [66], S.-C. Hsu [142], T. Hsu [67], M. Hu [18a], Q. Hu [63a],
S. Huang [33], X. Huang [14,114c], Y. Huang [143], Y. Huang [102], Y. Huang [14], Z. Huang [103],
Z. Hubacek [135], M. Huebner [25], F. Huegging [25], T.B. Huffman [129],
M. Hufnagel Maranha De Faria[84a], C.A. Hugli [49], M. Huhtinen [37], S.K. Huiberts [17],
R. Hulsken [106], N. Huseynov [12,f], J. Huston [109], J. Huth [62], R. Hyneman [147], G. Iacobucci [57],
G. Iakovidis [30], L. Iconomidou-Fayard [67], J.P. Iddon [37], P. Iengo [73a,73b], R. Iguchi [157],
Y. Iiyama [157], T. Iizawa [129], Y. Ikegami [85], N. Ilic [158], H. Imam [84c], G. Inacio Goncalves [84d],
T. Ingebretsen Carlson [48a,48b], J.M. Inglis [96], G. Introzzi [74a,74b], M. Iodice [78a], V. Ippolito [76a,76b],
R.K. Irwin [94], M. Ishino [157], W. Islam [173], C. Issever [19], S. Istin [22a,ah], H. Ito [171],
R. Iuppa [79a,79b], A. Ivina [172], J.M. Izen [46], V. Izzo [73a], P. Jacka [134], P. Jackson [1],
C.S. Jagfeld [111], G. Jain [159a], P. Jain [49], K. Jakobs [55], T. Jakoubek [172], J. Jamieson [60],
W. Jang [157], M. Javurkova [105], P. Jawahar [103], L. Jeanty [126], J. Jejelava [153a,z], P. Jenni [55,e],
C.E. Jessiman [35], C. Jia [63b], H. Jia [167], J. Jia [149], X. Jia [14,114c], Z. Jia [114a], C. Jiang [53],
S. Jiggins [49], J. Jimenez Pena [13], S. Jin [114a], A. Jinaru [28b], O. Jinnouchi [141], P. Johansson [143],
K.A. Johns [7], J.W. Johnson [139], F.A. Jolly [49], D.M. Jones [150], E. Jones [49], K.S. Jones[8],
P. Jones [33], R.W.L. Jones [93], T.J. Jones [94], H.L. Joos [56,37], R. Joshi [122], J. Jovicevic [16],
X. Ju [18a], J.J. Junggeburth [105], T. Junkermann [64a], A. Juste Rozas [13,t], M.K. Juzek [88],
S. Kabana [140e], A. Kaczmarska [88], M. Kado [112], H. Kagan [122], M. Kagan [147], A. Kahn [131],

55

C. Kahra [102], T. Kaji [157], E. Kajomovitz [154], N. Kakati [172], I. Kalaitzidou [55], C.W. Kalderon [30], N.J. Kang [139], D. Kar [34g], K. Karava [129], M.J. Kareem [159b], E. Karentzos [55], O. Karkout [117], S.N. Karpov [39], Z.M. Karpova [39], V. Kartvelishvili [93], A.N. Karyukhin [38], E. Kasimi [156], J. Katzy [49], S. Kaur [35], K. Kawade [144], M.P. Kawale [123], C. Kawamoto [89], T. Kawamoto [63a], E.F. Kay [37], F.I. Kaya [161], S. Kazakos [109], V.F. Kazanin [38], Y. Ke [149], J.M. Keaveney [34a], R. Keeler [168], G.V. Kehris [62], J.S. Keller [35], J.J. Kempster [150], O. Kepka [134], B.P. Kerridge [137], S. Kersten [174], B.P. Kerševan [95], L. Keszeghova [29a], S. Ketabchi Haghighat [158], R.A. Khan [132], A. Khanov [124], A.G. Kharlamov [38], T. Kharlamova [38], E.E. Khoda [142], M. Kholodenko [133a], T.J. Khoo [19], G. Khoriauli [169], J. Khubua [153b,*], Y.A.R. Khwaira [130], B. Kibirige[34g], D. Kim [6], D.W. Kim [48a,48b], Y.K. Kim [40], N. Kimura [98], M.K. Kingston [56], A. Kirchhoff [56], C. Kirfel [25], F. Kirfel [25], J. Kirk [137], A.E. Kiryunin [112], S. Kita [160], C. Kitsaki [10], O. Kivernyk [25], M. Klassen [161], C. Klein [35], L. Klein [169], M.H. Klein [45], S.B. Klein [57], U. Klein [94], A. Klimentov [30], T. Klioutchnikova [37], P. Kluit [117], S. Kluth [112], E. Kneringer [80], T.M. Knight [158], A. Knue [50], D. Kobylianskii [172], S.F. Koch [129], M. Kocian [147], P. Kodyš [136], D.M. Koeck [126], P.T. Koenig [25], T. Koffas [35], O. Kolay [51], I. Koletsou [4], T. Komarek [88], K. Köneke [55], A.X.Y. Kong [1], T. Kono [121], N. Konstantinidis [98], P. Kontaxakis [57], B. Konya [100], R. Kopeliansky [42], S. Koperny [87a], K. Korcyl [88], K. Kordas [156,d], A. Korn [98], S. Korn [56], I. Korolkov [13], N. Korotkova [38], B. Kortman [117], O. Kortner [112], S. Kortner [112], W.H. Kostecka [118], V.V. Kostyukhin [145], A. Kotsokechagia [37], A. Kotwal [52], A. Koulouris [37], A. Kourkoumeli-Charalampidi [74a,74b], C. Kourkoumelis [9], E. Kourlitis [112,ab], O. Kovanda [126], R. Kowalewski [168], W. Kozanecki [126], A.S. Kozhin [38], V.A. Kramarenko [38], G. Kramberger [95], P. Kramer [102], M.W. Krasny [130], A. Krasznahorkay [37], A.C. Kraus [118], J.W. Kraus [174], J.A. Kremer [49], T. Kresse [51], L. Kretschmann [174], J. Kretzschmar [94], K. Kreul [19], P. Krieger [158], M. Krivos [136], K. Krizka [21], K. Kroeninger [50], H. Kroha [112], J. Kroll [134], J. Kroll [131], K.S. Krowpman [109], U. Kruchonak [39], H. Krüger [25], N. Krumnack[82], M.C. Kruse [52], O. Kuchinskaia [38], S. Kuday [3a], S. Kuehn [37], R. Kuesters [55], T. Kuhl [49], V. Kukhtin [39], Y. Kulchitsky [38,a], S. Kuleshov [140d,140b], M. Kumar [34g], N. Kumari [49], P. Kumari [159b], A. Kupco [134], T. Kupfer[50], A. Kupich [38], O. Kuprash [55], H. Kurashige [86], L.L. Kurchaninov [159a], O. Kurdysh [67], Y.A. Kurochkin [38], A. Kurova [38], M. Kuze [141], A.K. Kvam [105], J. Kvita [125], T. Kwan [106], N.G. Kyriacou [108], L.A.O. Laatu [104], C. Lacasta [166], F. Lacava [76a,76b], H. Lacker [19], D. Lacour [130], N.N. Lad [98], E. Ladygin [39], A. Lafarge [41], B. Laforge [130], T. Lagouri [175], F.Z. Lahbabi [36a], S. Lai [56], J.E. Lambert [168], S. Lammers [69], W. Lampl [7], C. Lampoudis [156,d], G. Lamprinoudis [102], A.N. Lancaster [118], E. Lançon [30], U. Landgraf [55], M.P.J. Landon [96], V.S. Lang [55], O.K.B. Langrekken [128], A.J. Lankford [162], F. Lanni [37], K. Lantzsch [25], A. Lanza [74a], M. Lanzac Berrocal [166], J.F. Laporte [138], T. Lari [72a], F. Lasagni Manghi [24b], M. Lassnig [37], V. Latonova [134], A. Laurier [154], S.D. Lawlor [143], Z. Lawrence [103], R. Lazaridou[170], M. Lazzaroni [72a,72b], B. Le[103], H.D.M. Le [109], E.M. Le Boulicaut [175], L.T. Le Pottier [18a], B. Leban [24b,24a], A. Lebedev [82], M. LeBlanc [103], F. Ledroit-Guillon [61], S.C. Lee [152], S. Lee [48a,48b], T.F. Lee [94], L.L. Leeuw [34c], H.P. Lefebvre [97], M. Lefebvre [168], C. Leggett [18a], G. Lehmann Miotto [37], M. Leigh [57], W.A. Leight [105], W. Leinonen [116], A. Leisos [156,r], M.A.L. Leite [84c], C.E. Leitgeb [19], R. Leitner [136], K.J.C. Leney [45], T. Lenz [25], S. Leone [75a], C. Leonidopoulos [53], A. Leopold [148], R. Les [109], C.G. Lester [33], M. Levchenko [38], J. Levêque [4], L.J. Levinson [172], G. Levrini [24b,24a], M.P. Lewicki [88], C. Lewis [142], D.J. Lewis [4], L. Lewitt [143], A. Li [30], B. Li [63b], C. Li[63a], C-Q. Li [112], H. Li [63a], H. Li [63b], H. Li [114a], H. Li [15], H. Li [63b], J. Li [63c], K. Li [14], L. Li [63c], M. Li [14,114c], S. Li [14,114c], S. Li [63d,63c], T. Li [5], X. Li [106], Z. Li [157], Z. Li [14,114c], Z. Li [63a], S. Liang [14,114c], Z. Liang [14], M. Liberatore [138], B. Liberti [77a], K. Lie [65c], J. Lieber Marin [84e],

56

H. Lien [69], H. Lin [108], K. Lin [109], L. Linden [111], R.E. Lindley [7], J.H. Lindon [2], J. Ling [62],
E. Lipeles [131], A. Lipniacka [17], A. Lister [167], J.D. Little [69], B. Liu [14], B.X. Liu [114b],
D. Liu [63d,63c], E.H.L. Liu [21], J.B. Liu [63a], J.K.K. Liu [33], K. Liu [63d], K. Liu [63d,63c], M. Liu [63a],
M.Y. Liu [63a], P. Liu [14], Q. Liu [63d,142,63c], X. Liu [63a], X. Liu [63b], Y. Liu [114b,114c], Y.L. Liu [63b],
Y.W. Liu [63a], S.L. Lloyd [96], E.M. Lobodzinska [49], P. Loch [7], E. Lodhi [158], T. Lohse [19],
K. Lohwasser [143], E. Loiacono [49], J.D. Lomas [21], J.D. Long [42], I. Longarini [162], R. Longo [165],
I. Lopez Paz [68], A. Lopez Solis [49], N.A. Lopez-canelas [7], N. Lorenzo Martinez [4], A.M. Lory [111],
M. Losada [119a], G. Löschcke Centeno [150], O. Loseva [38], X. Lou [48a,48b], X. Lou [14,114c],
A. Lounis [67], P.A. Love [93], G. Lu [14,114c], M. Lu [67], S. Lu [131], Y.J. Lu [66], H.J. Lubatti [142],
C. Luci [76a,76b], F.L. Lucio Alves [114a], F. Luehring [69], O. Lukianchuk [67], B.S. Lunday [131],
O. Lundberg [148], B. Lund-Jensen [148,*], N.A. Luongo [6], M.S. Lutz [37], A.B. Lux [26], D. Lynn [30],
R. Lysak [134], E. Lytken [100], V. Lyubushkin [39], T. Lyubushkina [39], M.M. Lyukova [149],
M.Firdaus M. Soberi [53], H. Ma [30], K. Ma [63a], L.L. Ma [63b], W. Ma [63a], Y. Ma [124],
J.C. MacDonald [102], P.C. Machado De Abreu Farias [84e], R. Madar [41], T. Madula [98], J. Maeda [86],
T. Maeno [30], H. Maguire [143], V. Maiboroda [138], A. Maio [133a,133b,133d], K. Maj [87a],
O. Majersky [49], S. Majewski [126], N. Makovec [67], V. Maksimovic [16], B. Malaescu [130],
Pa. Malecki [88], V.P. Maleev [38], F. Malek [61,m], M. Mali [95], D. Malito [97], U. Mallik [81,*],
S. Maltezos [10], S. Malyukov [39], J. Mamuzic [13], G. Mancini [54], M.N. Mancini [27], G. Manco [74a,74b],
J.P. Mandalia [96], S.S. Mandarry [150], I. Mandić [95], L. Manhaes de Andrade Filho [84a],
I.M. Maniatis [172], J. Manjarres Ramos [91], D.C. Mankad [172], A. Mann [111], S. Manzoni [37],
L. Mao [63c], X. Mapekula [34c], A. Marantis [156,r], G. Marchiori [5], M. Marcisovsky [134],
C. Marcon [72a], M. Marinescu [21], S. Marium [49], M. Marjanovic [123], A. Markhoos [55],
M. Markovitch [67], E.J. Marshall [93], Z. Marshall [18a], S. Marti-Garcia [166], J. Martin [98],
T.A. Martin [137], V.J. Martin [53], B. Martin dit Latour [17], L. Martinelli [76a,76b], M. Martinez [13,t],
P. Martinez Agullo [166], V.I. Martinez Outschoorn [105], P. Martinez Suarez [13], S. Martin-Haugh [137],
G. Martinovicova [136], V.S. Martoiu [28b], A.C. Martyniuk [98], A. Marzin [37], D. Mascione [79a,79b],
L. Masetti [102], J. Masik [103], A.L. Maslennikov [38], S.L. Mason [42], P. Massarotti [73a,73b],
P. Mastrandrea [75a,75b], A. Mastroberardino [44b,44a], T. Masubuchi [127], T.T. Mathew [126],
T. Mathisen [164], J. Matousek [136], D.M. Mattern [50], J. Maurer [28b], T. Maurin [60], A.J. Maury [67],
B. Maček [95], D.A. Maximov [38], A.E. May [103], R. Mazini [152], I. Maznas [118], M. Mazza [109],
S.M. Mazza [139], E. Mazzeo [72a,72b], C. Mc Ginn [30], J.P. Mc Gowan [168], S.P. Mc Kee [108],
C.A. Mc Lean [6], C.C. McCracken [167], E.F. McDonald [107], A.E. McDougall [117],
J.A. Mcfayden [150], R.P. McGovern [131], R.P. Mckenzie [34g], T.C. Mclachlan [49], D.J. Mclaughlin [98],
S.J. McMahon [137], C.M. Mcpartland [94], R.A. McPherson [168,x], S. Mehlhase [111], A. Mehta [94],
D. Melini [166], B.R. Mellado Garcia [34g], A.H. Melo [56], F. Meloni [49],
A.M. Mendes Jacques Da Costa [103], H.Y. Meng [158], L. Meng [93], S. Menke [112], M. Mentink [37],
E. Meoni [44b,44a], G. Mercado [118], S. Merianos [156], C. Merlassino [70a,70c], L. Merola [73a,73b],
C. Meroni [72a,72b], J. Metcalfe [6], A.S. Mete [6], E. Meuser [102], C. Meyer [69], J-P. Meyer [138],
R.P. Middleton [137], L. Mijović [53], G. Mikenberg [172], M. Mikestikova [134], M. Mikuž [95],
H. Mildner [102], A. Milic [37], D.W. Miller [40], E.H. Miller [147], L.S. Miller [35], A. Milov [172],
D.A. Milstead [48a,48b], T. Min [114a], A.A. Minaenko [38], I.A. Minashvili [153b], L. Mince [60],
A.I. Mincer [120], B. Mindur [87a], M. Mineev [39], Y. Mino [89], L.M. Mir [13], M. Miralles Lopez [60],
M. Mironova [18a], M.C. Missio [116], A. Mitra [170], V.A. Mitsou [166], Y. Mitsumori [113], O. Miu [158],
P.S. Miyagawa [96], T. Mkrtchyan [64a], M. Mlinarevic [98], T. Mlinarevic [98], M. Mlynarikova [37],
S. Mobius [20], P. Mogg [111], M.H. Mohamed Farook [115], A.F. Mohammed [14,114c], S. Mohapatra [42],
G. Mokgatitswane [34g], L. Moleri [172], B. Mondal [145], S. Mondal [135], K. Mönig [49],
E. Monnier [104], L. Monsonis Romero [166], J. Montejo Berlingen [13], A. Montella [48a,48b],

M. Montella [122], F. Montereali [78a,78b], F. Monticelli [92], S. Monzani [70a,70c], A. Morancho Tarda [43],
N. Morange [67], A.L. Moreira De Carvalho [49], M. Moreno Llácer [166], C. Moreno Martinez [57],
J.M. Moreno Perez[23b], P. Morettini [58b], S. Morgenstern [37], M. Morii [62], M. Morinaga [157],
M. Moritsu [90], F. Morodei [76a,76b], P. Moschovakos [37], B. Moser [129], M. Mosidze [153b],
T. Moskalets [45], P. Moskvitina [116], J. Moss [32,j], P. Moszkowicz [87a], A. Moussa [36d],
Y. Moyal [172], E.J.W. Moyse [105], O. Mtintsilana [34g], S. Muanza [104], J. Mueller [132],
D. Muenstermann [93], R. Müller [37], G.A. Mullier [164], A.J. Mullin[33], J.J. Mullin[131], A.E. Mulski [62],
D.P. Mungo [158], D. Munoz Perez [166], F.J. Munoz Sanchez [103], M. Murin [103], W.J. Murray [170,137],
M. Muškinja [95], C. Mwewa [30], A.G. Myagkov [38,a], A.J. Myers [8], G. Myers [108], M. Myska [135],
B.P. Nachman [18a], O. Nackenhorst [50], K. Nagai [129], K. Nagano [85], R. Nagasaka[157],
J.L. Nagle [30,af], E. Nagy [104], A.M. Nairz [37], Y. Nakahama [85], K. Nakamura [85], K. Nakkalil [5],
H. Nanjo [127], E.A. Narayanan [45], I. Naryshkin [38], L. Nasella [72a,72b], M. Naseri [35], S. Nasri [119b],
C. Nass [25], G. Navarro [23a], J. Navarro-Gonzalez [166], R. Nayak [155], A. Nayaz [19],
P.Y. Nechaeva [38], S. Nechaeva [24b,24a], F. Nechansky [134], L. Nedic [129], T.J. Neep [21],
A. Negri [74a,74b], M. Negrini [24b], C. Nellist [117], C. Nelson [106], K. Nelson [108], S. Nemecek [134],
M. Nessi [37,g], M.S. Neubauer [165], F. Neuhaus [102], J. Neundorf [49], J. Newell [94], P.R. Newman [21],
C.W. Ng [132], Y.W.Y. Ng [49], B. Ngair [119a], H.D.N. Nguyen [110], R.B. Nickerson [129],
R. Nicolaidou [138], J. Nielsen [139], M. Niemeyer [56], J. Niermann [56], N. Nikiforou [37],
V. Nikolaenko [38,a], I. Nikolic-Audit [130], K. Nikolopoulos [21], P. Nilsson [30], I. Ninca [49],
G. Ninio [155], A. Nisati [76a], N. Nishu [2], R. Nisius [112], N. Nitika [70a,70c], J-E. Nitschke [51],
E.K. Nkadimeng [34g], T. Nobe [157], T. Nommensen [151], M.B. Norfolk [143], B.J. Norman [35],
M. Noury [36a], J. Novak [95], T. Novak [95], L. Novotny [135], R. Novotny [115], L. Nozka [125],
K. Ntekas [162], N.M.J. Nunes De Moura Junior [84b], J. Ocariz [130], A. Ochi [86], I. Ochoa [133a],
S. Oerdek [49,u], J.T. Offermann [40], A. Ogrodnik [136], A. Oh [103], C.C. Ohm [148], H. Oide [85],
R. Oishi [157], M.L. Ojeda [37], Y. Okumura [157], L.F. Oleiro Seabra [133a], I. Oleksiyuk [57],
S.A. Olivares Pino [140d], G. Oliveira Correa [13], D. Oliveira Damazio [30], J.L. Oliver [162],
Ö.O. Öncel [55], A.P. O'Neill [20], A. Onofre [133a,133e], P.U.E. Onyisi [11], M.J. Oreglia [40],
G.E. Orellana [92], D. Orestano [78a,78b], N. Orlando [13], R.S. Orr [158], L.M. Osojnak [131],
R. Ospanov [63a], Y. Osumi[113], G. Otero y Garzon [31], H. Otono [90], P.S. Ott [64a], G.J. Ottino [18a],
M. Ouchrif [36d], F. Ould-Saada [128], T. Ovsiannikova [142], M. Owen [60], R.E. Owen [137],
V.E. Ozcan [22a], F. Ozturk [88], N. Ozturk [8], S. Ozturk [83], H.A. Pacey [129], A. Pacheco Pages [13],
C. Padilla Aranda [13], G. Padovano [76a,76b], S. Pagan Griso [18a], G. Palacino [69], A. Palazzo [71a,71b],
J. Pampel [25], J. Pan [175], T. Pan [65a], D.K. Panchal [11], C.E. Pandini [117], J.G. Panduro Vazquez [137],
H.D. Pandya [1], H. Pang [15], P. Pani [49], G. Panizzo [70a,70c], L. Panwar [130], L. Paolozzi [57],
S. Parajuli [165], A. Paramonov [6], C. Paraskevopoulos [54], D. Paredes Hernandez [65b],
A. Pareti [74a,74b], K.R. Park [42], T.H. Park [158], M.A. Parker [33], F. Parodi [58b,58a], E.W. Parrish [118],
V.A. Parrish [53], J.A. Parsons [42], U. Parzefall [55], B. Pascual Dias [110], L. Pascual Dominguez [101],
E. Pasqualucci [76a], S. Passaggio [58b], F. Pastore [97], P. Patel [88], U.M. Patel [52], J.R. Pater [103],
T. Pauly [37], F. Pauwels [136], C.I. Pazos [161], M. Pedersen [128], R. Pedro [133a], S.V. Peleganchuk [38],
O. Penc [37], E.A. Pender [53], S. Peng [15], G.D. Penn [175], K.E. Penski [111], M. Penzin [38],
B.S. Peralva [84d], A.P. Pereira Peixoto [142], L. Pereira Sanchez [147], D.V. Perepelitsa [30,af],
G. Perera [105], E. Perez Codina [159a], M. Perganti [10], H. Pernegger [37], S. Perrella [76a,76b],
O. Perrin [41], K. Peters [49], R.F.Y. Peters [103], B.A. Petersen [37], T.C. Petersen [43], E. Petit [104],
V. Petousis [135], C. Petridou [156,d], T. Petru [136], A. Petrukhin [145], M. Pettee [18a], A. Petukhov [38],
K. Petukhova [37], R. Pezoa [140f], L. Pezzotti [37], G. Pezzullo [175], A.J. Pfleger [37], T.M. Pham [173],
T. Pham [107], P.W. Phillips [137], G. Piacquadio [149], E. Pianori [18a], F. Piazza [126], R. Piegaia [31],
D. Pietreanu [28b], A.D. Pilkington [103], M. Pinamonti [70a,70c], J.L. Pinfold [2],

B.C. Pinheiro Pereira [133a], J. Pinol Bel [13], A.E. Pinto Pinoargote [138,138], L. Pintucci [70a,70c],
K.M. Piper [150], A. Pirttikoski [57], D.A. Pizzi [35], L. Pizzimento [65b], A. Pizzini [117],
M.-A. Pleier [30], V. Pleskot [136], E. Plotnikova [39], G. Poddar [96], R. Poettgen [100], L. Poggioli [130],
I. Pokharel [56], S. Polacek [136], G. Polesello [74a], A. Poley [146,159a], A. Polini [24b], C.S. Pollard [170],
Z.B. Pollock [122], E. Pompa Pacchi [76a,76b], N.I. Pond [98], D. Ponomarenko [69], L. Pontecorvo [37],
S. Popa [28a], G.A. Popeneciu [28d], A. Poreba [37], D.M. Portillo Quintero [159a], S. Pospisil [135],
M.A. Postill [143], P. Postolache [28c], K. Potamianos [170], P.A. Potepa [87a], I.N. Potrap [39],
C.J. Potter [33], H. Potti [151], J. Poveda [166], M.E. Pozo Astigarraga [37], A. Prades Ibanez [77a,77b],
J. Pretel [168], D. Price [103], M. Primavera [71a], L. Primomo [70a,70c], M.A. Principe Martin [101],
R. Privara [125], T. Procter [60], M.L. Proffitt [142], N. Proklova [131], K. Prokofiev [65c], G. Proto [112],
J. Proudfoot [6], M. Przybycien [87a], W.W. Przygoda [87b], A. Psallidas [47], J.E. Puddefoot [143],
D. Pudzha [55], D. Pyatiizbyantseva [38], J. Qian [108], R. Qian [109], D. Qichen [103], Y. Qin [13],
T. Qiu [53], A. Quadt [56], M. Queitsch-Maitland [103], G. Quetant [57], R.P. Quinn [167],
G. Rabanal Bolanos [62], D. Rafanoharana [55], F. Raffaeli [77a,77b], F. Ragusa [72a,72b], J.L. Rainbolt [40],
J.A. Raine [57], S. Rajagopalan [30], E. Ramakoti [38], L. Rambelli [58b,58a], I.A. Ramirez-Berend [35],
K. Ran [49,114c], D.S. Rankin [131], N.P. Rapheeha [34g], H. Rasheed [28b], V. Raskina [130],
D.F. Rassloff [64a], A. Rastogi [18a], S. Rave [102], S. Ravera [58b,58a], B. Ravina [56], I. Ravinovich [172],
M. Raymond [37], A.L. Read [128], N.P. Readioff [143], D.M. Rebuzzi [74a,74b], G. Redlinger [30],
A.S. Reed [112], K. Reeves [27], J.A. Reidelsturz [174], D. Reikher [126], A. Rej [50], C. Rembser [37],
M. Renda [28b], F. Renner [49], A.G. Rennie [162], A.L. Rescia [49], S. Resconi [72a],
M. Ressegotti [58b,58a], S. Rettie [37], J.G. Reyes Rivera [109], E. Reynolds [18a], O.L. Rezanova [38],
P. Reznicek [136], H. Riani [36d], N. Ribaric [52], E. Ricci [79a,79b], R. Richter [112], S. Richter [48a,48b],
E. Richter-Was [87b], M. Ridel [130], S. Ridouani [36d], P. Rieck [120], P. Riedler [37], E.M. Riefel [48a,48b],
J.O. Rieger [117], M. Rijssenbeek [149], M. Rimoldi [37], L. Rinaldi [24b,24a], P. Rincke [56,164],
T.T. Rinn [30], M.P. Rinnagel [111], G. Ripellino [164], I. Riu [13], J.C. Rivera Vergara [168],
F. Rizatdinova [124], E. Rizvi [96], B.R. Roberts [18a], S.S. Roberts [139], S.H. Robertson [106,x],
D. Robinson [33], M. Robles Manzano [102], A. Robson [60], A. Rocchi [77a,77b], C. Roda [75a,75b],
S. Rodriguez Bosca [37], Y. Rodriguez Garcia [23a], A. Rodriguez Rodriguez [55],
A.M. Rodríguez Vera [118], S. Roe [37], J.T. Roemer [37], A.R. Roepe-Gier [139], O. Røhne [128],
R.A. Rojas [105], C.P.A. Roland [130], J. Roloff [30], A. Romaniouk [80], E. Romano [74a,74b],
M. Romano [24b], A.C. Romero Hernandez [165], N. Rompotis [94], L. Roos [130], S. Rosati [76a],
B.J. Rosser [40], E. Rossi [129], E. Rossi [73a,73b], L.P. Rossi [62], L. Rossini [55], R. Rosten [122],
M. Rotaru [28b], B. Rottler [55], C. Rougier [91], D. Rousseau [67], D. Rousso [49], A. Roy [165],
S. Roy-Garand [158], A. Rozanov [104], Z.M.A. Rozario [60], Y. Rozen [154], A. Rubio Jimenez [166],
A.J. Ruby [94], V.H. Ruelas Rivera [19], T.A. Ruggeri [1], A. Ruggiero [129], A. Ruiz-Martinez [166],
A. Rummler [37], Z. Rurikova [55], N.A. Rusakovich [39], H.L. Russell [168], G. Russo [76a,76b],
J.P. Rutherfoord [7], S. Rutherford Colmenares [33], M. Rybar [136], E.B. Rye [128], A. Ryzhov [45],
J.A. Sabater Iglesias [57], H.F-W. Sadrozinski [139], F. Safai Tehrani [76a], B. Safarzadeh Samani [137],
S. Saha [1], M. Sahinsoy [83], A. Saibel [166], M. Saimpert [138], M. Saito [157], T. Saito [157],
A. Sala [72a,72b], D. Salamani [37], A. Salnikov [147], J. Salt [166], A. Salvador Salas [155],
D. Salvatore [44b,44a], F. Salvatore [150], A. Salzburger [37], D. Sammel [55], E. Sampson [93],
D. Sampsonidis [156,d], D. Sampsonidou [126], J. Sánchez [166], V. Sanchez Sebastian [166],
H. Sandaker [128], C.O. Sander [49], J.A. Sandesara [105], M. Sandhoff [174], C. Sandoval [23b],
L. Sanfilippo [64a], D.P.C. Sankey [137], T. Sano [89], A. Sansoni [54], L. Santi [37,76b], C. Santoni [41],
H. Santos [133a,133b], A. Santra [172], E. Sanzani [24b,24a], K.A. Saoucha [163], J.G. Saraiva [133a,133d],
J. Sardain [7], O. Sasaki [85], K. Sato [160], C. Sauer [64b], E. Sauvan [4], P. Savard [158,ad], R. Sawada [157],
C. Sawyer [137], L. Sawyer [99], C. Sbarra [24b], A. Sbrizzi [24b,24a], T. Scanlon [98],

J. Schaarschmidt [142], U. Schäfer [102], A.C. Schaffer [67,45], D. Schaile [111], R.D. Schamberger [149],
C. Scharf [19], M.M. Schefer [20], V.A. Schegelsky [38], D. Scheirich [136], M. Schernau [162],
C. Scheulen [56], C. Schiavi [58b,58a], M. Schioppa [44b,44a], B. Schlag [147], S. Schlenker [37],
J. Schmeing [174], M.A. Schmidt [174], K. Schmieden [102], C. Schmitt [102], N. Schmitt [102],
S. Schmitt [49], L. Schoeffel [138], A. Schoening [64b], P.G. Scholer [35], E. Schopf [129], M. Schott [25],
J. Schovancova [37], S. Schramm [57], T. Schroer [57], H-C. Schultz-Coulon [64a], M. Schumacher [55],
B.A. Schumm [139], Ph. Schune [138], A.J. Schuy [142], H.R. Schwartz [139], A. Schwartzman [147],
T.A. Schwarz [108], Ph. Schwemling [138], R. Schwienhorst [109], F.G. Sciacca [20], A. Sciandra [30],
G. Sciolla [27], F. Scuri [75a], C.D. Sebastiani [94], K. Sedlaczek [118], S.C. Seidel [115], A. Seiden [139],
B.D. Seidlitz [42], C. Seitz [49], J.M. Seixas [84b], G. Sekhniaidze [73a], L. Selem [61],
N. Semprini-Cesari [24b,24a], D. Sengupta [57], V. Senthilkumar [166], L. Serin [67], M. Sessa [77a,77b],
H. Severini [123], F. Sforza [58b,58a], A. Sfyrla [57], Q. Sha [14], E. Shabalina [56], A.H. Shah [33],
R. Shaheen [148], J.D. Shahinian [131], D. Shaked Renous [172], L.Y. Shan [14], M. Shapiro [18a],
A. Sharma [37], A.S. Sharma [167], P. Sharma [81], P.B. Shatalov [38], K. Shaw [150], S.M. Shaw [103],
Q. Shen [63c], D.J. Sheppard [146], P. Sherwood [98], L. Shi [98], X. Shi [14], S. Shimizu [85],
C.O. Shimmin [175], J.D. Shinner [97], I.P.J. Shipsey [129,*], S. Shirabe [90], M. Shiyakova [39,v],
M.J. Shochet [40], D.R. Shope [128], B. Shrestha [123], S. Shrestha [122,ag], I. Shreyber [38],
M.J. Shroff [168], P. Sicho [134], A.M. Sickles [165], E. Sideras Haddad [34g], A.C. Sidley [117],
A. Sidoti [24b], F. Siegert [51], Dj. Sijacki [16], F. Sili [92], J.M. Silva [53], I. Silva Ferreira [84b],
M.V. Silva Oliveira [30], S.B. Silverstein [48a], S. Simion [67], R. Simoniello [37], E.L. Simpson [103],
H. Simpson [150], L.R. Simpson [108], S. Simsek [83], S. Sindhu [56], P. Sinervo [158], S. Singh [30],
S. Sinha [49], S. Sinha [103], M. Sioli [24b,24a], I. Siral [37], E. Sitnikova [49], J. Sjölin [48a,48b],
A. Skaf [56], E. Skorda [21], P. Skubic [123], M. Slawinska [88], V. Smakhtin [172], B.H. Smart [137],
S.Yu. Smirnov [38], Y. Smirnov [38], L.N. Smirnova [38,a], O. Smirnova [100], A.C. Smith [42],
D.R. Smith [162], E.A. Smith [40], J.L. Smith [103], R. Smith [147], H. Smitmanns [102], M. Smizanska [93],
K. Smolek [135], A.A. Snesarev [38], H.L. Snoek [117], S. Snyder [30], R. Sobie [168,x], A. Soffer [155],
C.A. Solans Sanchez [37], E.Yu. Soldatov [38], U. Soldevila [166], A.A. Solodkov [38], S. Solomon [27],
A. Soloshenko [39], K. Solovieva [55], O.V. Solovyanov [41], P. Sommer [51], A. Sonay [13],
W.Y. Song [159b], A. Sopczak [135], A.L. Sopio [53], F. Sopkova [29b], J.D. Sorenson [115],
I.R. Sotarriva Alvarez [141], V. Sothilingam [64a], O.J. Soto Sandoval [140c,140b], S. Sottocornola [69],
R. Soualah [163], Z. Soumaimi [36e], D. South [49], N. Soybelman [172], S. Spagnolo [71a,71b],
M. Spalla [112], D. Sperlich [55], G. Spigo [37], B. Spisso [73a,73b], D.P. Spiteri [60], M. Spousta [136],
E.J. Staats [35], R. Stamen [64a], A. Stampekis [21], E. Stanecka [88], W. Stanek-Maslouska [49],
M.V. Stange [51], B. Stanislaus [18a], M.M. Stanitzki [49], B. Stapf [49], E.A. Starchenko [38],
G.H. Stark [139], J. Stark [91], P. Staroba [134], P. Starovoitov [64a], S. Stärz [106], R. Staszewski [88],
G. Stavropoulos [47], A. Stefl [37], P. Steinberg [30], B. Stelzer [146,159a], H.J. Stelzer [132],
O. Stelzer-Chilton [159a], H. Stenzel [59], T.J. Stevenson [150], G.A. Stewart [37], J.R. Stewart [124],
M.C. Stockton [37], G. Stoicea [28b], M. Stolarski [133a], S. Stonjek [112], A. Straessner [51],
J. Strandberg [148], S. Strandberg [48a,48b], M. Stratmann [174], M. Strauss [123], T. Strebler [104],
P. Strizenec [29b], R. Ströhmer [169], D.M. Strom [126], R. Stroynowski [45], A. Strubig [48a,48b],
S.A. Stucci [30], B. Stugu [17], J. Stupak [123], N.A. Styles [49], D. Su [147], S. Su [63a], W. Su [63d],
X. Su [63a], D. Suchy [29a], K. Sugizaki [157], V.V. Sulin [38], M.J. Sullivan [94], D.M.S. Sultan [129],
L. Sultanaliyeva [38], S. Sultansoy [3b], T. Sumida [89], S. Sun [173], O. Sunneborn Gudnadottir [164],
N. Sur [104], M.R. Sutton [150], H. Suzuki [160], M. Svatos [134], M. Swiatlowski [159a], T. Swirski [169],
I. Sykora [29a], M. Sykora [136], T. Sykora [136], D. Ta [102], K. Tackmann [49,u], A. Taffard [162],
R. Tafirout [159a], J.S. Tafoya Vargas [67], Y. Takubo [85], M. Talby [104], A.A. Talyshev [38],
K.C. Tam [65b], N.M. Tamir [155], A. Tanaka [157], J. Tanaka [157], R. Tanaka [67], M. Tanasini [149],

Z. Tao [167], S. Tapia Araya [140f], S. Tapprogge [102], A. Tarek Abouelfadl Mohamed [109],
S. Tarem [154], K. Tariq [14], G. Tarna [28b], G.F. Tartarelli [72a], M.J. Tartarin [91], P. Tas [136],
M. Tasevsky [134], E. Tassi [44b,44a], A.C. Tate [165], G. Tateno [157], Y. Tayalati [36e,w], G.N. Taylor [107],
W. Taylor [159b], R. Teixeira De Lima [147], P. Teixeira-Dias [97], J.J. Teoh [158], K. Terashi [157],
J. Terron [101], S. Terzo [13], M. Testa [54], R.J. Teuscher [158,x], A. Thaler [80], O. Theiner [57],
T. Theveneaux-Pelzer [104], O. Thielmann [174], D.W. Thomas[97], J.P. Thomas [21], E.A. Thompson [18a],
P.D. Thompson [21], E. Thomson [131], R.E. Thornberry [45], C. Tian [63a], Y. Tian [57],
V. Tikhomirov [38,a], Yu.A. Tikhonov [38], S. Timoshenko[38], D. Timoshyn [136], E.X.L. Ting [1],
P. Tipton [175], A. Tishelman-Charny [30], S.H. Tlou [34g], K. Todome [141], S. Todorova-Nova [136],
S. Todt[51], L. Toffolin [70a,70c], M. Togawa [85], J. Tojo [90], S. Tokár [29a], K. Tokushuku [85],
O. Toldaiev [69], M. Tomoto [85,113], L. Tompkins [147,l], K.W. Topolnicki [87b], E. Torrence [126],
H. Torres [91], E. Torró Pastor [166], M. Toscani [31], C. Tosciri [40], M. Tost [11], D.R. Tovey [143],
I.S. Trandafir [28b], T. Trefzger [169], A. Tricoli [30], I.M. Trigger [159a], S. Trincaz-Duvoid [130],
D.A. Trischuk [27], B. Trocmé [61], A. Tropina[39], L. Truong [34c], M. Trzebinski [88], A. Trzupek [88],
F. Tsai [149], M. Tsai [108], A. Tsiamis [156], P.V. Tsiareshka[38], S. Tsigaridas [159a], A. Tsirigotis [156,r],
V. Tsiskaridze [158], E.G. Tskhadadze [153a], M. Tsopoulou [156], Y. Tsujikawa [89], I.I. Tsukerman [38],
V. Tsulaia [18a], S. Tsuno [85], K. Tsuri [121], D. Tsybychev [149], Y. Tu [65b], A. Tudorache [28b],
V. Tudorache [28b], A.N. Tuna [62], S. Turchikhin [58b,58a], I. Turk Cakir [3a], R. Turra [72a],
T. Turtuvshin [39], P.M. Tuts [42], S. Tzamarias [156,d], E. Tzovara [102], F. Ukegawa [160],
P.A. Ulloa Poblete [140c,140b], E.N. Umaka [30], G. Unal [37], A. Undrus [30], G. Unel [162], J. Urban [29b],
P. Urrejola [140a], G. Usai [8], R. Ushioda [141], M. Usman [110], F. Ustuner [53], Z. Uysal [83],
V. Vacek [135], B. Vachon [106], T. Vafeiadis [37], A. Vaitkus [98], C. Valderanis [111],
E. Valdes Santurio [48a,48b], M. Valente [159a], S. Valentinetti [24b,24a], A. Valero [166],
E. Valiente Moreno [166], A. Vallier [91], J.A. Valls Ferrer [166], D.R. Van Arneman [117],
T.R. Van Daalen [142], A. Van Der Graaf [50], P. Van Gemmeren [6], M. Van Rijnbach [37],
S. Van Stroud [98], I. Van Vulpen [117], P. Vana [136], M. Vanadia [77a,77b], U.M. Vande Voorde [148],
W. Vandelli [37], E.R. Vandewall [124], D. Vannicola [155], L. Vannoli [54], R. Vari [76a], E.W. Varnes [7],
C. Varni [18b], T. Varol [152], D. Varouchas [67], L. Varriale [166], K.E. Varvell [151], M.E. Vasile [28b],
L. Vaslin[85], G.A. Vasquez [168], A. Vasyukov [39], L.M. Vaughan [124], R. Vavricka[102],
T. Vazquez Schroeder [37], J. Veatch [32], V. Vecchio [103], M.J. Veen [105], I. Veliscek [30],
L.M. Veloce [158], F. Veloso [133a,133c], S. Veneziano [76a], A. Ventura [71a,71b], S. Ventura Gonzalez [138],
A. Verbytskyi [112], M. Verducci [75a,75b], C. Vergis [96], M. Verissimo De Araujo [84b],
W. Verkerke [117], J.C. Vermeulen [117], C. Vernieri [147], M. Vessella [105], M.C. Vetterli [146,ad],
A. Vgenopoulos [102], N. Viaux Maira [140f], T. Vickey [143], O.E. Vickey Boeriu [143],
G.H.A. Viehhauser [129], L. Vigani [64b], M. Vigl [112], M. Villa [24b,24a], M. Villaplana Perez [166],
E.M. Villhauer[53], E. Vilucchi [54], M.G. Vincter [35], A. Visibile[117], C. Vittori [37], I. Vivarelli [24b,24a],
E. Voevodina [112], F. Vogel [111], J.C. Voigt [51], P. Vokac [135], Yu. Volkotrub [87b], E. Von Toerne [25],
B. Vormwald [37], V. Vorobel [136], K. Vorobev [38], M. Vos [166], K. Voss [145], M. Vozak [117],
L. Vozdecky [123], N. Vranjes [16], M. Vranjes Milosavljevic [16], M. Vreeswijk [117], N.K. Vu [63d,63c],
R. Vuillermet [37], O. Vujinovic [102], I. Vukotic [40], I.K. Vyas [35], S. Wada [160], C. Wagner[147],
J.M. Wagner [18a], W. Wagner [174], S. Wahdan [174], H. Wahlberg [92], C.H. Waits[123], J. Walder [137],
R. Walker [111], W. Walkowiak [145], A. Wall [131], E.J. Wallin [100], T. Wamorkar [6], A.Z. Wang [139],
C. Wang [102], C. Wang [11], H. Wang [18a], J. Wang [65c], P. Wang [98], R. Wang [62], R. Wang [6],
S.M. Wang [152], S. Wang [63b], S. Wang [14], T. Wang [63a], W.T. Wang [81], W. Wang [14],
X. Wang [114a], X. Wang [165], X. Wang [63c], Y. Wang [63d], Y. Wang [114a], Y. Wang [63a],
Z. Wang [108], Z. Wang [63d,52,63c], Z. Wang [108], A. Warburton [106], R.J. Ward [21], N. Warrack [60],
S. Waterhouse [97], A.T. Watson [21], H. Watson [53], M.F. Watson [21], E. Watton [60,137], G. Watts [142],

B.M. Waugh [98], J.M. Webb [55], C. Weber [30], H.A. Weber [19], M.S. Weber [20], S.M. Weber [64a], C. Wei [63a], Y. Wei [55], A.R. Weidberg [129], E.J. Weik [120], J. Weingarten [50], C. Weiser [55], C.J. Wells [49], T. Wenaus [30], B. Wendland [50], T. Wengler [37], N.S. Wenke[112], N. Wermes [25], M. Wessels [64a], A.M. Wharton [93], A.S. White [62], A. White [8], M.J. White [1], D. Whiteson [162], L. Wickremasinghe [127], W. Wiedenmann [173], M. Wielers [137], C. Wiglesworth [43], D.J. Wilbern[123], H.G. Wilkens [37], J.J.H. Wilkinson [33], D.M. Williams [42], H.H. Williams[131], S. Williams [33], S. Willocq [105], B.J. Wilson [103], P.J. Windischhofer [40], F.I. Winkel [31], F. Winklmeier [126], B.T. Winter [55], J.K. Winter [103], M. Wittgen[147], M. Wobisch [99], T. Wojtkowski[61], Z. Wolffs [117], J. Wollrath[162], M.W. Wolter [88], H. Wolters [133a,133c], M.C. Wong[139], E.L. Woodward [42], S.D. Worm [49], B.K. Wosiek [88], K.W. Woźniak [88], S. Wozniewski [56], K. Wraight [60], C. Wu [21], M. Wu [114b], M. Wu [116], S.L. Wu [173], X. Wu [57], Y. Wu [63a], Z. Wu [4], J. Wuerzinger [112,ab], T.R. Wyatt [103], B.M. Wynne [53], S. Xella [43], L. Xia [114a], M. Xia [15], M. Xie [63a], S. Xin [14,114c], A. Xiong [126], J. Xiong [18a], D. Xu [14], H. Xu [63a], L. Xu [63a], R. Xu [131], T. Xu [108], Y. Xu [15], Z. Xu [53], Z. Xu[114a], B. Yabsley [151], S. Yacoob [34a], Y. Yamaguchi [85], E. Yamashita [157], H. Yamauchi [160], T. Yamazaki [18a], Y. Yamazaki [86], S. Yan [60], Z. Yan [105], H.J. Yang [63c,63d], H.T. Yang [63a], S. Yang [63a], T. Yang [65c], X. Yang [37], X. Yang [14], Y. Yang [45], Y. Yang[63a], Z. Yang [63a], W-M. Yao [18a], H. Ye [114a], H. Ye [56], J. Ye [14], S. Ye [30], X. Ye [63a], Y. Yeh [98], I. Yeletskikh [39], B. Yeo [18b], M.R. Yexley [98], T.P. Yildirim [129], P. Yin [42], K. Yorita [171], S. Younas [28b], C.J.S. Young [37], C. Young [147], C. Yu [14,114c], Y. Yu [63a], J. Yuan [14,114c], M. Yuan [108], R. Yuan [63d,63c], L. Yue [98], M. Zaazoua [63a], B. Zabinski [88], E. Zaid[53], Z.K. Zak [88], T. Zakareishvili [166], S. Zambito [57], J.A. Zamora Saa [140d,140b], J. Zang [157], D. Zanzi [55], O. Zaplatilek [135], C. Zeitnitz [174], H. Zeng [14], J.C. Zeng [165], D.T. Zenger Jr [27], O. Zenin [38], T. Ženiš [29a], S. Zenz [96], S. Zerradi [36a], D. Zerwas [67], M. Zhai [14,114c], D.F. Zhang [143], J. Zhang [63b], J. Zhang [6], K. Zhang [14,114c], L. Zhang [63a], L. Zhang [114a], P. Zhang [14,114c], R. Zhang [173], S. Zhang [108], S. Zhang [91], T. Zhang [157], X. Zhang [63c], Y. Zhang [142], Y. Zhang [98], Y. Zhang [114a], Z. Zhang [18a], Z. Zhang [63b], Z. Zhang [67], H. Zhao [142], T. Zhao [63b], Y. Zhao [139], Z. Zhao [63a], Z. Zhao [63a], A. Zhemchugov [39], J. Zheng [114a], K. Zheng [165], X. Zheng [63a], Z. Zheng [147], D. Zhong [165], B. Zhou [108], H. Zhou [7], N. Zhou [63c], Y. Zhou [15], Y. Zhou [114a], Y. Zhou[7], C.G. Zhu [63b], J. Zhu [108], X. Zhu[63d], Y. Zhu [63c], Y. Zhu [63a], X. Zhuang [14], K. Zhukov [69], N.I. Zimine [39], J. Zinsser [64b], M. Ziolkowski [145], L. Živković [16], A. Zoccoli [24b,24a], K. Zoch [62], T.G. Zorbas [143], O. Zormpa [47], W. Zou [42], L. Zwalinski [37].

[1]Department of Physics, University of Adelaide, Adelaide; Australia.

[2]Department of Physics, University of Alberta, Edmonton AB; Canada.

[3](a)Department of Physics, Ankara University, Ankara;(b)Division of Physics, TOBB University of Economics and Technology, Ankara; Türkiye.

[4]LAPP, Université Savoie Mont Blanc, CNRS/IN2P3, Annecy; France.

[5]APC, Université Paris Cité, CNRS/IN2P3, Paris; France.

[6]High Energy Physics Division, Argonne National Laboratory, Argonne IL; United States of America.

[7]Department of Physics, University of Arizona, Tucson AZ; United States of America.

[8]Department of Physics, University of Texas at Arlington, Arlington TX; United States of America.

[9]Physics Department, National and Kapodistrian University of Athens, Athens; Greece.

[10]Physics Department, National Technical University of Athens, Zografou; Greece.

[11]Department of Physics, University of Texas at Austin, Austin TX; United States of America.

[12]Institute of Physics, Azerbaijan Academy of Sciences, Baku; Azerbaijan.

[13]Institut de Física d'Altes Energies (IFAE), Barcelona Institute of Science and Technology, Barcelona; Spain.

[14]Institute of High Energy Physics, Chinese Academy of Sciences, Beijing; China.

[15]Physics Department, Tsinghua University, Beijing; China.

[16]Institute of Physics, University of Belgrade, Belgrade; Serbia.

[17]Department for Physics and Technology, University of Bergen, Bergen; Norway.

[18][a]Physics Division, Lawrence Berkeley National Laboratory, Berkeley CA;[b]University of California, Berkeley CA; United States of America.

[19]Institut für Physik, Humboldt Universität zu Berlin, Berlin; Germany.

[20]Albert Einstein Center for Fundamental Physics and Laboratory for High Energy Physics, University of Bern, Bern; Switzerland.

[21]School of Physics and Astronomy, University of Birmingham, Birmingham; United Kingdom.

[22][a]Department of Physics, Bogazici University, Istanbul;[b]Department of Physics Engineering, Gaziantep University, Gaziantep;[c]Department of Physics, Istanbul University, Istanbul; Türkiye.

[23][a]Facultad de Ciencias y Centro de Investigaciónes, Universidad Antonio Nariño, Bogotá;[b]Departamento de Física, Universidad Nacional de Colombia, Bogotá; Colombia.

[24][a]Dipartimento di Fisica e Astronomia A. Righi, Università di Bologna, Bologna;[b]INFN Sezione di Bologna; Italy.

[25]Physikalisches Institut, Universität Bonn, Bonn; Germany.

[26]Department of Physics, Boston University, Boston MA; United States of America.

[27]Department of Physics, Brandeis University, Waltham MA; United States of America.

[28][a]Transilvania University of Brasov, Brasov;[b]Horia Hulubei National Institute of Physics and Nuclear Engineering, Bucharest;[c]Department of Physics, Alexandru Ioan Cuza University of Iasi, Iasi;[d]National Institute for Research and Development of Isotopic and Molecular Technologies, Physics Department, Cluj-Napoca;[e]National University of Science and Technology Politechnica, Bucharest;[f]West University in Timisoara, Timisoara;[g]Faculty of Physics, University of Bucharest, Bucharest; Romania.

[29][a]Faculty of Mathematics, Physics and Informatics, Comenius University, Bratislava;[b]Department of Subnuclear Physics, Institute of Experimental Physics of the Slovak Academy of Sciences, Kosice; Slovak Republic.

[30]Physics Department, Brookhaven National Laboratory, Upton NY; United States of America.

[31]Universidad de Buenos Aires, Facultad de Ciencias Exactas y Naturales, Departamento de Física, y CONICET, Instituto de Física de Buenos Aires (IFIBA), Buenos Aires; Argentina.

[32]California State University, CA; United States of America.

[33]Cavendish Laboratory, University of Cambridge, Cambridge; United Kingdom.

[34][a]Department of Physics, University of Cape Town, Cape Town;[b]iThemba Labs, Western Cape;[c]Department of Mechanical Engineering Science, University of Johannesburg, Johannesburg;[d]National Institute of Physics, University of the Philippines Diliman (Philippines);[e]University of South Africa, Department of Physics, Pretoria;[f]University of Zululand, KwaDlangezwa;[g]School of Physics, University of the Witwatersrand, Johannesburg; South Africa.

[35]Department of Physics, Carleton University, Ottawa ON; Canada.

[36][a]Faculté des Sciences Ain Chock, Université Hassan II de Casablanca;[b]Faculté des Sciences, Université Ibn-Tofail, Kénitra;[c]Faculté des Sciences Semlalia, Université Cadi Ayyad, LPHEA-Marrakech;[d]LPMR, Faculté des Sciences, Université Mohamed Premier, Oujda;[e]Faculté des sciences, Université Mohammed V, Rabat;[f]Institute of Applied Physics, Mohammed VI Polytechnic University, Ben Guerir; Morocco.

[37]CERN, Geneva; Switzerland.

[38]Affiliated with an institute covered by a cooperation agreement with CERN.

[39]Affiliated with an international laboratory covered by a cooperation agreement with CERN.

[40]Enrico Fermi Institute, University of Chicago, Chicago IL; United States of America.

[41]LPC, Université Clermont Auvergne, CNRS/IN2P3, Clermont-Ferrand; France.

[42]Nevis Laboratory, Columbia University, Irvington NY; United States of America.

[43]Niels Bohr Institute, University of Copenhagen, Copenhagen; Denmark.

[44][a]Dipartimento di Fisica, Università della Calabria, Rende;[b]INFN Gruppo Collegato di Cosenza, Laboratori Nazionali di Frascati; Italy.

[45]Physics Department, Southern Methodist University, Dallas TX; United States of America.

[46]Physics Department, University of Texas at Dallas, Richardson TX; United States of America.

[47]National Centre for Scientific Research "Demokritos", Agia Paraskevi; Greece.

[48][a]Department of Physics, Stockholm University;[b]Oskar Klein Centre, Stockholm; Sweden.

[49]Deutsches Elektronen-Synchrotron DESY, Hamburg and Zeuthen; Germany.

[50]Fakultät Physik , Technische Universität Dortmund, Dortmund; Germany.

[51]Institut für Kern- und Teilchenphysik, Technische Universität Dresden, Dresden; Germany.

[52]Department of Physics, Duke University, Durham NC; United States of America.

[53]SUPA - School of Physics and Astronomy, University of Edinburgh, Edinburgh; United Kingdom.

[54]INFN e Laboratori Nazionali di Frascati, Frascati; Italy.

[55]Physikalisches Institut, Albert-Ludwigs-Universität Freiburg, Freiburg; Germany.

[56]II. Physikalisches Institut, Georg-August-Universität Göttingen, Göttingen; Germany.

[57]Département de Physique Nucléaire et Corpusculaire, Université de Genève, Genève; Switzerland.

[58][a]Dipartimento di Fisica, Università di Genova, Genova;[b]INFN Sezione di Genova; Italy.

[59]II. Physikalisches Institut, Justus-Liebig-Universität Giessen, Giessen; Germany.

[60]SUPA - School of Physics and Astronomy, University of Glasgow, Glasgow; United Kingdom.

[61]LPSC, Université Grenoble Alpes, CNRS/IN2P3, Grenoble INP, Grenoble; France.

[62]Laboratory for Particle Physics and Cosmology, Harvard University, Cambridge MA; United States of America.

[63][a]Department of Modern Physics and State Key Laboratory of Particle Detection and Electronics, University of Science and Technology of China, Hefei;[b]Institute of Frontier and Interdisciplinary Science and Key Laboratory of Particle Physics and Particle Irradiation (MOE), Shandong University, Qingdao;[c]School of Physics and Astronomy, Shanghai Jiao Tong University, Key Laboratory for Particle Astrophysics and Cosmology (MOE), SKLPPC, Shanghai;[d]Tsung-Dao Lee Institute, Shanghai;[e]School of Physics, Zhengzhou University; China.

[64][a]Kirchhoff-Institut für Physik, Ruprecht-Karls-Universität Heidelberg, Heidelberg;[b]Physikalisches Institut, Ruprecht-Karls-Universität Heidelberg, Heidelberg; Germany.

[65][a]Department of Physics, Chinese University of Hong Kong, Shatin, N.T., Hong Kong;[b]Department of Physics, University of Hong Kong, Hong Kong;[c]Department of Physics and Institute for Advanced Study, Hong Kong University of Science and Technology, Clear Water Bay, Kowloon, Hong Kong; China.

[66]Department of Physics, National Tsing Hua University, Hsinchu; Taiwan.

[67]IJCLab, Université Paris-Saclay, CNRS/IN2P3, 91405, Orsay; France.

[68]Centro Nacional de Microelectrónica (IMB-CNM-CSIC), Barcelona; Spain.

[69]Department of Physics, Indiana University, Bloomington IN; United States of America.

[70][a]INFN Gruppo Collegato di Udine, Sezione di Trieste, Udine;[b]ICTP, Trieste;[c]Dipartimento Politecnico di Ingegneria e Architettura, Università di Udine, Udine; Italy.

[71][a]INFN Sezione di Lecce;[b]Dipartimento di Matematica e Fisica, Università del Salento, Lecce; Italy.

[72][a]INFN Sezione di Milano;[b]Dipartimento di Fisica, Università di Milano, Milano; Italy.

[73][a]INFN Sezione di Napoli;[b]Dipartimento di Fisica, Università di Napoli, Napoli; Italy.

[74][a]INFN Sezione di Pavia;[b]Dipartimento di Fisica, Università di Pavia, Pavia; Italy.

[75][a]INFN Sezione di Pisa;[b]Dipartimento di Fisica E. Fermi, Università di Pisa, Pisa; Italy.

[76][a]INFN Sezione di Roma;[b]Dipartimento di Fisica, Sapienza Università di Roma, Roma; Italy.

[77](a)INFN Sezione di Roma Tor Vergata;(b)Dipartimento di Fisica, Università di Roma Tor Vergata, Roma; Italy.

[78](a)INFN Sezione di Roma Tre;(b)Dipartimento di Matematica e Fisica, Università Roma Tre, Roma; Italy.

[79](a)INFN-TIFPA;(b)Università degli Studi di Trento, Trento; Italy.

[80]Universität Innsbruck, Department of Astro and Particle Physics, Innsbruck; Austria.

[81]University of Iowa, Iowa City IA; United States of America.

[82]Department of Physics and Astronomy, Iowa State University, Ames IA; United States of America.

[83]Istinye University, Sariyer, Istanbul; Türkiye.

[84](a)Departamento de Engenharia Elétrica, Universidade Federal de Juiz de Fora (UFJF), Juiz de Fora;(b)Universidade Federal do Rio De Janeiro COPPE/EE/IF, Rio de Janeiro;(c)Instituto de Física, Universidade de São Paulo, São Paulo;(d)Rio de Janeiro State University, Rio de Janeiro;(e)Federal University of Bahia, Bahia; Brazil.

[85]KEK, High Energy Accelerator Research Organization, Tsukuba; Japan.

[86]Graduate School of Science, Kobe University, Kobe; Japan.

[87](a)AGH University of Krakow, Faculty of Physics and Applied Computer Science, Krakow;(b)Marian Smoluchowski Institute of Physics, Jagiellonian University, Krakow; Poland.

[88]Institute of Nuclear Physics Polish Academy of Sciences, Krakow; Poland.

[89]Faculty of Science, Kyoto University, Kyoto; Japan.

[90]Research Center for Advanced Particle Physics and Department of Physics, Kyushu University, Fukuoka ; Japan.

[91]L2IT, Université de Toulouse, CNRS/IN2P3, UPS, Toulouse; France.

[92]Instituto de Física La Plata, Universidad Nacional de La Plata and CONICET, La Plata; Argentina.

[93]Physics Department, Lancaster University, Lancaster; United Kingdom.

[94]Oliver Lodge Laboratory, University of Liverpool, Liverpool; United Kingdom.

[95]Department of Experimental Particle Physics, Jožef Stefan Institute and Department of Physics, University of Ljubljana, Ljubljana; Slovenia.

[96]School of Physics and Astronomy, Queen Mary University of London, London; United Kingdom.

[97]Department of Physics, Royal Holloway University of London, Egham; United Kingdom.

[98]Department of Physics and Astronomy, University College London, London; United Kingdom.

[99]Louisiana Tech University, Ruston LA; United States of America.

[100]Fysiska institutionen, Lunds universitet, Lund; Sweden.

[101]Departamento de Física Teorica C-15 and CIAFF, Universidad Autónoma de Madrid, Madrid; Spain.

[102]Institut für Physik, Universität Mainz, Mainz; Germany.

[103]School of Physics and Astronomy, University of Manchester, Manchester; United Kingdom.

[104]CPPM, Aix-Marseille Université, CNRS/IN2P3, Marseille; France.

[105]Department of Physics, University of Massachusetts, Amherst MA; United States of America.

[106]Department of Physics, McGill University, Montreal QC; Canada.

[107]School of Physics, University of Melbourne, Victoria; Australia.

[108]Department of Physics, University of Michigan, Ann Arbor MI; United States of America.

[109]Department of Physics and Astronomy, Michigan State University, East Lansing MI; United States of America.

[110]Group of Particle Physics, University of Montreal, Montreal QC; Canada.

[111]Fakultät für Physik, Ludwig-Maximilians-Universität München, München; Germany.

[112]Max-Planck-Institut für Physik (Werner-Heisenberg-Institut), München; Germany.

[113]Graduate School of Science and Kobayashi-Maskawa Institute, Nagoya University, Nagoya; Japan.

[114](a)Department of Physics, Nanjing University, Nanjing;(b)School of Science, Shenzhen Campus of Sun

Yat-sen University;[(c)]University of Chinese Academy of Science (UCAS), Beijing; China.

[115]Department of Physics and Astronomy, University of New Mexico, Albuquerque NM; United States of America.

[116]Institute for Mathematics, Astrophysics and Particle Physics, Radboud University/Nikhef, Nijmegen; Netherlands.

[117]Nikhef National Institute for Subatomic Physics and University of Amsterdam, Amsterdam; Netherlands.

[118]Department of Physics, Northern Illinois University, DeKalb IL; United States of America.

[119][(a)]New York University Abu Dhabi, Abu Dhabi;[(b)]United Arab Emirates University, Al Ain; United Arab Emirates.

[120]Department of Physics, New York University, New York NY; United States of America.

[121]Ochanomizu University, Otsuka, Bunkyo-ku, Tokyo; Japan.

[122]Ohio State University, Columbus OH; United States of America.

[123]Homer L. Dodge Department of Physics and Astronomy, University of Oklahoma, Norman OK; United States of America.

[124]Department of Physics, Oklahoma State University, Stillwater OK; United States of America.

[125]Palacký University, Joint Laboratory of Optics, Olomouc; Czech Republic.

[126]Institute for Fundamental Science, University of Oregon, Eugene, OR; United States of America.

[127]Graduate School of Science, Osaka University, Osaka; Japan.

[128]Department of Physics, University of Oslo, Oslo; Norway.

[129]Department of Physics, Oxford University, Oxford; United Kingdom.

[130]LPNHE, Sorbonne Université, Université Paris Cité, CNRS/IN2P3, Paris; France.

[131]Department of Physics, University of Pennsylvania, Philadelphia PA; United States of America.

[132]Department of Physics and Astronomy, University of Pittsburgh, Pittsburgh PA; United States of America.

[133][(a)]Laboratório de Instrumentação e Física Experimental de Partículas - LIP, Lisboa;[(b)]Departamento de Física, Faculdade de Ciências, Universidade de Lisboa, Lisboa;[(c)]Departamento de Física, Universidade de Coimbra, Coimbra;[(d)]Centro de Física Nuclear da Universidade de Lisboa, Lisboa;[(e)]Departamento de Física, Universidade do Minho, Braga;[(f)]Departamento de Física Teórica y del Cosmos, Universidad de Granada, Granada (Spain);[(g)]Departamento de Física, Instituto Superior Técnico, Universidade de Lisboa, Lisboa; Portugal.

[134]Institute of Physics of the Czech Academy of Sciences, Prague; Czech Republic.

[135]Czech Technical University in Prague, Prague; Czech Republic.

[136]Charles University, Faculty of Mathematics and Physics, Prague; Czech Republic.

[137]Particle Physics Department, Rutherford Appleton Laboratory, Didcot; United Kingdom.

[138]IRFU, CEA, Université Paris-Saclay, Gif-sur-Yvette; France.

[139]Santa Cruz Institute for Particle Physics, University of California Santa Cruz, Santa Cruz CA; United States of America.

[140][(a)]Departamento de Física, Pontificia Universidad Católica de Chile, Santiago;[(b)]Millennium Institute for Subatomic physics at high energy frontier (SAPHIR), Santiago;[(c)]Instituto de Investigación Multidisciplinario en Ciencia y Tecnología, y Departamento de Física, Universidad de La Serena;[(d)]Universidad Andres Bello, Department of Physics, Santiago;[(e)]Instituto de Alta Investigación, Universidad de Tarapacá, Arica;[(f)]Departamento de Física, Universidad Técnica Federico Santa María, Valparaíso; Chile.

[141]Department of Physics, Institute of Science, Tokyo; Japan.

[142]Department of Physics, University of Washington, Seattle WA; United States of America.

[143]Department of Physics and Astronomy, University of Sheffield, Sheffield; United Kingdom.

[144] Department of Physics, Shinshu University, Nagano; Japan.

[145] Department Physik, Universität Siegen, Siegen; Germany.

[146] Department of Physics, Simon Fraser University, Burnaby BC; Canada.

[147] SLAC National Accelerator Laboratory, Stanford CA; United States of America.

[148] Department of Physics, Royal Institute of Technology, Stockholm; Sweden.

[149] Departments of Physics and Astronomy, Stony Brook University, Stony Brook NY; United States of America.

[150] Department of Physics and Astronomy, University of Sussex, Brighton; United Kingdom.

[151] School of Physics, University of Sydney, Sydney; Australia.

[152] Institute of Physics, Academia Sinica, Taipei; Taiwan.

[153] [a] E. Andronikashvili Institute of Physics, Iv. Javakhishvili Tbilisi State University, Tbilisi; [b] High Energy Physics Institute, Tbilisi State University, Tbilisi; [c] University of Georgia, Tbilisi; Georgia.

[154] Department of Physics, Technion, Israel Institute of Technology, Haifa; Israel.

[155] Raymond and Beverly Sackler School of Physics and Astronomy, Tel Aviv University, Tel Aviv; Israel.

[156] Department of Physics, Aristotle University of Thessaloniki, Thessaloniki; Greece.

[157] International Center for Elementary Particle Physics and Department of Physics, University of Tokyo, Tokyo; Japan.

[158] Department of Physics, University of Toronto, Toronto ON; Canada.

[159] [a] TRIUMF, Vancouver BC; [b] Department of Physics and Astronomy, York University, Toronto ON; Canada.

[160] Division of Physics and Tomonaga Center for the History of the Universe, Faculty of Pure and Applied Sciences, University of Tsukuba, Tsukuba; Japan.

[161] Department of Physics and Astronomy, Tufts University, Medford MA; United States of America.

[162] Department of Physics and Astronomy, University of California Irvine, Irvine CA; United States of America.

[163] University of Sharjah, Sharjah; United Arab Emirates.

[164] Department of Physics and Astronomy, University of Uppsala, Uppsala; Sweden.

[165] Department of Physics, University of Illinois, Urbana IL; United States of America.

[166] Instituto de Física Corpuscular (IFIC), Centro Mixto Universidad de Valencia - CSIC, Valencia; Spain.

[167] Department of Physics, University of British Columbia, Vancouver BC; Canada.

[168] Department of Physics and Astronomy, University of Victoria, Victoria BC; Canada.

[169] Fakultät für Physik und Astronomie, Julius-Maximilians-Universität Würzburg, Würzburg; Germany.

[170] Department of Physics, University of Warwick, Coventry; United Kingdom.

[171] Waseda University, Tokyo; Japan.

[172] Department of Particle Physics and Astrophysics, Weizmann Institute of Science, Rehovot; Israel.

[173] Department of Physics, University of Wisconsin, Madison WI; United States of America.

[174] Fakultät für Mathematik und Naturwissenschaften, Fachgruppe Physik, Bergische Universität Wuppertal, Wuppertal; Germany.

[175] Department of Physics, Yale University, New Haven CT; United States of America.

[176] Yerevan Physics Institute, Yerevan; Armenia.

[a] Also Affiliated with an institute covered by a cooperation agreement with CERN.

[b] Also at An-Najah National University, Nablus; Palestine.

[c] Also at Borough of Manhattan Community College, City University of New York, New York NY; United States of America.

[d] Also at Center for Interdisciplinary Research and Innovation (CIRI-AUTH), Thessaloniki; Greece.

[e] Also at CERN, Geneva; Switzerland.

[f] Also at CMD-AC UNEC Research Center, Azerbaijan State University of Economics (UNEC);

Azerbaijan.

[g] Also at Département de Physique Nucléaire et Corpusculaire, Université de Genève, Genève; Switzerland.

[h] Also at Departament de Fisica de la Universitat Autonoma de Barcelona, Barcelona; Spain.

[i] Also at Department of Financial and Management Engineering, University of the Aegean, Chios; Greece.

[j] Also at Department of Physics, California State University, Sacramento; United States of America.

[k] Also at Department of Physics, King's College London, London; United Kingdom.

[l] Also at Department of Physics, Stanford University, Stanford CA; United States of America.

[m] Also at Department of Physics, Stellenbosch University; South Africa.

[n] Also at Department of Physics, University of Fribourg, Fribourg; Switzerland.

[o] Also at Department of Physics, University of Thessaly; Greece.

[p] Also at Department of Physics, Westmont College, Santa Barbara; United States of America.

[q] Also at Faculty of Physics, Sofia University, 'St. Kliment Ohridski', Sofia; Bulgaria.

[r] Also at Hellenic Open University, Patras; Greece.

[s] Also at Imam Mohammad Ibn Saud Islamic University; Saudi Arabia.

[t] Also at Institucio Catalana de Recerca i Estudis Avancats, ICREA, Barcelona; Spain.

[u] Also at Institut für Experimentalphysik, Universität Hamburg, Hamburg; Germany.

[v] Also at Institute for Nuclear Research and Nuclear Energy (INRNE) of the Bulgarian Academy of Sciences, Sofia; Bulgaria.

[w] Also at Institute of Applied Physics, Mohammed VI Polytechnic University, Ben Guerir; Morocco.

[x] Also at Institute of Particle Physics (IPP); Canada.

[y] Also at Institute of Physics, Azerbaijan Academy of Sciences, Baku; Azerbaijan.

[z] Also at Institute of Theoretical Physics, Ilia State University, Tbilisi; Georgia.

[aa] Also at National Institute of Physics, University of the Philippines Diliman (Philippines); Philippines.

[ab] Also at Technical University of Munich, Munich; Germany.

[ac] Also at The Collaborative Innovation Center of Quantum Matter (CICQM), Beijing; China.

[ad] Also at TRIUMF, Vancouver BC; Canada.

[ae] Also at Università di Napoli Parthenope, Napoli; Italy.

[af] Also at University of Colorado Boulder, Department of Physics, Colorado; United States of America.

[ag] Also at Washington College, Chestertown, MD; United States of America.

[ah] Also at Yeditepe University, Physics Department, Istanbul; Türkiye.

[*] Deceased